

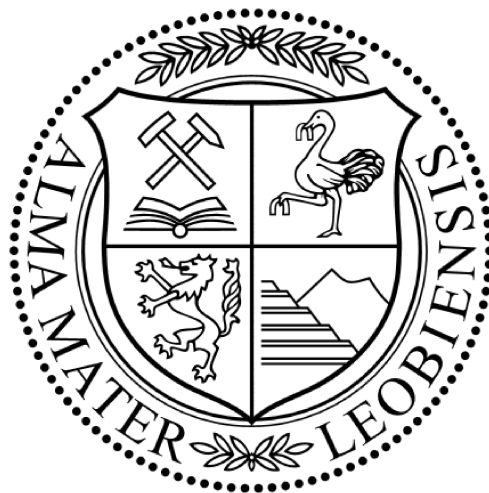
Dissolution kinetics of CaO and MgO in converter steelmaking slags

A Thesis submitted to the Montanuniversitaet Leoben
for the degree of Doctor in Mining and Metallurgical Sciences

written by

Cheremisina Elizaveta

Leoben, December 2016



Acknowledgement

First of all, I would like to express my sincere gratitude to Prof. Dr. Johannes Schenk for his continuous support and assistance throughout my research work. Moreover, his guidance and valuable suggestions helped to achieve the desired results in the scientific work and to develop professionally.

I am thankful to Dr. Abdellah Kharicha for introducing me into the flow dynamics simulation. I appreciate the knowledge I have gained from our consultations regarding thermodynamics. Our productive discussions made a great contribution for my research work.

This work was carried out in the frames of the K1-Met project - the member of COMET – Competence Centers for Excellent Technologies.

Furthermore, I wish to acknowledge the crucial role of my parents and signify my sincere appreciation for their unconditional support and the encouragement to go on the rocky path of science.

This thesis is dedicated to my parents

Abstract

In this work the dissolution kinetics of pure CaO, lime and dololime containing various amounts of magnesium oxide in steelmaking slags has been studied in a non-steady-state diffusion, at temperatures ranging from 1300-1600°C, directly in the hot process. Experiments were carried out in stagnant regime and under forced convection.

In the frames of the K1-Met project - the member of COMET – Competence Centers for Excellent Technologies, the standardized method for the study of kinetics of lime and dololime dissolution in the converter slag has been developed. To control and improve the steelmaking process it is important to know the rate-limiting step of lime dissolution in the melt in the process of interaction between metal and slag.

To describe the kinetics of metallurgical processes physico-mathematical method based on fundamental laws of physical chemistry was applied. Using differential equations of mass balance of the dissolving substance values of mass transfer coefficients were determined experimentally and allow estimating the rate of conjugated mass transfer processes or chemical reactions.

Pure CaO dissolved more rapidly and of bigger mass compared to industrial limes. Calculated apparent activation energy value for the dissolution of pure CaO and lime in the slag is less than 200 kJ/mol, which characterizes the diffusion limiting step in the process. The dependence of the linear rate of lime samples dissolution on the saturation concentration of CaO in the slag has been derived, indicating the diffusion regime of the CaO dissolution in the melt.

It was revealed that the decrease in solubility of lime with the increasing content of magnesium oxide in lime is due to the formation of high temperature solid chemical compounds (Ca_2SiO_4 , $(\text{Mg}, \text{Fe})_2\text{SiO}_4$) and solutions based on MgO like $(\text{Mg}, \text{Fe})\text{O}$ on the surface and in the volume of samples. Slightly soluble compounds formed at the interface of liquid slag-lime hinder the process of lime dissolution.

Using non-stationary linear and spatial diffusion models on the basis of experimental data diffusion coefficients and diffusion activation energy were calculated. It was found that the rate limiting step in the process of lime dissolution in slag is the diffusion of MgO in the melt for slag systems containing high amount of FeO.

Dicalcium, tricalcium silicates and magnesiowustite formed in the process of lime dissolution envelop the dissolved lime particles and limit the diffusion through a solid layer, where the rate-limiting step of the process is internal diffusion.

Kurzfassung

Die Beschreibung der Auflösungskinetik von reinem CaO, Kalk und dolomitischem Kalk mit variablen Gehalten von Magnesiumoxid in Stahlwerksschlacken ist Inhalt dieser Arbeit. Die experimentelle Untersuchung der Diffusion erfolgte dabei in einer nicht stationären Strömung im Temperaturbereich von 1300 – 1600 °C. Die Experimente wurden dabei in einem stehenden Regime bei erzwungener Konvektion der Probe durchgeführt.

Im Rahmen eines K1-MET Projektes – einem Mitglied von COMET - Competence Centers for Excellent Technologies, ist dafür eine standardisierte Methode zur Untersuchung der Auflösungskinetik von Kalk und dolomitischem Kalk in Konverterschlacke entwickelt worden. Zur Kontrolle und kontinuierlichen Verbesserung des Stahlwerksprozesses ist es wichtig die limitierenden Schritte der Kalkauflösung zwischen der Interaktionsfläche zwischen Metallbad und Schlacke zu kennen.

Zur Beschreibung der Kinetik des metallurgischen Prozesses wurden physikalisch-mathematische Methoden und fundamentale Gesetze der physikalischen Chemie verwendet. Mittels der Massenerhaltungsgleichungen der aufzulösenden Substanzen wurden die Massentransferkoeffizienten experimentell bestimmt.

Reines CaO löst sich schneller verglichen mit industriellen Kalksorten. Die berechnete Aktivierungsenergie für die Auflösung von reinem CaO und Kalk in der Schlacke ist kleiner 200 kJ/mol. Dies zeigt, dass die Diffusion der limitierende Prozessschritt ist. Daraus konnte eine lineare Abhängigkeit zwischen Kalkauflösung und der Sättigungskonzentration von CaO in der Schlacke abgeleitet werden.

Es konnte festgestellt werden, dass eine Abnahme der Löslichkeit von Kalk mit einem Anstieg des MgO-Anteils erfolgt. Dies resultiert aufgrund der Bildung von hochschmelzenden chemischen Verbindungen (Ca_2SiO_4 , $(\text{Mg}, \text{Fe})_2\text{SiO}_4$) sowie auf MgO-basierten Lösungen wie $(\text{Mg}, \text{Fe})\text{O}$ auf der Oberfläche und im Inneren des Probenkörpers. Die schwerlöslichen Verbindungen bilden eine Deckschicht an der Grenzfläche zwischen Schlacke und Kalk aus, welche die Kalkauflösung hemmt.

Unter Verwendung nicht stationärer linearer und räumlicher Diffusionsmodelle wurden auf Basis experimenteller Daten die Diffusionskoeffizienten und die Aktivierungsenergie der Diffusion kalkuliert. Der limitierende Schritt der Kalkauflösung in der Schlacke ist die Diffusion von MgO. Dies ist speziell bei Schlackensystemen mit einem hohen FeO-Gehalt beobachtet worden.

Dikalzium- und Trikalzium-Silikate sowie Magnesiawüstite umhüllen das unaufgelöste Kalkpartikel. Dadurch bildet sich eine feste Deckschicht, welche die weitere Kalkauflösung hemmt und somit eine Festkörperdiffusion stattfindet.

Affidavit

I declare in lieu of oath, that I wrote this thesis and performed the associated research myself, using only literature cited in this volume.

Elizaveta Cheremisina

Leoben, December 2016

Table of Contents

Table of Contents	I
List of Symbols	III
1 Introduction	1
2 Oxygen Steelmaking fundamentals	3
2.1 Types of Oxygen Steelmaking Processes	4
2.2 Basic Oxygen furnace structure	6
2.3 The Lance	8
2.4 Sublance Equipment	9
2.5 Steelmaking Operation.....	9
2.6 Raw materials	13
2.7 Refractories.....	16
2.8 Environmental issues	17
3 Thermodynamic for oxygen steelmaking	18
3.1 Refining Reactions in BOF Steelmaking.....	19
3.2 Slag Formation in BOF Steelmaking	22
4 Kinetics of CaO and MgO dissolution in the converter steelmaking process	24
4.1 Factors affecting dissolution.....	26
4.2 Mixing and Mass transfer	27
4.3 Diffusion	28
4.3.1 Diffusion coefficient	29
4.4 Mass transfer in the presence of flow	30
4.5 Mass Transfer Correlations	31
4.6 Kinetic models applied for present work	32
4.6.1 Kinetic model 1	32
4.6.2 Kinetic model 2	35
5 Objects of the study and research techniques	38
6 The methodology of the experiment	45
6.1 The research methodology for the selection of crucible material	45
6.2 Methods for determination of phase transformations in model slag	46
6.3 The methodology of the Kinetic investigations.....	48
7 Refractory materials used in the metallurgical experiment	50
7.1 The results of experimental studies for the crucible material choice	52

8	Experimental results of the study of slag phase transformations.....	63
9	Experimental results of the study of CaO and lime dissolution in slags	72
10	Experimental results of the study of lime dissolution containing various amounts of MgO in model slag	83
	10.1 The calculation of the diffusion coefficients of lime dissolution in model slag containing various amounts of MgO	95
11	The results of experimental study of dolomite dissolution containing 20, 50 and 80% MgO.....	101
12	CFD calculations	112
13	Rotating cylinder experiment.....	115
14	Summary.....	122
15	Bibliography	124
16	List of Figures	128
17	List of Tables.....	133
18	Appendix.....	135

List of Symbols

Latin Letters

A	m^2	Surface area
B	-	Slag Basicity
C_s	$\text{mol}\cdot\text{cm}^{-3}$	Substance concentration near the surface
C_i	$\text{mol}\cdot\text{cm}^{-3}$	The concentration of species in moles/volume
Cx_i	$\text{mol}\cdot\text{cm}^{-3}$	The concentration of species in mass/volume
C_b	$\text{mol}\cdot\text{cm}^{-3}$	Bulk concentration
\bar{C}_i	$\text{mol}\cdot\text{cm}^{-3}$	Interfacial concentration
(CaO)	%	Concentration of calcium oxide in the slag
$(\text{CaO})_{\text{sat}}$	%	Saturation concentration of calcium oxide in the slag
$\bar{\text{CaO}}$	%	Content of CaO in the slag
$\text{CaO}\%_{\text{sol}}$	%	Concentration of CaO in the initial lime which is dissolved
D	cm^2/s	Diffusion coefficient
$\frac{dn_i}{dt}$	mol/s	Number of atoms per unit time
$\frac{dm_i}{dt}$	g/s	Mass of atoms per unit time
D_0	m^2/s	The maximum diffusion coefficient at infinite temperature
D_E	m^2/s	Eddy diffusivity

d	cm^2	Diameter of particle/sample
$\Delta_f G$	$\text{J}\cdot\text{mol}^{-1}$	Gibbs energy of formation
dM	g	Mass of the dissolved substance
$-\frac{d(\text{CaO})}{dt}$	g/s	Mass of CaO consumed
$(-\frac{dM_{\text{sol}}}{dt})$	g/s	Mass of dissolved solid phase in time
dM_{sol}	g	Mass of lime dissolved
d_{prim}	cm^2	Primary diameter of the particle in the beginning of the process
$\Delta(\%\text{MgO})$	$\%$	Difference between the concentration of MgO in the slag phase and its saturation in the slag phase
$\frac{\Delta h}{\Delta \tau}$	cm/s	Linear rate of sample dissolution
E_A	$\text{J}\cdot\text{mol}^{-1}$	The activation energy for reaction
E_D	$\text{J}\cdot\text{mol}^{-1}$	The activation energy for diffusion
J	$\text{kg}\cdot\text{s}^{-1}\cdot\text{m}^{-2}$	Mass flux of the substance
J_x	$\text{kg}\cdot\text{s}^{-1}\cdot\text{m}^{-2}$	Incoming mass flux in the direction x
J_{x+dx}	$\text{kg}\cdot\text{s}^{-1}\cdot\text{m}^{-2}$	Outgoing mass flux from the elementary volume
k_i	cm/s	Mass transfer coefficient
k	J/K	The Boltzmann constant
L	m	Typical length for a system
M	kg	Mass of solid phase at time intervals

M_{sol}	kg	Mass of lime
$M_{sol,prim}$	kg	Mass of initial solid phase
$M_{liq,prim}$	kg	Mass of liquid slag
M_{CaO}	kg	Mass of CaO
N	-	Number of particles
p	N/m ²	Ambient pressure of the system
r	cm ²	The radius of the diffusing particle
R	J · K ⁻¹ mol ⁻¹	Universal gas constant
Re	-	Reynolds number
S	cm ²	Contact surface of sample and slag
Sc	-	Schmidt number
Sh	-	Sherwood number
St	-	Stanton number
T	K	Absolute temperature
t	s	Time
U	m/s	Velocity of the fluid
V	cm ³	Volume
V_i	cm ³	Volume of a single particle
v_r	m/min	Rate of decrease of the radius of solid particle

Greek Letters

π	-	A mathematical constant approximated as 3.14159
ρ	kg/m ³	Density
v	m/s	The mass average velocity
ω_{CaO}	-	Mass fraction of CaO
K_s	-	Shape ratio
ν	m ² /s	Kinematic viscosity
μ	kg/(m·s)	Dynamic viscosity of the fluid
δ	m·10 ⁻⁵	The thickness of interfacial boundary layer
α	-	The empirical constant
β	-	The empirical constant
η	Pa·s	Fluid viscosity

Superscripts, Subscripts

A	Activation
b	Bulk
D	Diffusion
E	Eddy
f	Formation

i	Component i
i	Interfacial
liq	Liquid
liq.prim	Liquid primary
s	Shape
s	Substance
sol	Solid
sol.prim	Solid primary
x	Vector x

Abbreviations

BOF	Basic Oxygen Furnace
BOP	Basic Oxygen Process
Q-BOP	Quick-quiet Basic Oxygen Process
LD slag	Linz-Donawitz (Converter) slag
OBM	Oxygen Blowing Machine or also Oxygen-Bottom-Maxhütte
ASTM	American Society for Testing and Materials
SEM	Scanning Electron Microscope
EDS	Energy-dispersive X-ray spectroscopy
XRF	X-ray fluorescence method of analysis
XRD	X-ray diffraction method of analysis

BN	Boron Nitride
UK	United Kingdom
DRI	Direct reduced iron
Wt%	Weight percent
BET	Brunauer–Emmett–Teller analysis
BJH	Barett-Joyner-Halenda analysis
CFD	Computational Fluid Dynamics

1 Introduction

The aim of the present study is the development of scientific-methodological approach, based on studies of the kinetics of heterogeneous processes in metallurgy, in order to optimize the dissolution of lime in steelmaking slags and ensure the formation of slag of the desired composition since the demand for high quality steel requires effective process control.

The research method applied is the calculation of kinetic characteristics of heterogeneous processes. The method consists of the experimental study of various limes dissolution in steelmaking slags and the choice of the kinetic model that takes into account the complete mass balance of the components. The novelty of this work is the new kinetic data obtained experimentally of various limes and dolomite dissolution in industrial and in model slag systems.

Experimental determination of diffusion characteristics in liquid metal solutions in general, in particular with iron, is followed by many difficulties and there is a very small amount of the experimental studies on the following topic. [1]

T. Deng [2] studied the dissolution mechanism and rate of lime in converter slag. The author investigated lime dissolution under forced convection using a molybdenum rod for stirring purposes. The experimental equipment allowed the system to be quenched at a high temperature. It was revealed that different lime samples had different dissolution rates, and that CaO dissolution in slag had progressed due to the removal of dicalcium silicate layer.

Nobuhiro Maruoka et al. [3] studied the dissolution rate of different limes into the slag. Authors measured the change in the slag composition after the dissolution test. Procedure was carried out using iron rod for stirring slag, iron crucible and Argon gas to flush the system from the bottom up. XRF method was applied to analyze slag samples. It was found that with the following CaO–FeO–SiO₂ slag a dense dicalcium silicate layer occurred on the lime particles and, therefore, lime porosity had low significance for the dissolution rate due to the formation of the reaction layer. However, porous lime tends to dissolve faster than a dense lime due to the filling of lime pores with slag.

Huang Fuxiang et.al. [4] studied the dissolution rate of oxides in the slag and investigated the effect of the interfacial layer on its dissolution rate. They prepared a mixture of oxides to imitate the interfacial layer from sintered reagents. Prepared sample was immersed in a molten slag stirred with Argon gas. It was found that the thickness and constitution of the interfacial layer affect the dissolution rate.

In the study on the dissolution of MgO from flux and BOF refractory, Nobuhiro Maruoka et al. [5] investigated the dissolution rate of MgO. Authors added different oxides containing MgO into the melt and defined the change in the MgO content. They found that solid formation of MgO and FeO occurred at the interface of the FeO–CaO–SiO₂ slag and sintered MgO.

Nikitin et al. [6] studied the kinetics of the interaction of metal and slag in crucibles made of fused MgO at temperature of 1580°C. The primary slag contained 9.8-52 % CaO, 70.4-6.8 % SiO₂, 19.8-41.2 % Al₂O₃. A polarizing method was used: an alternating current of small intensity was applied through the cell, consisting of two liquid metal electrodes and molten slag connecting them. By measuring resistivity of melt, diffusion coefficient of ions in the slag was calculated.

This work was performed to investigate the kinetic characteristics of steelmaking processes. The primary kinetic task is a description of the mechanism and rate of metal impurities oxidation, and solid materials transition in the liquid phase, including lime dissolution in the slag. As a result of mixing in steelmaking process turbulent diffusion coefficients increase, so that in each phase concentrations of components are roughly constant. However, at interfaces in the fixed or unstirred boundary layers, the mass transfer is ensured by molecular diffusion. The transfer of matter from one phase to another is a complex process with a limiting step, which is the molecular diffusion in the slag boundary layer. Determination of molecular diffusion coefficients of lime and dolomite with various amounts of magnesium oxide carried out in this thesis shows the kinetics of slag formation.

An investigation of the kinetic regime of slag formation helps to achieve a desirable composition of slag and, reduces the melting time as well as refractory wear. This generally leads to greater productivity of the steelmaking converter and lowers the cost of steel production.

2 Oxygen Steelmaking fundamentals

The BOF process is a natural successor to the Bessemer converter process. It is a method of primary steelmaking in which molten pig iron rich in carbon at 1400°C is converted to steel at 1650°C by the exothermic oxidation of components dissolved in the iron. The first commercial operation of steelmaking with oxygen top blowing in the converter started in the early 1950s at Linz and Donawitz (Austria). The Basic Oxygen Process has become the most substantial and effective steel making method. It has become the basis of a major process for steel production all over the world and became known as Linz-Donawitz or LD process. The raise of the top-blown basic oxygen converter steel making process has revolutionized steel making industry in the world and is the result of continuous developments over the past years. In 2014 world crude steel production in oxygen blown converters reached 1 229 325 tons. [7] For a long time now, most of the steel has been made by top oxygen blowing. Several improvements took place over time in order to optimize the process. During the period since 1952 the time to complete a heat of steel has been cut from about one hour to less than 30 minutes; meanwhile the size of the charge has increased from 35 net tons to more than 400. Process has various names all over the world, but they all denote top-blown converter steelmaking process. For example, in European steel plants the process is still called LD; in the UK, BOS (basic oxygen steelmaking); in the Far East and America, BOF (basic oxygen furnace), with the exception of U.S. where it is called BOP (basic oxygen process).

In the early 1970s, another but less common - a bottom-blown oxygen steelmaking process was developed in Canada and Germany. This process is known as OBM in Europe and Q-BOP elsewhere. Further progress in oxygen steelmaking led to the present practices of various types of top and bottom blowing. It is known as combined blowing, as illustrated schematically in Figure 2-1 for BOF and Q-BOP processes. The oxygen steelmaking process rapidly refines a charge of molten pig iron and scrap into steel with a desired carbon content and temperature using high purity oxygen. Steel is made in discrete cycles called heats. The furnace or converter is a barrel shaped, open topped, refractory lined vessel that can rotate on a horizontal trunnion axis. [8,9]

The Basic Oxygen Steelmaking process is autogenous or self-sufficient in energy which requires no additional fuel due to the strong exothermic reactions. The charge materials for the basic oxygen process are 70-80% liquid hot metal from the blast furnace and steel scrap which are charged into the Basic Oxygen Furnace (BOF) vessel. Oxygen of greater than 99.9% purity is blown at supersonic velocity, through water cooled copper, multihole lance onto the surface of the mixture of hot metal, scrap and fluxes in the steelmaking vessel. After the oxidation of impurities and at the end of oxygen blowing process the composition of the charge is typically modified as follows [10]:

Hot metal

at 1400°C	4.6 %C	0.7 %Si	0.4 %Mn	0.05 %S	0.08 %P
-----------	--------	---------	---------	---------	---------

Steel

at 1650°C	0.05 %C	Trace Si	0.2 %Mn	0.03 %S	0.01 %P
-----------	---------	----------	---------	---------	---------

The oxidation of carbon and silicon contained in the hot metal is the main heat source due to the strong exothermic reactions. It liberating great quantities of heat and melts the scrap. There are lesser energy contributions from the oxidation of iron, manganese, and phosphorus. The post combustion of carbon monoxide as it exits the vessel also transmits heat back to the bath. The overall purpose of this process is to reduce the carbon from about 4% to less than 1% (usually less than 0.1%), to reduce or control the sulphur and phosphorus, and finally, to raise the temperature of the liquid steel made from scrap and liquid hot metal to approximately 1635°C.

The required quantities of hot metal, scrap, oxygen, and fluxes vary according to their chemical compositions and temperatures, and to the desired chemistry and temperature of the steel to be tapped. Fluxes are added early in the oxygen blow, to control sulphur and phosphorous and to limit erosion of the furnace refractory lining. Input process parameters such as analysed data (hot metal, scrap, flux and alloy) and measured data (weighing and temperature) lead to the chemical, thermal and time variations of the process. The principal elements are iron, silicon, carbon, manganese and phosphorous. The liquid pig iron or hot metal provides almost all of the silicon, carbon, manganese and phosphorous, and lesser amounts are contained in the scrap. Both the high temperatures of the liquid pig iron and the intense stirring provided when the oxygen jet is introduced, contribute to the fast oxidation (burning or combustion) of these elements and a resultant rapid, large energy release. Silicon, manganese, iron and phosphorous form oxides which in combination with the fluxes create a liquid slag. The vigorous stirring provides a rapid reaction and enables the transfer of energy to the slag and steel bath. Carbon, when oxidized, leaves the process in gaseous form, principally as carbon monoxide. During the blow, the slag, reaction gases and steel (as tiny droplets) make up a foamy emulsion. The large surface area of the steel droplets, in contact with the slag, at high temperatures allow quick reactions and rapid mass transfer of elements from metal and gas phases to the slag. At the end of the process the slag floats on top of the steel bath.

The product of the BOF is molten crude steel with a specified chemical composition. From here it undergo further refining in a secondary refining process and after that it is sent to the continuous caster where it is solidified into semi-finished shapes: blooms, billets, or slabs. [11]

2.1 Types of Oxygen Steelmaking Processes

There are three primary ways in the Oxygen Steelmaking process in which oxygen can be supplied to the vessel. In the 70's the most common was the top-blown converter (BOF). In the BOF all of the oxygen is introduced via a water-cooled lance

the end of which has three to six special nozzles that allow the gas blow at supersonic velocities. In top blowing, the stirring is ensured by supersonic jets which create the necessary slag emulsion and vigorous bath stirring and provide the rapid reactions. The lance is positioned above the furnace and lowered into it. When the lance is lowered into the furnace oxygen starts blowing. Slag forming fluxes are charged from above the furnace via a chute in the waste gas hood. [12]

By 1978, the bottom-blown oxygen process appeared as a new technology with specific metallurgical advantages. By this time, this process had been applied in some greenfield installations and in some conversions from the open hearth steelmaking process. In the bottom-blown converters (OBM or Q-BOP), oxygen is introduced through the bottom via several tuyeres which consist of two pipes with the oxygen passing through the center pipe and a coolant hydrocarbon passing through the annulus between the pipes (see Figure 2-1). To cool the tuyere methane (natural gas) or propane is used. The coolant chemically decomposes when introduced at high temperatures and absorbs heat. It is protecting the tuyere from overheating by formation a mushroom shaped deposition of porous carbon. In bottom blowing, all of the oxygen is introduced through the bottom, and passes through the bath and slag, creating intensive bath stirring and formation of a slag emulsion. Powdered fluxes are added into the bath through the tuyeres located in the bottom of the furnace. [9]

Combination-blown processes emerged, mainly by modification of existing top-blown or bottom-blown oxygen steelmaking processes. This came about because of the desire to approach the metallurgical advantages of bottom-blowing without abandoning the advantages of top-blowing. The combination blowing or top and bottom blowing, or mixed blowing process is characterized by both a top blowing lance and a bottom stirring. One general class of combination-blown processes utilizes oxygen through a top lance, and an inert gas through tuyeres or permeable elements in the furnace bottom to stir the bath. A second class of combined blowing processes utilizes some of the oxygen through a top lance or tuyeres mounted in the top cone of the vessel, and the balance of the oxygen through Q-BOP type tuyeres mounted in the vessel bottom. These processes generally can also switch the bottom gas from oxygen to argon or nitrogen for stirring purposes.

The plant layout and main sequence of operation are similar for the different processes. The major differences between the processes are in the design of the furnace and the equipment for introducing the oxygen and fluxes, and also the main refining steps. The methods of controlling the different processes are similar. [9,13]

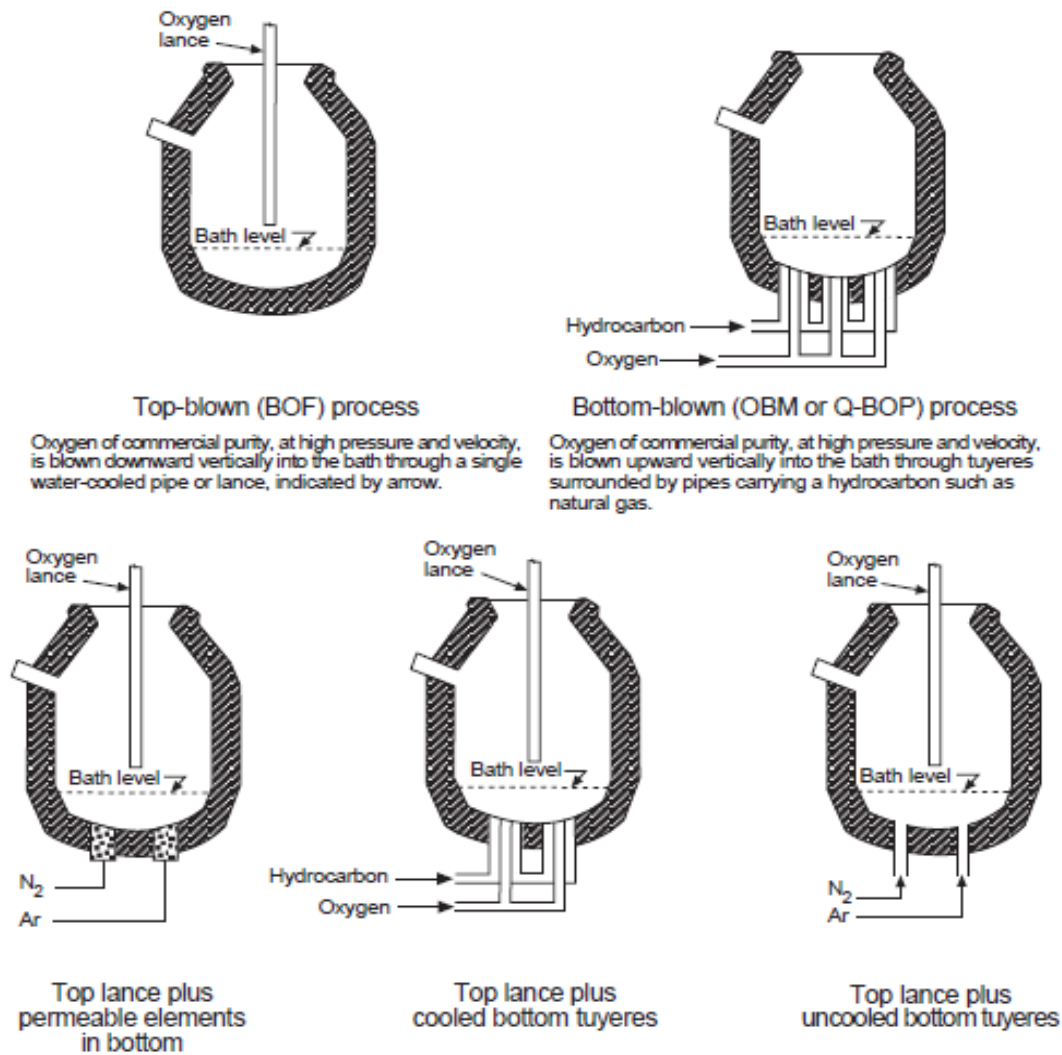


Figure 2-1: BOF and Q-BOP steelmaking with and without combined blowing [12]

2.2 Basic Oxygen furnace structure

The Basic Oxygen Furnace (BOF) is presented on Figure 2-2. It consists of a vertical vessel lined with refractory lining, vessel protective slag shields, the trunnion ring, a vessel suspension system supporting the vessel within the trunnion ring, trunnion pins and support bearings, and the oxygen lance.

BOF installation consists of the basic oxygen furnace, furnace support foundation, furnace tilt drive and controls, furnace water cooling system, fume exhaust and cleaning system, oxygen injection system, auxiliary furnace bottom stirring system, process additives system, scrap and hot metal charging system, molten steel delivery and slag disposal system and other steelmaking requirements such as sampling, refractory inspection and relining systems, computers, etc.

The BOF vessel has a spherical bottom, cylindrical shell and upper cone and is equipped with: rotating device that allows proper positioning of the vessel, lance carriage to keep the water-cooled lance in the vertical position, nose cone section through which the gases exit, tap hole for draining metal/slag, overhead bins for adding iron ore, fluxes, slag-forming agents, etc. as required during the blow.

The vessel is attached to a supporting ring equipped with trunnions. The supporting ring provides stable position of the vessel during oxygen blowing. The converter is capable to rotate about its horizontal axis on trunnions driven by electric motors. This rotation is necessary for charging raw materials, sampling the melt and pouring the steel out of the converter.

Only 8-12% of the furnace volume is filled with the treated molten metal. The bath depth is about 1.2-1.9 m. The typical capacity of the Basic Oxygen Furnace is 250-400 t. The top blown basic oxygen furnace is equipped with the water cooled oxygen for blowing oxygen into the melt through 4-6 nozzles. The oxygen pressure is about 1-1.5 MPa. Service life of oxygen lance is about 400 heats. The bottom blown basic oxygen furnace is equipped with 15-20 tuyeres for injection of oxygen (or oxygen with lime powder). The tuyeres are cooled by either hydrocarbon gas (propane, methane) or oil supplied to the outer jacket of the tube. [12,13]

The refractory lining in the converter vessel usually consists of a safety layer and a working layer. Working lining degrades after each campaign that can normally last between 3000 and 10,000 heats. When the campaign is longer, magnesite carbon refractories are used instead of the normal pitch-bonded dolomite or pitch impregnated fired magnesite. Magnesia based refractory lining are used for Basic Oxygen Furnace due to their high corrosion resistance and excellent high temperature strength. However, even these linings undergo degradation due to mechanical abrasion and chemical reactions with the liquid slags at high temperatures. After each campaign, the degraded lining is mechanically removed. Once relining is completed, the converter is ready for use. The whole relining procedure can take up to 4-5 days. [9,12]

From 1980s, refractory lining technology has been improved significantly as well as entire converter campaign. The refractory cost per ton of steel has been reduced, but also the downtime. One of the major improvements that have been done is called slag splashing. In order to prolong the lining life the residual slag from the previous heat is used as a coating on the refractory lining before the next heat is charged. Using high pressure gas molten slag is forced to the upper part of the vessel where it connects to the converter working lining. This significantly decreases the amount of refractories that are exposed to the refining reactions, and reduces the refractory wear. However, the upper sidewalls of the converter which were not covered with the molten slag are under intensive slag attack in the subsequent heat, due to temperature variations between two heats.

Even though all BOF vessels have a very large inner volume, the converter contents often overflow through the tap hole or get ejected through the mouth opening. This is referred to as spitting (for metal droplets) or slopping (for slag-metal emulsion). Therefore the bath depth is an important parameter. With increasing wear

of the lining, the bath depth can vary substantially, and in the most shops the depth is measured by lance equipment every 8 hours. In combined blown BOF vessels the usual problem is local wear of the refractory components at the converter bottom itself due to bottom blowing through tuyeres and the resultant bath agitation. Such refractory wear and erosion of the converter components is caused by turbulent flow of molten metal and thermal stress caused by the passage of cold gases. In such cases pitch bonded impregnated magnesite carbon based upon fused magnesia with high density and low porosity is used in the corroded part of the vessel. [9,12]

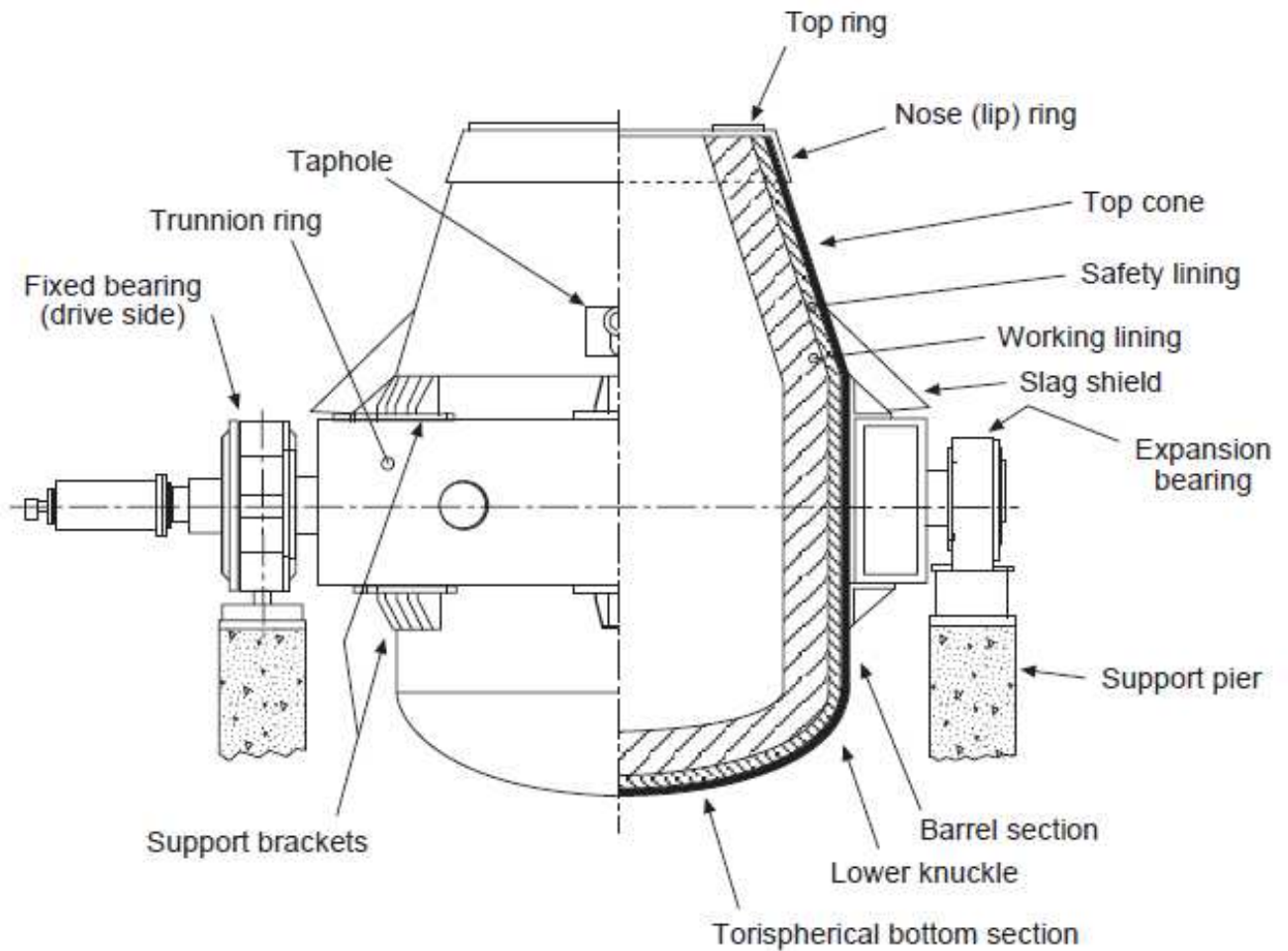


Figure 2-2: Schematic section of the BOF [12]

2.3 The Lance

In BOF steelmaking, oxygen of high purity (at least 99.9% oxygen) is blown at supersonic velocity onto the surface of the bath using a vertical lance, inserted through the mouth of the vessel. In the past during the development of the process only single-hole lances were used. Under the influence of growing industry the vessel size has increased and multi-hole lances went into operation so that large volumes of oxygen (typically 1000-1200 Nm³/min. for 160-180 t converters) can be blown within the restricted blowing time of 15-20 minutes. Due to the bigger amount of holes the total jet energy gets dispersed along the diameter of the vessel which reduces the chances

of any individual oxygen jet penetrating anywhere near the vessel bottom. As the result of such development high productivity of the process has been achieved as larger amount of liquid metal is exposed to oxygen. Furthermore, the larger the number of holes in the lance, the faster will be the slag-metal reactions like dephosphorization. Such reactions can then take place at a greater number of reaction sites. [9,11]

2.4 Sublance Equipment

Modern BOF shops are equipped with sublances. It is an important tool in basic oxygen steelmaking which allows assessment of the liquid steel while the converter is still in its vertical position and without interrupting the blow. A sublance is used for performing measurements and taking samples in a metallurgical furnace. Sublances are supplied by number of companies through all over the world such as Danieli Corus (Netherlands, India, China), Primetals Technologies (Austria) etc.

The use of sublances leads to increased plant output, reduces tap-to-tap time and rate of overblows or reblows, prolongs refractory lining life, avoids converter titling and provides information on bath temperature, carbon content, oxygen activity and bath level as automated measuring and sampling. The purpose of a sublance is also to measure bath level and to secure a steel sample in an oxygen steelmaking vessel while in the upright position. Such sublance systems employ mechanical and electrical devices to perform measuring and monitoring functions, and to provide a steel sample for spectrographic analysis. [14]

During the heat cycle, after a predetermined amount of oxygen has been blown, the oxygen blow rate is reduced and an in-blow test is made by lowering the sublance at a controlled speed through the hood opening. The sublance is stopped at the test elevation below the bath surface. This test elevation is fixed and is regulated from heat to heat by the process computer to compensate for lining wear throughout the campaign. All pertinent data gathered is transmitted to process computers for adjustments to the oxygen blow cycle and coolant additions to finish the heat at the tap carbon and temperature aims. After the blow cycle is completed, the sublance is lowered to the test elevation to measure the finished tap carbon and temperature and to retrieve a metal sample for spectrographic analysis. The metal sample may then be sent via pneumatic tube transport to the laboratory. [15]

2.5 Steelmaking Operation

In the BOF, hot metal containing carbon ranging from 4.0% to 4.5%, 0.4% to 1.5% silicon, manganese varying from 0.15% to 1.5% (sometimes even more), 0.045% to 2.5% phosphorus (normally between 0.060% and 0.250%), and sulphur 0.150% maximum (normally 0.050-0.080%) is refined. In the steelmaking process, all these impurities are removed virtually to zero levels so that steel of the desired composition can be

produced. When the hot metal temperature and chemical analysis are known, a computer determines the optimum proportions of scrap and hot metal, flux additions, lance height and oxygen blowing time. The basic operational steps of the BOF presented on the Figure 2-3.

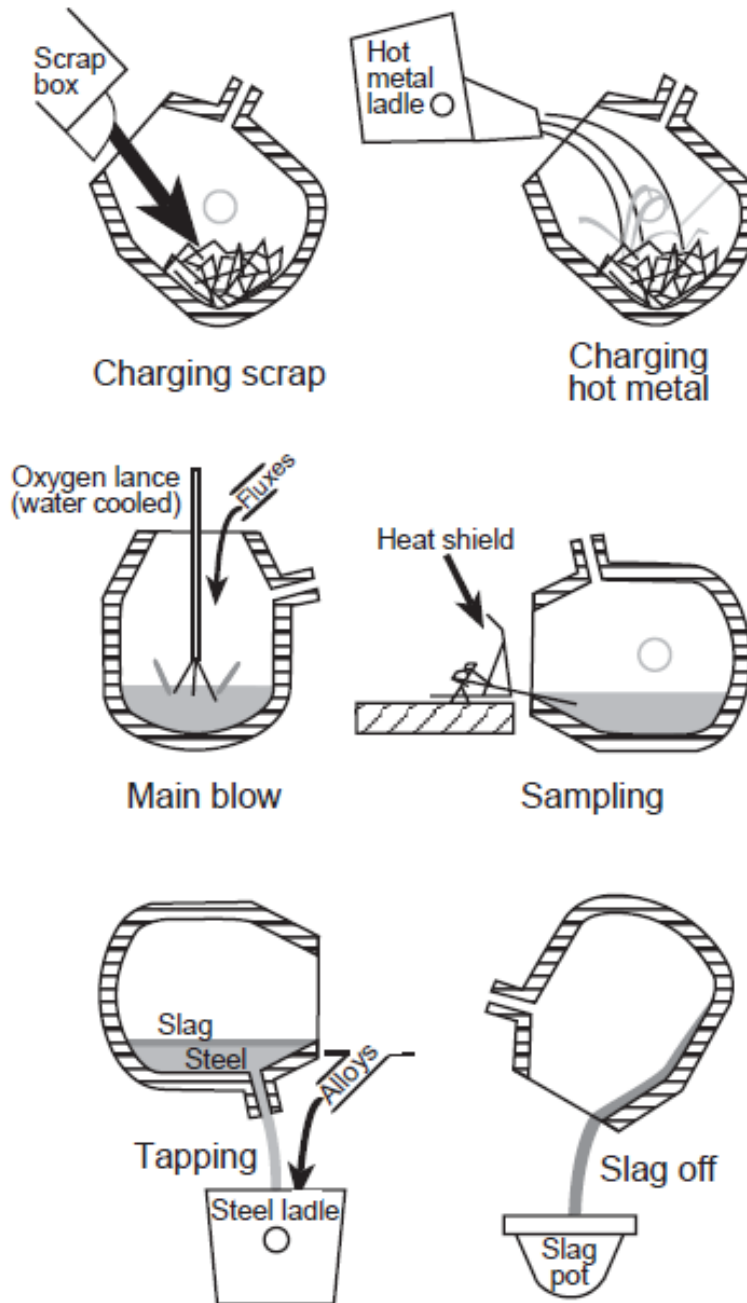


Figure 2-3: Schematic of operational steps in oxygen steelmaking process (BOF) [13]

The tap-to-tap time of each BOF heat is usually around 30 minutes and is typically consist of the following steps: [13]

1. Scrap charging

Scrap charging begins when the BOF vessel is tilted about 45 degrees towards the charging aisle. The charge is usually about 25 to 30% of the total charge weight dumped from a charging box into the mouth of the cylindrical BOF. Sometimes in order to accelerate the slag forming a part of lime is charged together with scrap.

2. Metal pouring

The hot metal from a transfer ladle is immediately poured directly onto the scrap in the converter using a charging crane with the vessel inclined towards the charging side. Fumes and kish (graphite flakes from the carbon saturated hot metal) are emitted from the vessel's mouth and collected by the pollution control system. Pouring takes 2-3 minutes.

3. Blowing

Then the vessel is rotated back to the vertical position and lime/dolomite fluxes are dropped onto the charge from overhead bins while the lance is lowered down to the vessel and the blowing process starts (flow rate 550-600 Nm³/min. for a 160-180t converter) for around 15-20 minutes. The lance is water-cooled with a multi-hole copper tip. Through this lance, oxygen of greater than 99.5% purity is blown into the mix. If the oxygen is lower in purity, nitrogen levels at tap become unacceptable.

4. Flux addition

After the oxygen is turned on, flux additions are started and are usually completed at the end of the second batch of oxygen. The fluxes are used to control the slag chemistry as well as sulfur and phosphorus levels in the steel. The principle active ingredients from the fluxes are CaO (from burnt lime) and MgO (from dolomitic lime). The CaO component is used to control sulphur and phosphorous. The dolomitic lime is used to saturate the slag with MgO in order to minimize the refractory wear in the furnace. Steelmaking slags without it are very corrosive to the lining. The corrosion rate is reduced dramatically when MgO is added to saturate the slag and it is much cheaper to saturate the slag with MgO from dolomitic lime than by dissolving it from the lining.

Another flux addition sometimes used in high carbon heats is fluorspar (CaF₂, or spar). This mineral is charged to dissolve the lime and to reduce the viscosity of the slag. However in the modern practice in many shops fluorspar is avoided due to its high corrosive effect on refractory linings. Furthermore, it causes significant fluoride emissions and serious pollution.

Coolants are also important additions charged at about the same time as fluxes. There are several types of coolants. Iron ore, either lump or pellets, are the most common type. Ore (iron oxide) should be added as soon as possible to achieve early lime dissolution.

5. Oxidation

As blowing begins, silicon from the hot metal is oxidized forming silica (SiO₂), which reacts with the basic fluxes to form a molten slag. The gas is primarily carbon

monoxide (CO) from the oxidation of carbon in the hot metal. These two oxidation reactions are strong exothermal reactions which produce enough heat to melt the scrap. Basic slag is forming due to the oxidation of hot metal impurities (SiO_2 , MnO , FeO , Fe_2O_3) and fluxes dissolution. Phosphorus and sulfur are removed into the slag. The rate of gas evolution is many times the volume of the vessel and it is common to see slag slopping over the lip of the vessel, especially if the slag is too viscous.

6. Sampling and testing

Blowing continues for a predetermined time based on the metallic charge chemistry and the melt specification. It takes normally 15 to 20 minutes, and the lance is generally preprogrammed to move to different heights during the blowing period. The lance is then raised and the vessel turned down towards the charging aisle for sampling and temperature tests. Temperature is measured by thermocouple. Blowing stops when carbon and phosphorus content in the steel reduced to certain level for certain steel type. Sublance is used for sampling and bath temperature measurements without interrupting the blow.

7. Tapping

Once the steel is ready for tapping the vessel is rotated it to the opposite side so that steel flows through the tap-hole in the nose portion of the vessel into a ladle. The preheated ladle is positioned in the ladle car under the furnace. When Steel flows from the tap-hole, ferroalloys, deoxidizing and desulfurizing agents are added to the molten steel in the ladle. During tapping of steel, simultaneous outflow of slag occurs. Slag has a strong oxidizing power and reoxidizes the molten steel. To prevent slag from flowing into the ladle to the maximum possible extent, pneumatic slag stopper arrangements are used at the tap hole, or different slag arresting devices are introduced into the converter like refractory darts, which are heavier than slag but lighter than steel. A number of new slag stopper technologies are introduced today by steelmaking companies.

8. Slag off (De-slagging)

After tapping steel into the ladle, and turning the vessel upside down and tapping the remaining slag into the "slag pot", the vessel is returned to the upright position. Tapping of slag takes 2-3 minutes. Sometimes slag is blown with nitrogen to coat the barrel areas of the vessel. This process is known as "slag splashing". At the end of process gunning with refractory materials in high wear areas may also be necessary. After maintenance is complete the vessel is ready to receive the next charge. The whole production cycle takes up to 40-50 minutes. In the Table 2-5 the duration of the process phases is presented.

The CO gas generated during blowing and dust (20 kg/tons liquid steel), are sent to the gas-cleaning plant before it is stored. [13,16]

Table 2-1: The duration of Basic Oxygen Steelmaking process stages [16]

Process stage	Time, min.	Description
Charging scrap and hot metal	5-10	Scrap at ambient temperature, hot metal at 1340°C
Blowing oxygen	14-23	Oxygen reacts with elements, Si, C, Fe, Mn, P in scrap and hot metal and flux additions to form a slag
Sampling-Chemical testing	4-15	Steel at 1650°C, chemistry and temperature
Tapping	4-8	Steel is poured from furnace into a ladle, typical size = 250 tons
Pouring slag off	3-9	Most slag is removed from furnace, in some shops slag is used to coat furnace walls

2.6 Raw materials

1. Hot metal

Hot metal is a blast furnace liquid iron combined with number of other chemical elements, the most common of which are carbon, silicon, manganese, phosphorus, and sulphur. Its quality is of primary importance in BOF steelmaking as well as its temperature. The hot metal temperature has to be high enough to permit easy transfer from the torpedo ladles to the transfer ladle, efficient pre-treatment without giving rise to problems like skull formation on the injection lance, smooth charging into the BOF, etc. From the blast furnace hot metal is transported either to a desulfurization station or directly to the BOF in torpedo cars or ladles. The hot metal chemistry depends significantly on how the blast furnace is operated and what iron-bearing materials are charged to it. The chemistry of hot metal can vary depending on the shop, but typically it contains about 4.0–4.5% carbon, 0.3–1.5% silicon, 0.25–2.2% manganese, 0.04–0.20% phosphorus and 0.03–0.08% sulfur (before hot metal desulfurization). The sulfur level in desulfurized hot metal can be as low as 0.001%. Blast furnace practice affects the composition of hot metal. With colder blast furnace practices usually there is a decrease in the silicon content and an increase in the sulfur in the hot metal and phosphorus contents of the hot metal increases if the BOF slag is recycled at the sinter plant. Carbon and silicon provide the most of energy. The bigger amount of scrap can be charged if the hot metal silicon is high and hence generate bigger amount of heat due to its oxidation. Hot metal silicon also affects the slag volume, and therefore the lime consumption and resultant iron yield. [17]

2. Scrap

In autogenous BOF operation scrap melting requires the most of heat. It is one of the most important and costly components of the charge. Steel scrap comes in many forms. The most common is scarp produced at the plant or so called "home scrap". Scrap is a large source of iron in the steelmaking operation after hot metal. Biggest part of scarp produced is recycled iron or steel products right from the mill (e.g. slab crops, pit scrap, cold iron or home scrap). It can also be purchased from an outside source. Scrap also can be in many sizes and has different chemical analyses and a variety of prices. Hence, the purchase and melting of scrap a very complex issue. For example, if scrap comes in very large pieces it is difficult to melt it and may also damage the vessel when charged. Some scrap may contain oil or hazardous elements. Obsolete scrap may contain a variety of other objects which could be hazardous or explosive. Obviously the chemical analysis of obsolete scrap is imprecise. When scrap is loaded in the scrap box it is being weighed and the crane operator loads the box according to the weight and requirements of the upcoming heat. Then the box is transported to the BOF. It is important to load the correct amounts and types of scrap (the scrap mix) as indicated by the computer or a fixed schedule. Otherwise the process of the heat will be affected. The light pieces of scarp must be loaded in the front prior the big pieces to protect the refractory lining and minimize the damage. Also, since heavy scrap is more difficult to melt than light scrap, it is preferable that it sits on top so that it is closest to the area of oxygen jet and melts faster. Scrap pieces that are too large to be charged into the furnace are cut into smaller pieces by means of shears or flame cutting. Thin, small pieces of scarp are compressed into block like bundles called bales using special hydraulic presses. Normally, larger, heavier pieces of scrap are more difficult to melt than lighter, smaller ones. It is better to avoid unmelted scrap as it can cause significant problems in the process like excessively high temperatures or missed chemistries at blow end. Bottom or mixed blowing, which can significantly enhance the mixing characteristics in the furnace, improves scrap melting of larger pieces. Since scrap contains various elements the removal of some of them may also be a problem in the steelmaking. Elements, such as copper, molybdenum, tin and nickel cannot be oxidized and hence cannot be removed by NaOH. Elements such as aluminum, silicon and zirconium can be fully oxidized from scrap and become included into the slag. Elements which fall in the middle category in terms of their tendency to react, such as phosphorus, manganese and chromium distribute themselves between the metal and slag. Most steelmaking shops typically use about 20 to 35% of their total metallic charge as scrap, with the exact amount depending on the steelmaking process. Scrap selection is very complicated and depends on the steel products. Deep drawing steels limit the maximum residual (%Cu +%Sn + %Ni +%Cr +%Mo) content to less than 0.13%, while other products allow this to range as high as 0.80%. [13,16]

3. Fluxes

Fluxes play a very important role in steelmaking process. First they combine with SiO_2 which is oxidized from the hot metal to form a "basic" slag. The forming oxides, sulphur and phosphorus from the hot metal are removed to the slag. The fluxes added to the process strongly depend on the hot metal silicon, the weight of hot metal, the lime to silica ratio ($\% \text{CaO} / \% \text{SiO}_2$), and the amount of MgO needed in the slag to avoid the damage of furnace refractories. In the process a basic slag is desired, therefore, the lime to silica ratio should range from two to four. The consumed amount of fluxes depends on the hot metal silicon, the proportion of hot metal to scrap, the initial (hot metal) and final (steel) sulphur and phosphorus contents.

Lime (burnt limestone) (95+% CaO) and dolomitic lime (burnt dolomite) (58% CaO, 39% MgO) are the two major fluxes in steelmaking. They are produced by calcining the carbonate minerals CaCO_3 and MgCO_3 . The calcining reaction generates CO_2 gas leaving CaO or MgO. There are "soft" and "hard"- burned limes available for the process. Soft burned fluxes form slag more quickly than hard-burned. In the short blowing cycle, this is critical for effective sulphur and phosphorus removal. The MgO addition is designed to be about 8 to 10% of the final slag weight to saturate the slag with MgO and reduces dissolution of the MgO vessel lining. Lime quality is also of a great importance in the BOF process, when big amount of lime is charged into the BOF within a short period of time. Lime quality is important to ensure its rapid dissolution in the slag. Usually, small limes with high porosity have higher reactivity and provide rapid slag formation due to the slag penetration in the pores. The most common quality problems with either burnt or dolomitic lime are uncalcined inner parts, excess fines and too low a reactivity (calcined too hot or too long). In some BOF operations lumpy dolomite is added directly into the furnace as a coolant as well as a source of MgO to saturate the slag.

Calcium fluoride or fluorspar (CaF_2) is also sometimes used in the BOF steelmaking. However in the most shops it is avoided due to serious pollution and health hazards. It increases slag fluidity and enhance lime dissolution in slag by dissolving the dicalcium silicate ($2\text{CaO} \cdot \text{SiO}_2$) layer formed around the lime particles which prevents the dissolution of the lime.

4. Coolants

Limestone, scrap, and iron ore are all potential coolants that are used in the case of excessively hot heat that has been overblown. The economics and handling facilities dictate the selection at each shop. Varieties of limestone (calcium and/or magnesium carbonates) are often used but the cooling effects are less than from ores. Some shops use DRI which cools 10% more efficiently than scrap for the same weight. The coolant amounts are calculated by the computer.

5. Alloys

The common alloys are ferromanganese, silicomanganese, and ferrosilicon. Aluminum can be added. Sulfur, carbon, calcium, and special elements like boron and titanium are fed at the ladle furnace as powders. [13]

6. Oxygen

Oxygen is also an important in BOF steelmaking and its quality should be emphasized. The minimum purity of oxygen to allow the production of the full range of carbon steel products should be 99.9%. The final turndown nitrogen and hydrogen contents of steel are dependent not only on the amounts of these elements present in hot metal/fluxes, but also on oxygen. [9,11,13]

2.7 Refractories

Nowadays most of refractories for oxygen steelmaking vessels is magnesia (MgO), obtained from minerals or seawater. Magnesia is produced from magnesium hydroxide $Mg(OH)_2$. Obtained calcined magnesia is then briquetted or pelletized for firing into dense refractory-grade magnesia, usually in shaft kilns under high temperatures around 2000°C. Magnesia based refractories have high corrosion and temperature resistance. Magnesia quality is of a great importance. The impurity levels should be as low as possible to achieve the desired strength of the brick. High purity is quite important because MgO has high refractoriness and good resistance to basic slags. All refractories are very expensive, and any failure in the refractories leads to a great loss of production time, equipment, energy consumption and the product quality. Refractories are generally subdivided into 3 groups: acid, basic, and neutral. Acid refractories should not be used in contact with basic slags, gases or fumes. Basic refractories are the best for a basic chemical environment. [18,19]

A high CaO/SiO₂ ratio, preferably 2:1 or slightly higher, is optimum for maintaining high refractoriness in magnesia. High density reduces infiltration and dissociation of magnesia grain by slag. Material with big crystallite size, like fused magnesia, has less surface area for slag attack.

Refractories are subjected to a variety of slag conditions under aggressive atmosphere. Slag basicity can vary from 2 to 4 during refining reactions. The iron oxide (FeO) content of the bath increases with blowing time especially as the carbon in the steel falls below 0.2 % and Fe is oxidized. Although all refractory materials are dissolved by FeO and MgO forms a solid solution with FeO, meaning they coexist as solids within a certain temperature range. The high concentrations of FeO formed late in the blow oxidize the carbon in the brick.

In some cases the refractoriness can be increased by sintering bricks made from pure MgO grains at a high temperature and then impregnating them with tar under a vacuum. However, many shops avoid this practice for environmental reasons and these materials are no longer used in oxygen steelmaking. Today's working lining

refractories are primarily resin-bonded magnesia-carbon bricks made with high quality sintered magnesite and high purity flake graphite. Resin-bonded brick are unfired and contain 5% to 25% high purity flake graphite and one or more powdered metals. Further refinements include using additional grains in the mix. Small additions of metal additives (Si, Al, and Mg) protect the graphite from oxidation because they are preferentially oxidized. Metallic carbides, nitrides, and magnesium-aluminate spinel add strength and resistance to slag attack. Manufacturing processes as well as purity and crystal sizes of the starting ingredients affect the refractory quality up to a great extent. For extra corrosion resistance up to 15% high purity graphite can be added to MgO refractories but more than 15% can result in the lower density of the brick. [13,19,20]

2.8 Environmental issues

The BOS is characterized by several pollution sources and require emission control equipment. Environmental challenges at BOS shops include: the capture and removal of contaminants in the hot and dirty primary off-gas from the converter; secondary emissions associated with charging and tapping the furnaces; control of emissions from ancillary operations such as hot metal transfer, desulfurization, or ladle metallurgy operations; the recycling and disposal of collected oxide dusts; and the disposition of slag. Thus, compliance to emission standards is an important design and operating cost factor for the operation. [20]

3 Thermodynamic for oxygen steelmaking

In steelmaking the impurities in hot metal like carbon, silicon, manganese, phosphorus and sulphur are refined through oxidation and slag formation to produce steel of desired chemistry and cleanliness. For this purpose oxygen is supplied and slag of desired chemistry is formed. When oxygen is supplied, oxidation of all impurities of hot metal including iron begins simultaneously.

The reactions occurring in iron - and steelmaking processes are essentially reduction and oxidation reactions. In the blast furnace, iron oxides are reduced to metallic iron saturated with carbon. The hot metal produced also contains a number of other impurities, e.g. Si, S, P, Mn, which together with carbon are removed by oxidation during the steelmaking operation. The steel thus produced is invariably overoxidized and, therefore, the final adjustments to the composition of the steel are made by adding suitable deoxidizers and alloying elements to satisfy the specifications requested by the steel users. The basic oxygen furnace needs no additional fuel. The pig iron impurities (carbon, silicon, manganese and phosphorous) serve as fuel. Iron and its impurities oxidize evolving heat necessary for the process. In the oxygen steelmaking process, elements such as carbon (C), silicon (Si), and manganese (Mn) dissolved in the hot metal are removed by oxidation to produce liquid steel.

Hot metal and scrap are charged into the furnace and high-purity oxygen gas is injected at high flow rates, through a lance to react with the metal bath. The products of oxidation reactions are CO, CO₂, SiO₂, MnO, and iron oxides. Most of these oxides formed during the blow (16-25 min) are dissolved with the fluxes added to the furnace, such as lime (CaO), to form a liquid slag to remove sulfur (S) and phosphorus (P) from the metal. The gaseous oxides, composed of about 90% CO and 10% CO₂, exit the furnace carrying small amounts of iron oxide and lime dust. The rate of oxygen injection is limited either by the capacity of the hood and gas cleaning system or by the available oxygen pressure. When oxygen is injected onto the metal bath a tremendous amount of gas is evolved forming an emulsion with the liquid slag and with metal droplets. This gas-metal-slag emulsion generates large surface areas that increase the rates of the refining reactions. [21–23]

3.1 Refining Reactions in BOF Steelmaking

Carbon oxidation

Decarburization is the most extensive and important reaction during oxygen steelmaking. About 4.5 wt% Carbon in the hot metal is oxidized to CO and CO₂ during the oxygen blow, and steel with less than 0.1 wt% carbon is produced. Carbon oxidation is complex and expressed by following reactions in metal (left column) and in slag (right column) [22,23]:



The resulting reaction is:



Silicon Oxidation

Almost all silicon is removed early in the blow due to the strong affinity of oxygen for silicon. The Si dissolved in the hot metal (0.25–1.3 wt.%) is oxidized to very low levels (<0.005 wt.%) in the first three to five minutes of the blow. The oxidation of Si to silica (SiO₂) is exothermic producing significant amounts of heat which raises the temperature of the bath. It also forms a silicate slag that reacts with the added lime (CaO) and dolomitic lime (MgO) to form the basic steelmaking slag. The content of Si in the hot metal is very important because it oxidizes nearly completely and produces the major amount of heat. It strongly affects the amount of scrap that can be melted. It also determines the slag volume and consequently affects the iron yield and dephosphorization of the metal.



Manganese Oxidation

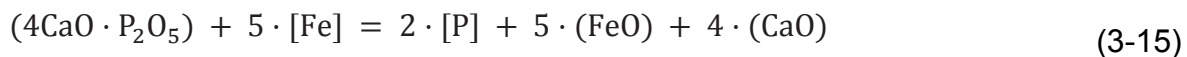
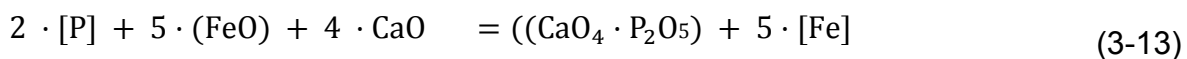
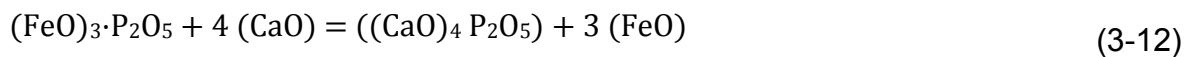
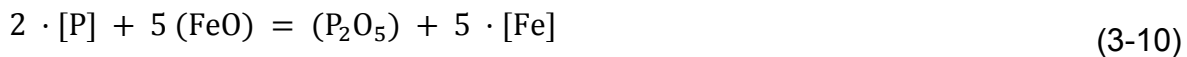
In top-blown processes Mn is oxidized to MnO early in the blow and after most of the silicon has been oxidized, the Mn reverts into the metal. Finally, towards the end

of the blow, the Mn in the metal decreases, as more oxygen is available for its oxidation.



Phosphorus Oxidation

Dephosphorization is due to the oxidizing conditions in the furnace. Phosphorus removal is favoured by low temperatures, high slag basicity (high CaO/SiO₂ ratio), high slag FeO, high slag fluidity, and good stirring. Stirring improves slag-metal mixing, which increases the rate of dephosphorization. Good stirring with additions of fluxing agents, such as fluorspar, also improves dephosphorization by increasing the dissolution of lime, resulting in a highly basic and fluid liquid slag.



Sulfur Reaction

The BOF is not very effective for sulfur removal due to its highly oxidizing conditions. In the BOF, about 10 to 20% of sulfur in the metal reacts directly with oxygen to form gaseous SO₂. The rest of the sulfur is removed by the following slag-metal reaction:



Sulfur removal by the slag is favored by high slag basicities (high CaO/SiO₂ ratio), and low FeO contents. The final sulfur content of steel is also affected by the sulfur contained in the furnace charge materials, such as hot metal and scrap. The sulfur content in the hot metal supplied from the blast furnace generally ranges from 0.020 to 0.040 wt.%, and if the hot metal is desulfurized before steelmaking the sulfur content in the hot metal can be as low as 0.001 wt.%. [23]

Other Elements

In the steel scrap the following elements can present: V, Ti, Cr, Pb, Zn, Hg etc. All elements in the steel scrap can be subdivided into 4 groups: 1. Elements which fully transfer in the slag phase: Si, Al, Ti, Zr, B. etc. V and W almost totally transfer to the slag phase. 2. Elements which are distributed between metal and slag: Mn, P, S, Cr. 3. Elements which totally dissolve in the steel: Cu, Ni, Sn, Mo, Co, As, Sb. 4. Elements which transfer as gaseous substance: Cd, Zn, Hg, Pb.

Under standard conditions the strength of the element-oxygen affinity decreases at 1600°C in the following order for first group of elements: Be, Ca, Mg, Al, Ti, C, Si, V, B, Mn, Cr, Fe. For the second –third group of elements: W, Mo, Co, Ni, Cu, As.

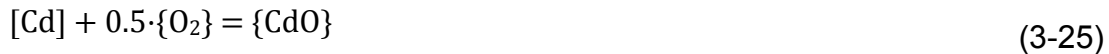
Elements of first group (from Be to Cr) have a stronger affinity to oxygen than Fe. Therefore in the converter where iron presents in metallic form, elements of first group easily oxidize and elements of third group almost do not oxidize [24]:



Cr, Ti and V react according to the reactions above. Ti is used as alloying element. Zr reacts according to the following reaction:



Cd, Zn, Pb, Hg – elements which are exit the slag and steel in the gaseous form as volatile oxides:



3.2 Slag Formation in BOF Steelmaking

The molten iron from the blast furnace process is saturated with graphite and contains undesirable amounts of impurities: silicon, manganese, phosphorus and sulphur which have to be removed during refining operation. With the exception of sulphur, the removal of these impurities is carried out by oxidation and solution of the oxides in the slag. To generate a slag with the desired chemical composition fluxes are charged into the furnace as the blow starts. The rate of assimilation of fluxes and slag and its interaction strongly affects the slag-metal reactions during the blow. Therefore, it is important to control the evolution of slag. The initial slag is rich in SiO₂ and FeO. In the first part of the process the lance is kept above the bath surface, at about 3.5 m. and large amounts of fluxes such as burnt lime and dolomitic lime are dropped into the furnace. The lance is then lowered and the slag starts to form due to the simultaneous oxidation of elements and CO generation. Also, as the blow starts, the CaO dissolution in the slag progresses and the slag mass increases.

Finally, after three quarters of the blow, the FeO content in the slag increases because of a decrease in the rate of decarburization. BOF slag consists primarily of calcium silicates together with oxides and compounds of iron, manganese, alumina and other trace elements. The chemical composition of BOF slag depends on the type of steel being produced (i.e. high, ordinary or low sulfur steel), fluxes and raw materials used (i.e. lime or dolomitic lime) and on the final products requirements. A typical chemical analysis on processed BOF slag aggregate is: 42-44% CaO, 27-31% Fe total, 10-12% SiO₂, 5-6% MgO, 3-4% Mn total, 1-2% P₂O₅, 1-2% Al₂O₃, 0.5% TiO₂, 0.1–0.3 % S. In low phosphorus practice, the silica content is in the range 15% to 20%. In high phosphorus practice, the slag contains 8% to 17% P₂O₅, or higher, and the silica content is in the range 8% to 16%.

BOF slag is a multiphase mixture. It usually contains dicalcium silicate (bredigite) (2CaO·SiO₂), and other elements up to 1-2% (e.g. Mn, Fe, Mg), tricalcium silicate (3CaO·SiO₂), wustite (FeO), calcium ferrite (also dicalcium ferrite and calcium

aluminoferrite), and minor amounts of periclase (MgO) and magnesiowustite (solid solution of FeO and MgO). Pieces of undissolved lime also present in the slag at turndown due to the formation of dicalcium silicate ($2\text{CaO}\cdot\text{SiO}_2$) film on the surface of lime particles, which prevents its rapid dissolution. [21]

Up to 1% of free metal in fine globules may also present. The quantity of phases depends on the CaO and SiO_2 proportions of the slag. Tricalcium silicate only appears at high lime/silica ratios (>3.0). Wustite and ferrites are major phases in iron-rich BOF slags. There are two important properties of steelmaking slags: the basicity and the state of oxidation of the slag.

Slag Basicity: The oxides, e.g. SiO_2 , P_2O_5 , and Al_2O_3 which form anion complexes in molten slags (network formers) are said to be acidic oxides. The oxides, e.g. CaO, MgO, MnO, FeO, which break down the anion complexes in the melt are known as the network modifiers and are said to be basic oxides. The ratio of the concentrations of basic oxides to those of the acidic oxides is called the "basicity" of the slag. There are numerous ways of representing the basicity of the industrial slags. Since this is an arbitrary way of expressing the general chemical behaviour of the slag, there is no particular rule dictating the manner in which the basicity should be represented.

In simple slags where lime and silica are the major constituent oxides, the basicity is usually defined by the concentration ratio $B_2 = \frac{\%(\text{CaO})}{\%(\text{SiO}_2)}$, which is often called the "V-ratio" or "basicity 2" which refers to the two components involved. It is the ratio of basic and acidic oxides of the slag. Metallurgical slags by their basicity are divided as low (0.93 -1.4)-, medium (1.4 -1.87)-, high (1.87-2.80) and multibasic (≥ 2.80). [25]

However, most of the industrial slags contain fair proportions of magnesia and phosphorus pentoxide; in such cases the basicity may be defined as follows: it is assumed that the concentrations of CaO and MgO are equivalent on molar basis; converting it to concentrations in weight percent, CaO equivalence of MgO becomes $1.4 \% \text{MgO} = \% \text{CaO}$. On molar basis $1/2 \text{P}_2\text{O}_5$ is assumed to be equivalent to SiO_2 ; therefore in terms of weight percent, SiO_2 equivalence of P_2O_5 is $0.84 \cdot \% \text{P}_2\text{O}_5 = \% \text{SiO}_2$. The basicity is then given by [21] :

$$\text{Slag basicity} = \frac{\text{CaO} + 1.4 \cdot \% \text{MgO}}{\% \text{SiO}_2 + 0.84 \cdot \% \text{P}_2\text{O}_5} \quad (3-29)$$

A large percentage of steel is made using basic slags which are best suited to yield steel low in silicon, phosphorus and sulphur. Most basic slags are saturated with lime and magnesia; in order to minimize the wear of the basic lining in the furnace so that and can withstand a large number of heats before relining. [13]

4 Kinetics of CaO and MgO dissolution in the converter steelmaking process

For several decades the theory of diffusion kinetics of steelmaking processes has been studied. Investigation of any diffusion characteristics of liquid metal melts is one of the most difficult problems in experimental metallurgy.

Lime and dolomitic lime are two primary fluxes charged in the converter bath to generate a slag of the desired chemical composition. In the process of interaction between metal and slag, it is important to know the rate-limiting step of lime dissolution in the melt. The rate of assimilation of fluxes with slag and its interaction strongly influences the slag-metal reactions during the blow. The impurities from the hot metal are removed into the slag in the steelmaking process. Therefore, to achieve the final product with the required quality, it is important to control the evolution of slag. Physicochemical properties of slag influence the productivity of the steelmaking processes to a great extent. The rapid formation of physically and chemically active slag facilitates removal of sulfur and phosphorus from the melt. It reduces metal loss and formation of *metal-regulus* in the slag; furthermore it decreases wear in the refractory lining. Viscous slag is physically poorly active and has a low refining capacity, thus, reaction processes with metal slow down. Such a viscous slag will lead to an increase in the metal losses due to the regulus formation and slag splashing. It often leads to the lance becoming clogged and formation of skulls on the neck of the vessel. High slag fluidity is also not desirable due to the increased refractory wear of the converter lining.

In the process of steelmaking in an oxygen converter it is necessary to obtain at the end of the blowing process a sufficiently flowable, physically and chemically active homogeneous slag with basicity $\text{CaO/SiO}_2 = 3.0\text{--}3.5$. As it is known, the chemical composition of the converter slag and intensity of lining destruction vary in different stages of the converter process. The highest rate of destruction of the lining in the converter is observed during the formation of slag with the basicity $\text{CaO/SiO}_2 = 1.0 - 1.5$ and a high oxidation state (up to 30% FeO).

Therefore, it is necessary to form a slag with maximum concentration of MgO, closer to the saturation for a desired temperature conditions in the first period of blowing. In order to increase the MgO content in the slag, it is efficient to use Magnesian fluxes. The consumption of slag-forming materials is determined by calculation, in accordance with the raw material composition and the desired slag. During the melting process a slag sample's composition may differ from the calculated value, and pieces of undissolved lime may be present in the sample of slag. Moreover, it can happen that a melting operation is over, slag of the desired composition is not formed and detrimental impurities are not fully removed

The sources for slag formation are oxides - oxidation products of hot metal components and impurities of scrap loaded into the converter, bulk materials (iron ore, flux materials) and refractory linings.

In the kinetic study the main difficulty lies in the suppression or elimination of convective mass transfer, which essentially depends on the viscosity of the fluid and temperature gradient. Therefore, there are not many literature sources and experimental works which provide the solution for the following problem. [26]

Study of L. Akselrod et.al [26] on the kinetics of slag saturation with magnesium oxide in simulation process of interaction of the refractory material MgO-C and slag with addition of magnesia flux, showed a significant decrease in the rate of dissolution of magnesium oxide in the slag, in 2.0 – 2.25 times accordingly.

Industrial research carried out by specialists of the Hamburger Stahlwerke Company, enables the dissolution degree of basic refractory in the slag to be estimated, depending on the content of magnesium oxide in the refractory. [27]

The authors considered the proportion of MgO transiting into the slag from the lining by calculating the material balance of the slag. In the experiment there was a clear tendency towards a decrease in magnesium oxide dissolution from the lining in the slag with the increase of the saturation of slag with MgO.

In industrial conditions there is a problem of even distribution of the dissolving MgO throughout the volume of the slag, which is why the rate of dissolution of magnesia material in the slag plays such an important role. Lime is essential for slag formation. The melting point of lime is 2570 °C, and the temperature of molten slag is 1250-1500°C. Therefore, one of the most important tasks of slag formation control is a fairly high assimilation rate of lime into the slag phase.

Dissolution of lime in slag occurs in the following stages:

1. A film of saturated solution with calcium oxide forms on the surface of lime particles with a concentration (C_s), which is higher than the CaO concentration in the liquid phase (C).

Film formation is accompanied by formation of solid and liquid solutions, as well as chemical compounds of the system CaO-FeO-MnO-SiO₂. The rate of dissolution is determined by the rate of further mass transport through this film.

2. Penetration of liquid slag through the pores and grain boundaries on the surface of lime.

3. Melting and transition of the remaining surface (film) layers into the slag.

As shown in the experimental studies, the rate of assimilation of lime by slag is limited by the rate of mass transfer of CaO through the film of chemical compounds formed on surface of lime particles. [28] The impact of the rate limiting step of major metallurgical process of lime dissolution in steelmaking slags provides information about the process' mechanism and methods of its intensification.

4.1 Factors affecting dissolution

Evolution of slag composition during the BOF blow depends essentially on the rate of flux dissolution into the slag and is influenced by certain factors:

1. The rate of dissolution is controlled by mass transfer in the slag. [28]
2. Solubility of oxide in the slag. The dissolution of solid oxides in molten slag is directly related to the saturation level of solid oxides in the slag. The higher the solubility of solids in the slag the larger the driving force for the solid oxide to dissolve. For the purpose of the present work, the solubility of lime and dolomite in the CaO–SiO₂–FeO slag at various temperatures can be obtained from ternary phase diagram.
3. Formation of solid phase at the interface between oxide and slag. In the CaO and MgO dissolution process solid impervious high melting outer coating of 2CaO SiO₂ and (Fe, Mg)O solid solution layer occurs on the surface of lime and dolomite particles. [28–30]
4. Viscosity of the slag. Viscosity influences the dissolution of fluxes in the slag up to a great extent. It affects the mass transfer of ions through the liquid slag.
5. Properties of solid oxides: density, porosity, reactivity, size etc. Smaller lime particles dissolve faster because of the larger specific surface area. In industrial practice, charge materials come in various sizes. [31]
6. Lime particles which have bigger volume fraction of pores are more reactive, and dissolve faster than less porous lime, due to the slag permeation into the pores which leads to an increase in the surface area for reaction, and the particles tend to disintegrate into smaller sizes owing to such penetration as well as the lower strength of porous lime. When calcination procedure of CaCO₃ is kept at a lower temperature for a longer time, the reagent is more porous. However, too low a temperature and/or too short a time of calcining results in a lime containing unacceptable percentage of undissociated CaCO₃. [9,32]
7. The generally applied lime reactivity test is the standard slaking test in which water is added at room temperature to indicate the rise in temperature.
8. At higher temperatures rate of dissolution increases as a general rule of kinetics. However, it has been observed that at 1600°C and above lime starts to sinter rapidly, making it dense and as the result the rate of dissolution drops.

9. Pieces of undissolved CaO, both free as well as with a coating of dicalcium silicate have been observed in the final converter slag. In usual practice free lime can range between 5% and 10% of the total slag weight. [33,34]

4.2 Mixing and Mass transfer

Steelmaking reactions are heterogeneous in nature, i.e. more than one phase is involved, such as slag, metal, gas and solid, etc. The chemical reactions between such phases occur at the phase boundaries (i.e. at interfaces). The rate of reactions, therefore, would be proportional to the interfacial areas. These heterogeneous reactions occur in a few stages. First is transport of the reactants to the interface and after reaction takes place transport of the reaction products away from the interface. This is achieved by the process of mass transfer. Mass transfer describes the transport of mass from one point to another and may be further subdivided into the following categories: [35,36]

- Mass transfer in the bulk phase away from the interface. This step is sufficiently rapid only in fluids, and even more rapid if the flow is turbulent in nature. The terminology mixing is commonly used in this connection.
- Mass transfer at or near the interface, which depends on the concentration at the interface, temperature, total area available, etc.

As a result, all heterogeneous reactions take place through a series of kinetic steps, such as:

1. Interfacial chemical reaction
2. Mixing in the volume of the fluid
3. Mass transfer at or near the interface.

Solids may be assumed to be pure in pyro-metallurgical processes since solid-state diffusion is extremely slow and can be neglected. Nevertheless, porous solids like iron ore, sinter, lime, etc. are used in these processes and react fast due to easy diffusion of gases or liquids through the pores of these materials.

New phases are formed after these reactions, for example, the formation of carbon monoxide bubbles during decarburisation and deoxidation products following the addition of deoxidants. Theoretically, the formation of such products requires nucleation and growth. However, it has been established that nucleation is not required in industrial processing and only growth is involved. [35–39]

The mass transfer coefficient is the measure of the dissolution rate and can be defined as the diffusivity divided by the boundary layer thickness, δ .

$$k_i = \frac{D}{\delta} \quad (4-1)$$

where D is the diffusion coefficient, (cm^2/s) and δ is the boundary layer thickness.

An estimate of the relation between the boundary layer thickness and a system's typical length is given by the Sherwood number:

$$\text{Sh} = \frac{k_i L}{D} \quad (4-2)$$

where L is a typical length for a system (e.g. the radius of a pipe or the width of a channel). Since the thickness of the boundary layer depends on the convection just outside an interface, the Sherwood number also gives a measurement of the convective and diffusive fluxes to such an interface. [40,41]

4.3 Diffusion

Diffusion is a mass transfer phenomenon which ensures the distribution of chemical substances in space and time in order to become more equal. The mass transfer of any species is the evolution of its concentration in space and time. If the concentration of a species is initially not uniform (it is greater in one region than in another) then, diffusion causes mass transfer in favour of a more uniform concentration.

The driving force for diffusion is the thermal motion of molecules. At temperatures above absolute zero, molecules are never at rest. Their kinetic energy means that they are always in motion, molecules start colliding with each other frequently and the direction of the motion becomes randomized. When molecules are moving and constantly changing direction, diffusion occurs because of the statistics of this movement. [42]

For example, in a volume of a solution with a non-uniform concentration of substances, diffusion induces the concentration to become uniform. Such uniform concentration means that the number of molecules moving in opposite directions is the same. However, at the interface between the region of high and low concentration, there will be more molecules moving to the region of low concentration. This is because there are more of them on one side of the interface than on the other. Such movement of molecules from one region to another is a net flux of material. This phenomenon is diffusion which drives a net flux of material from regions of high concentration to low concentration, or in other words, down a concentration gradient. Once the concentration has become uniform, the molecules are all still in motion in different, random directions and there are the same number of molecules moving from the boundary interface in either direction. Even though the molecules are in random motion, there is no statistical driving force for them to start accumulating anywhere if their distribution is uniform.

Diffusion is governed by the Fick's first law of diffusion. It describes quantitatively the diffusion process and indicates that the molar flux in the direction x is proportional to the concentration gradient. Concentration profile does not change with time i.e. steady-state diffusion. [43]

$$\text{Molar flux} = \frac{dni}{A} = -D_i \cdot \frac{\delta C_i}{\delta x} \quad (4-3)$$

$$\text{Mass flux} = \frac{dmi}{A} = -D_i \cdot \frac{\delta C_{xi}}{\delta x} \quad (4-4)$$

for diffusion of species i along the direction x . C_i is the concentration of i in moles/volume, C_{xi} is the concentration of i in mass/volume and D_i is the diffusion coefficient (i.e. diffusivity) of i , $\text{cm}^2 \cdot \text{s}^{-1}$ or $\text{m}^2 \cdot \text{s}^{-1}$. Values of D (in $\text{m}^2 \cdot \text{s}^{-1}$) at ironmaking and steelmaking temperatures are of the order of 10^{-2} to 10^{-3} for gases, $5 \cdot 10^{-8}$ to $5 \cdot 10^{-9}$ for liquid steel, and $5 \cdot 10^{-10}$ to $5 \cdot 10^{-11}$ for liquid slags.

Fick's second law describes concentration profile and the concentration gradient change with time. The flux of atoms in the diffusion process may vary. It is called the unsteady flow or non-steady state diffusion. The rate of accumulation of diffusing substance in a given volume is the difference between incoming and outgoing fluxes per unit time. [44]

$$\frac{\partial C}{\partial t} = \frac{1}{dx} \cdot (J_x - J_{x+dx}) = -\frac{\partial J}{\partial x} \quad (4-5)$$

$$\frac{\partial C}{\partial t} = \frac{\partial}{\partial x} \left(D \frac{\partial C}{\partial x} \right)$$

$$\frac{\partial C}{\partial t} = D \frac{\partial^2 C}{\partial x^2}$$

4.3.1 Diffusion coefficient

Diffusion coefficient indicates the rate of the diffusion process. It is most simply understood as the magnitude of the molar flux through a surface per unit concentration gradient. It is analogous to the property of thermal diffusivity in heat transfer: [45,46]

$$D_i = \frac{|J|}{|\nabla C_i|} \quad (4-6)$$

There are numerous ways in which Diffusion coefficient can be defined. It obeys the following relation to temperature and pressure:

$$D = \frac{T^{\frac{3}{2}}}{p} \quad (4-7)$$

For particles or large molecules in a viscous fluid (usually a liquid solution), the Stokes-Einstein equation can be applied:

$$D = \frac{k \cdot T}{6\pi\mu r} \quad (4-8)$$

where k is the Boltzmann constant, μ is the solvent viscosity, and r is the radius of the diffusing particle.

The diffusion coefficient in solids at different temperatures is generally found to be well predicted by the Arrhenius equation:

$$D = D_0 e^{-\frac{E_a}{kT}} \quad (4-9)$$

where D is the diffusion coefficient (m^2/s), D_0 is the maximum diffusion coefficient (at infinite temperature; m^2/s), E_A is the activation energy for diffusion in dimensions of ($J \cdot atom^{-1}$), T is the absolute temperature (K), k is the Boltzmann constant. [47–49]

4.4 Mass transfer in the presence of flow

There are two types of flow exist: laminar or turbulent. The movement of substances in laminar flow is only in the direction of the flow (see streamlines as shown in Figure 4-1(left). In the turbulent flow elements also move at right angles to the direction of the flow, however, they produce local eddies. On the Fig. 4-1 (right) flow past a cylinder is moving much faster than in laminar flow. The eddies produced by the obstruction form a wake downstream. [50]

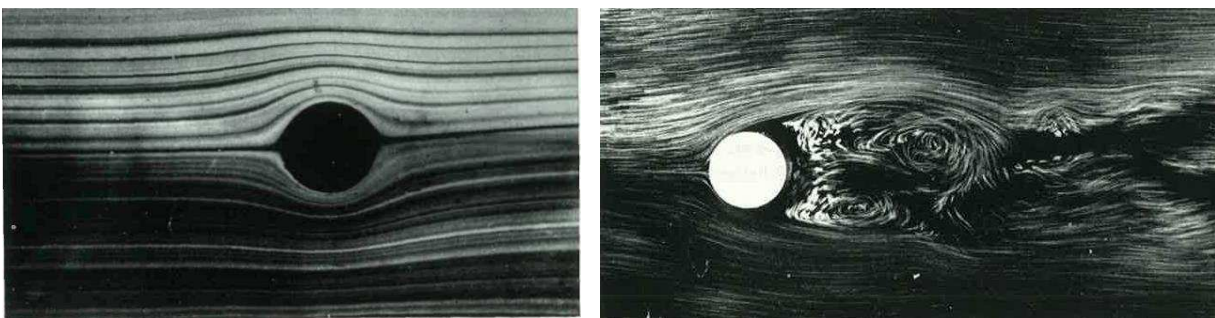


Figure 4-1: Laminar (left), turbulent (right) flow [50]

In most metallurgical operations, a system in which flow is turbulent is associated with many difficulties. Because in turbulence mixing occurs not only by diffusion but by the movement of eddies. For such case it is possible to measure eddy diffusivity in the same way as diffusivities are measured. In a turbulent liquid the eddy diffusivity D_E is defined by the equation [50]:

$$J = D_E \frac{\Delta C}{L} \quad (4-10)$$

where L is the distance over which the concentration difference ΔC exists.

In the stirred systems the mixing is usually vigorous enough to keep the bulk concentrations uniform, so that gradients of concentration exist only near the interface. For example, in a single stirred phase M, with bulk and interfacial concentrations C_b and C_i the solute is removed from the surface in a manner that keeps C_i constant. The flux of solute J from the bulk phase to the interface can be defined by the equation [50]:

$$J = k_M A (C_b - C_i) \quad (4-11)$$

where k_M is a mass transfer coefficient, and A the area of the interface. If J is in mole·s⁻¹, A in cm² and C_b and C_i in mole·cm⁻³, the units of k_M are cm·s⁻¹.

4.5 Mass Transfer Correlations

Mass transfer coefficients can be correlated to several dimensionless groups. The Reynolds number physically estimates the ratio of inertial forces to viscous forces [51–53]:

$$Re = \frac{\rho v L}{\mu} \quad (4-12)$$

where v is the mass average velocity (m/s), L is the characteristic length (diameter of a sphere, diameter of a cylinder, or length of a flat surface) (m), ρ is the fluid density (kg/m³), μ is the fluid viscosity (kg/(m·s)).

The Schmidt number gives an estimate of the relation between viscosity and mass diffusivity in a fluid:

$$Sc = \frac{\mu}{\rho \cdot D} \quad (4-13)$$

where D is the diffusion coefficient (m²/s).

The Sherwood number describes the ratio of mass transfer rate to diffusion rate. It also can be defined as a function of the Reynolds and Schmidt numbers.

$$Sh = \frac{k \cdot L}{D} \quad (4-14)$$

The mass transfer coefficient can be estimated from the relation between the Sherwood number, the Reynolds and Schmidt numbers. For example, for forced convection the following expression can be used:

$$Sh = k \cdot Re^\alpha \cdot Sc^\beta \quad (4-15)$$

where α and β are exponents and k is a constant. Another equation is used for free convection:

$$Sh = k \cdot Gr^\alpha \cdot Sc^\beta \quad (4-16)$$

4.6 Kinetic models applied for present work

4.6.1 Kinetic model 1

The dissolution of oxides in the slag can be described by kinetic model of dissolution of solid particles in liquids. The following kinetic model is based on few main principles: all reactions in the steel bath are heterogeneous, as the substances present in different phases any chemical process in the bath consists of three stages:

1. Transportation of the reagents to the reaction side where the reagents react with each other.
2. The chemical reaction (interaction). Particles with a certain energy level greater than the level of the activation energy in the primary particles are transformed into reaction products.
3. Transport of the reaction products from the reaction side.

The first and second process stages subdivided into more stages such as diffusion, adsorption and chemical stage.

For small solid CaO and MgO particles of (less than 0.1 mm) diffusion in micro-heterogeneous systems can be greatly intensified by increasing the contact surface of liquid (molten slag) and particles and hence the mass transfer. The acceleration of mass transfer using powdered materials can be obtained with decreasing particle size d , if the relative velocity of the liquid phase is constant. [29]

It is well known that the total surface of the particles increases in inverse proportion to their effective size. If we assume that the particle is spherical, the ratio of its surface area to volume would be [54]:

$$\frac{S_i}{V_i} = \frac{\pi d^2}{\frac{\pi d^3}{6}} = \frac{6}{d} = \frac{3}{r} \quad (4-17)$$

Total surface of particles:

$$S_{\Sigma} = S_i \cdot N = \frac{6V_i \cdot N}{d} = \frac{6V_{\Sigma}}{d} = \frac{6M}{d\rho_{solid}} \quad (4-18)$$

where S_i and V_i are surface and volume of a single particle (such as CaO); N – is the number of particles; V_{Σ} and M - are the total volume and the total mass of particles; d and r - are the diameter and radius of the particle; ρ_{solid} - is the density of the particle.

In the process of lime dissolution in slag the determination of the process kinetics is limited to the measurement of mass transfer coefficient k . Mass transfer coefficient in the melt can be determined if the reliable data on the rate of dissolution of lime is provided and all of the parameters in the kinetic equation (4-19) are known.

As CaO dissolving in the slag, its weight will decrease over time as it enters the molten slag phase. Therefore, in the kinetic equation (4-19) the "minus" sign means that the mass of CaO decreases:

$$-\frac{d(CaO)}{dt} = k_{CaO} \cdot ((CaO)_{sat} - (CaO)) \cdot S \quad (4-19)$$

where the subscript 'sat' refers to the saturation concentration; $-\frac{d(CaO)}{dt}$ – is mass of CaO consumed; $(CaO)_{sat}$ - is the concentration of calcium oxide in the slag at the surface of lime particles (saturation concentration), (kg/m^3); (CaO) - is the concentration of calcium oxide in the slag, (kg/m^3); k_{CaO} - is the mass transfer coefficient; S – is the total surface of lime (m^2). This equation is applicable only in cases where the process of lime dissolution is limited by mass transfer of calcium oxide.

The following equation is used to recalculate the mass concentration into percent:

$$(CaO) = \frac{CaO\%}{100\%} \cdot \rho_{liq} \quad \text{and} \quad (CaO)_{sat} = \frac{CaO\%_{sat}}{100\%} \cdot \rho_{liq} \quad (4-20)$$

where ρ_{liq} is the density of slag (kg/m^3).

The equation (4-19) is modified into equation (4-21):

$$-\frac{dCaO}{dt} = k_{CaO} \cdot \frac{((CaO\%)_{sat} - (CaO\%)) \cdot \rho_{liq} \cdot S}{100\%} \quad (4-21)$$

Since in the process not pure CaO is dissolved but lime which contains a certain percentage of CaO, the equation (4-19) is modified:

$$\begin{aligned}
 -\frac{dCaO}{dt} &= -\frac{dM_{sol}}{dt} \cdot \omega_{CaO} = & (4-22) \\
 &= -\frac{dM_{sol}}{dt} \cdot \frac{CaO_{sol}}{\rho_{sol}} = k_{CaO} \cdot ((CaO)_{sat} - (CaO))
 \end{aligned}$$

where M_{sol} is mass of lime, and $(-\frac{dM_{sol}}{dt})$ is mass of lime decreasing in time, ω_{CaO} is mass fraction of CaO equal to $\frac{CaO_{sol}}{\rho_{sol}}$

$$-\frac{dM_{sol}}{dt} = \frac{k_{CaO} \cdot ((CaO)_{sat} - (CaO))}{(CaO)_{sol}} \cdot S \cdot \rho_{sol} \quad (4-23)$$

$$\begin{aligned}
 -\frac{dM_{sol}}{dt} &= k_{CaO} \cdot \frac{\left(\frac{CaO\%_{sat}}{100\%} \rho_{liq} - \frac{CaO\%}{100\%} \rho_{liq}\right)}{\frac{(CaO\%)_{sol}}{100\%} \rho_{sol}} \cdot S \cdot \rho_{sol} = & (4-24) \\
 &= \frac{k_{CaO} \cdot ((CaO\%)_{sat} - (CaO\%))}{(CaO\%)_{sol}} S \cdot \rho_{liq}
 \end{aligned}$$

Equation (4-23) in percent:

$$-\frac{dM_{sol}}{dt} = \frac{k_{CaO} \cdot ((CaO\%)_{sat} - (CaO\%))}{(CaO\%)_{sol}} S \cdot \rho_{liq} \quad (4-25)$$

The size of lime particles continuously reduces during the dissolution in the slag and, consequently, lime surface S decreases, hence, the mass dissolution rate continuously decreases. In practice it is easier to determine the linear rate than the mass change and the solid-lime surface change. Therefore, in experiment it is possible to use $\frac{dx}{dt}$ parameter, where x is the lime particle linear size, for example, the radius of the spherical particle (or half of an edge of the cube, cylinder height, etc.).

The linear rate of dissolution of spherical lime particles can be calculated by the following equation:

$$-\frac{dM_{sol}}{dt} = -\frac{dV_{sol} \cdot \rho_{sol}}{dt} = -\frac{dr \cdot S \cdot \rho_{sol}}{dt} \quad (4-26)$$

$$v_r = -\frac{dr}{dt} = \frac{k_{CaO} \cdot ((CaO\%)_{sat} - (CaO\%)) \cdot \rho_{liq}}{(CaO\%)_{sol} \cdot \rho_{sol}} \quad (4-27)$$

$$k = \frac{-\frac{dr}{dt} \cdot (\text{CaO}\%)_{sol} \cdot \rho_{sol}}{((\text{CaO}\%)_{sat} - (\text{CaO}\%)) \cdot \rho_{liq}} \quad (4-28)$$

All equations can be also applied to the MgO dissolution process.

After the value of mass transfer coefficient is defined the correlation between $\ln(k)$ and the inverse temperature $\frac{1}{T}$ should be examined to determine the activation energy of the dissolution reaction. The activation energy value reveals if the rate determining step is diffusion or chemical reaction and is calculated by the equation (4-29) using the experimental data [29]:

$$E = \frac{8.314 \cdot \ln\left(\frac{K_2}{K_1}\right)}{\frac{1}{T_1} - \frac{1}{T_2}} \quad (4-29)$$

The low activation energy value of less than 200 kJ/mol shows that the dissolution process of CaO or lime in steel slag is limited by diffusion. If the value of activation energy is higher than 200 kJ/mol, the rate-limiting step of the process is a chemical reaction.

4.6.2 Kinetic model 2

The following kinetic model is suggested to be more accurate, as it considers the total mass balance of CaO dissolution (its transition and accumulation in the bulk slag):

Lime with mass dM_{solid} dissolved in the selected time interval dt . Consequently, CaO (contained in lime dM_{solid}) is transported into the slag in the time dt :

$$dCaO = \frac{dM_{sol}}{100\%} \cdot \text{CaO}\% = 0,01 \cdot dM_{sol} \cdot \text{CaO}\%_{sol} \quad (4-30)$$

where the subscript 'sol' refers to the solid, dM_{sol} is a mass of lime dissolved, CaO% is the content of CaO in the lime.

From the lime dissolved in the given time dt the CaO diffuses into the slag phase according to the main kinetic equation:

$$0,01 \cdot k_{CaO} ((\text{CaO}\%)_{sat} - (\text{CaO}\%)) \cdot S \cdot \rho_{liq} \cdot dt \quad (4-31)$$

Here, the surface area of lime sample is calculated as the sum of the base and side surfaces of the cylinder, considering its linear size (height of the cylinder).

Therefore the balance would be (due to the concentration gradient):

$(0,01 \cdot dM_{sol} \cdot \text{CaO}\%_{sol})$ - came to the slag phase;

$(0,01 \cdot k_{CaO} ((CaO\%)_{sat} - (CaO\%)) S \cdot \rho_{liq} \cdot dt)$ -diffuses into the slag;

$0,01 \cdot dM_{liq} \cdot CaO\%$ - remained into the slag;

Therefore, the following equation has been obtained:

$$0,01 \cdot dM_{sol} \cdot CaO\%_{sol} - 0,01 \cdot k_{CaO} \cdot ((CaO\%)_{sat} - (CaO\%)) S \cdot \rho_{liq} \cdot dt = 0,01 \cdot dM_{liq} \cdot CaO\% \quad (4-32)$$

where $CaO\%_{sol}$ is the concentration of CaO in lime, $CaO\%_{sat}$ is the concentration of CaO in the saturated layer of slag, $CaO\%$ -is the concentration of CaO in the slag phase.

As the mass of lime dissolved (dM_{sol}) became equal to the melt mass (dM_{liq}) occurring in the slag ($dM_{liq} = dM_{sol}$), consequently, (dM_{liq}) can be replaced with (dM_{sol}) in the equation (4-32):

$$0,01 \cdot dM_{sol} \cdot CaO\%_{sol} - 0,01 \cdot k_{CaO} \cdot ((CaO\%)_{sat} - (CaO\%)) S \cdot \rho_{liq} \cdot dt = 0,01 \cdot dM_{sol} \cdot CaO\% \quad (4-33)$$

$$-\frac{dM_{sol}}{dt} = \frac{k_{CaO} \cdot ((CaO\%)_{sat} - (CaO\%)) S \cdot \rho_{liq}}{CaO\%_{sol} - CaO\%} \quad (4-34)$$

Similar equation is applied for MgO:

$$-\frac{dM_{sol}}{dt} = \frac{k_{MgO} \cdot ((MgO\%)_{sat} - (MgO\%)) S \cdot \rho_{liq}}{MgO\%_{sol} - MgO\%} \quad (4-35)$$

The linear rate is expressed as follows:

$$dM_{sol} = dV_{sol} \cdot \rho_{sol} = d \frac{4}{3} \pi r^3 \cdot \rho_{sol} = dr \cdot S \cdot \rho_{sol} \quad (4-36)$$

$$\frac{dM_{sol}}{dt} = \frac{dr}{dt} \cdot S \cdot \rho_{sol}$$

$$\frac{dr}{dt} = \frac{dM_{sol}}{dt} \cdot \frac{1}{S \cdot \rho_{sol}} = \frac{k_{CaO} \cdot ((CaO\%)_{sat} - (CaO\%)) \cdot \rho_{liq}}{(CaO\%_{sol} - CaO\%) \rho_{sol}}$$

For more precise calculation it is necessary to consider that the concentration of CaO in the liquid slag phase (% CaO) is variable in equation (4-34), so that at any time interval the concentration will vary. Therefore, the changing concentrations of CaO in the liquid slag phase can be expressed by the following equation:

$$\text{CaO}\% = \text{CaO}\%_{\text{prim}} + \frac{(M_{\text{sol.prim}} - M) \cdot \text{CaO}\%_{\text{sol}}}{(M_{\text{liq.prim}} + M_{\text{sol.prim}} - M)} \quad (4-37)$$

where the subscript 'sol.prim' refers to solid primary and 'liq.prim' to liquid primary; $M_{\text{sol.prim}}$ is the weight of lime at the beginning of the process (kg), $M_{\text{liq.prim}}$ is the mass of the liquid slag (kg) at the beginning of the process at time $t = 0$, M is the mass of the solid lime phase (kg) at any time t , $\text{CaO}\%_{\text{prim}}$ is the primary concentration of CaO in the slag before the experiment, $\text{CaO}\%_{\text{sol}}$ is the concentration of CaO in the lime.

5 Objects of the study and research techniques

The objects of the study were samples of industrial and model slags with different content of main slag components: CaO, SiO₂ and FeO.

X-ray fluorescence method of analysis (XRF) and Scanning Electron spectroscopy SEM (Scanning Electron Microscope, QUANTA FEI 200 FEG-ESEM) were used to study the elemental composition of slag. Phase analysis of slag was studied using X-ray diffraction method XRD (Bragg-Brentano diffractometer Difrey-401 with Cu anod tube and K-alpha monochromatized x-ray source).

The elemental composition of slag carried out by XRF method is shown in Table 5-1 and SEM results are presented in Table 5-2. The phase composition of the slag is shown in Table 5-3.

Table 5-1: The elemental composition of the industrial slags carried out by X-ray fluorescence method

№	Content, %										
	Fe	Al ₂ O ₃	CaO	MnO	MgO	P ₂ O ₅	SiO ₂	TiO ₂	Cr ₂ O ₃	C	S
LD-Slag №1	24.16	2.05	38.73	6.55	5.50	1.13	11.09	0.34	0.49	0.26	0.07
LD-Slag №2	18.46	1.74	46.68	5.96	6.54	1.21	11.08	0.21	0.41	0.04	0.04

Table 5-2: The elemental composition of the industrial slag №1 by SEM

№ Sample	Content, %									
	CO	C	MgO	Al ₂ O ₃	SiO ₂	P ₂ O ₅	CaO	MnO	FeO	The Sum
1.00	37.03	15.87	2.20	1.17	4.65	1.15	30.58	4.26	23.58	67.58
2.00	19.86	8.51	1.87	1.17	6.84	1.24	42.42	2.93	25.91	82.37
3.00	19.86	8.51	1.10	1.17	9.26	1.37	40.25	2.78	13.67	69.59
max	37.03	15.87	2.20	1.17	9.26	1.37	42.42	4.26	25.91	86.59
min	19.86	8.51	1.10	1.17	4.65	1.15	30.58	2.78	13.67	55.09
Average	28.44	12.19	1.65	1.17	6.95	1.26	36.50	3.52	19.79	70.84

Table 5-3: Industrial slags phase composition (XRD analysis of slag carried out by MCL-Leoben)

№	Content, %							
	(MgO) _{0,59} (MnO) _{0,41}	NaFe ₂ O ₃	Fe	Mg ₂ SiO ₄	CaO	CaFe ₂ O ₅	MgO	Fe-Oxide
LD-Slag №1	56.0	8.9	2.6	1.8	21.1	6.6	2.2	bal.
LD-Slag №2	68.2	-	1.4	1.7	6.5	17.5	-	bal.

Tables 5-4 and 5-5 show the phase composition of LD slags №1 and 2, carried out in the laboratory of the State Mining University in Saint – Petersburg. Rietveld investigation of slags is presented on Figures 5-1 and 5-2.

Table 5-4: The results of quantitative X-ray analysis of the industrial slag №1

Phase composition	Quantity (Mass.%)
Wustite FeO	32±3%
Larnite Ca ₂ SiO ₄	21±2%
Merwinite Ca ₃ Mg(SiO ₄) ₂	15±4%
Brownmillerite Ca ₂ (Al,Fe) ₂ O ₅	13±3%
Rankinite Ca ₃ Si ₂ O ₇	9±2%
Tephroite Mn ₂ SiO ₄	6±2%
Hematite Fe ₂ O ₃	3±1%
Whitlockite Ca ₃ (PO ₄) ₂	≈1%

Table 5-5: The results of quantitative X-ray analysis of the industrial slag № 2

Phase composition	Content (Mass, %)
Srebrodolskite Ca ₂ Fe ₂ O ₅	37±3%
Wustite FeO	24±3%
Larnite Ca ₂ SiO ₄	21±3%
Berringerite FeP	5±3%
Marokite CaMn ₂ O ₄	5±2%
Manganite MnO	3±1%
Hematite Fe ₂ O ₃	3±1%

Whitlockite $\text{Ca}_3(\text{PO}_4)_2$	$\approx 1\%$
Hauerite MnS	$\approx 1\%$

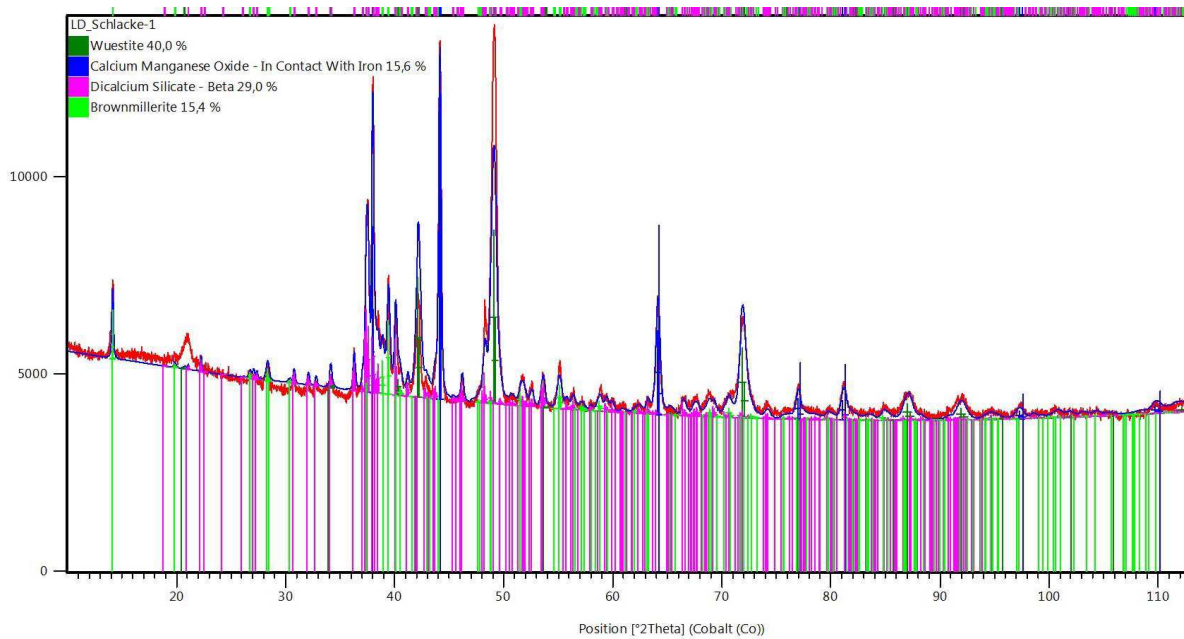


Figure 5-1: Rietveld investigation of phases of LD slag №1

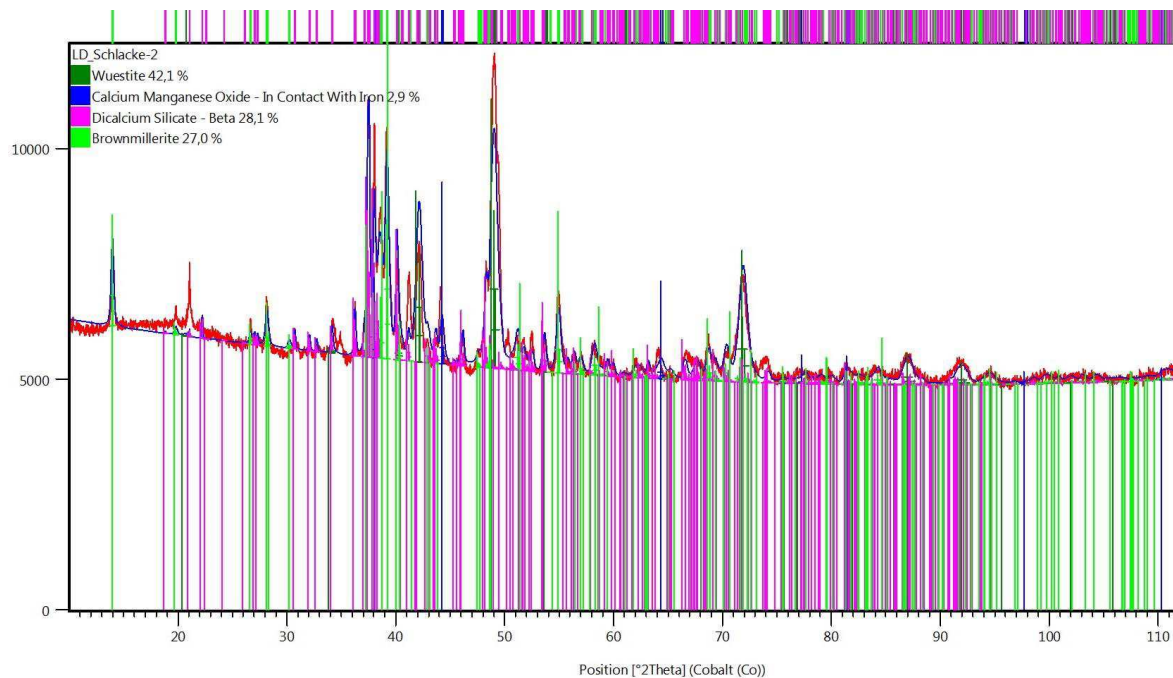


Figure 5-2: Rietveld investigation of phases of LD slag №2

Slag analysis carried out in independent laboratories and by different methods show good agreement with respect to the slag phase composition and phase quantity. The summarized results are presented in Table 5-6.

Table 5-6: Comparison of XRD and Rietveld results for investigation of Industrial slag phase composition

XRD analysis		Rietveld analysis by Voestalpine, Linz	
Phase composition	Quantity (Mass.%)	Phase composition	Quantity (Mass.%)
Wustite FeO	32±3%	Wustite	40%
Larnite Ca ₂ SiO ₄	21±2%	Dicalcium silicate	29%
Merwinite Ca ₃ Mg(SiO ₄) ₂	15±4%		
Brownmellerite Ca ₂ (Al,Fe) ₂ O ₅	13±3%	Brownmellerite	15.4%
Rankinite Ca ₃ Si ₂ O ₇	9±2%	-	-
Tephroite Mn ₂ SiO ₄	6±2%	-	-
Hematite Fe ₂ O ₃	3±1%	-	-
Whitlockite Ca ₃ (PO ₄) ₂	≈1%	-	-

Microscopic investigation of LD slag phases was carried out by Polyvar Reichert-Jung Microscope. The following phases of primary and secondary dicalcium silicate, tricalcium silicate, wustite, hematite, calcium oxide and Fe can be observed on the Figures 5-3 – 5-7:

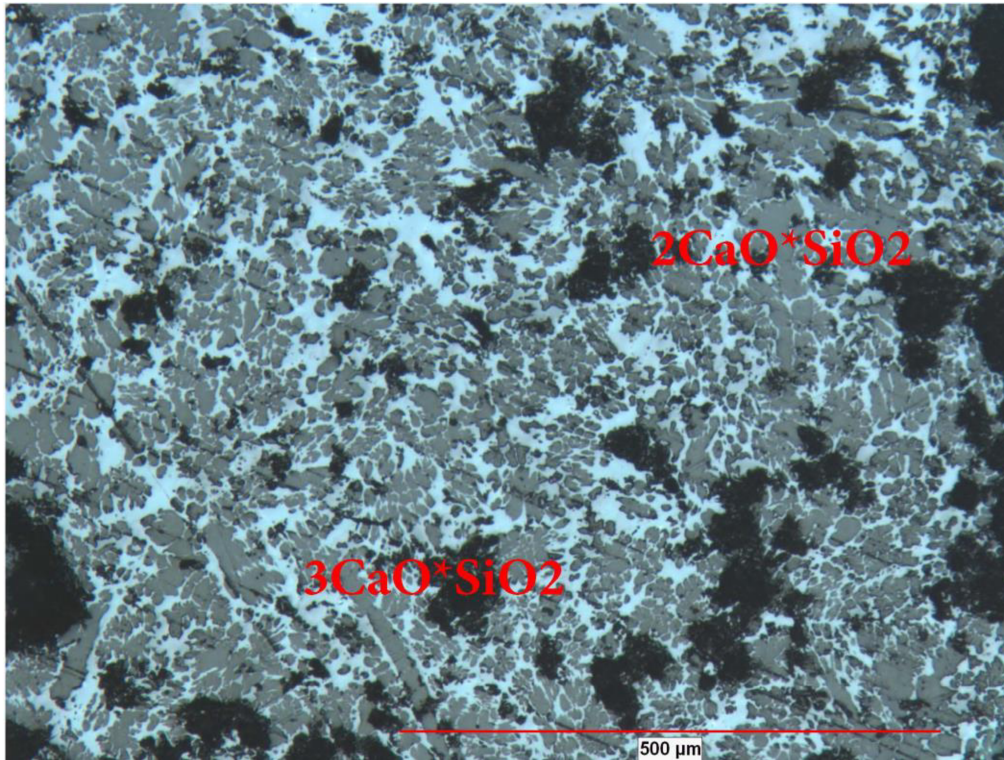


Figure 5-3: Microscopic investigation of LD slag phases

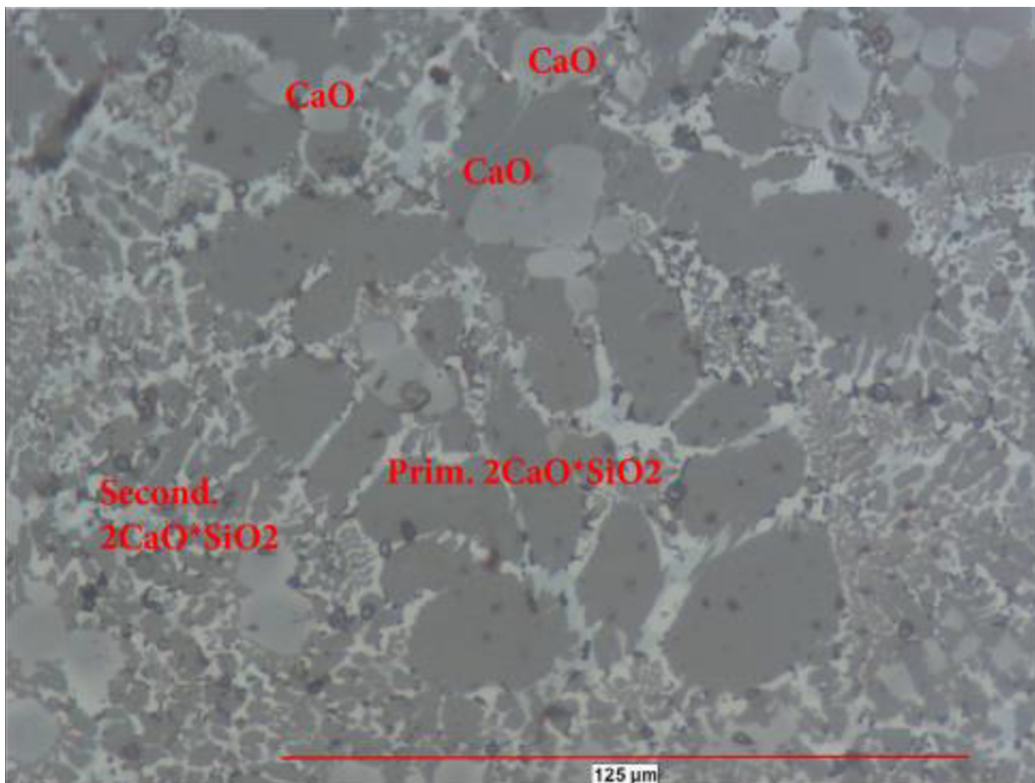


Figure 5-4: Microscopic investigation of LD slag phases

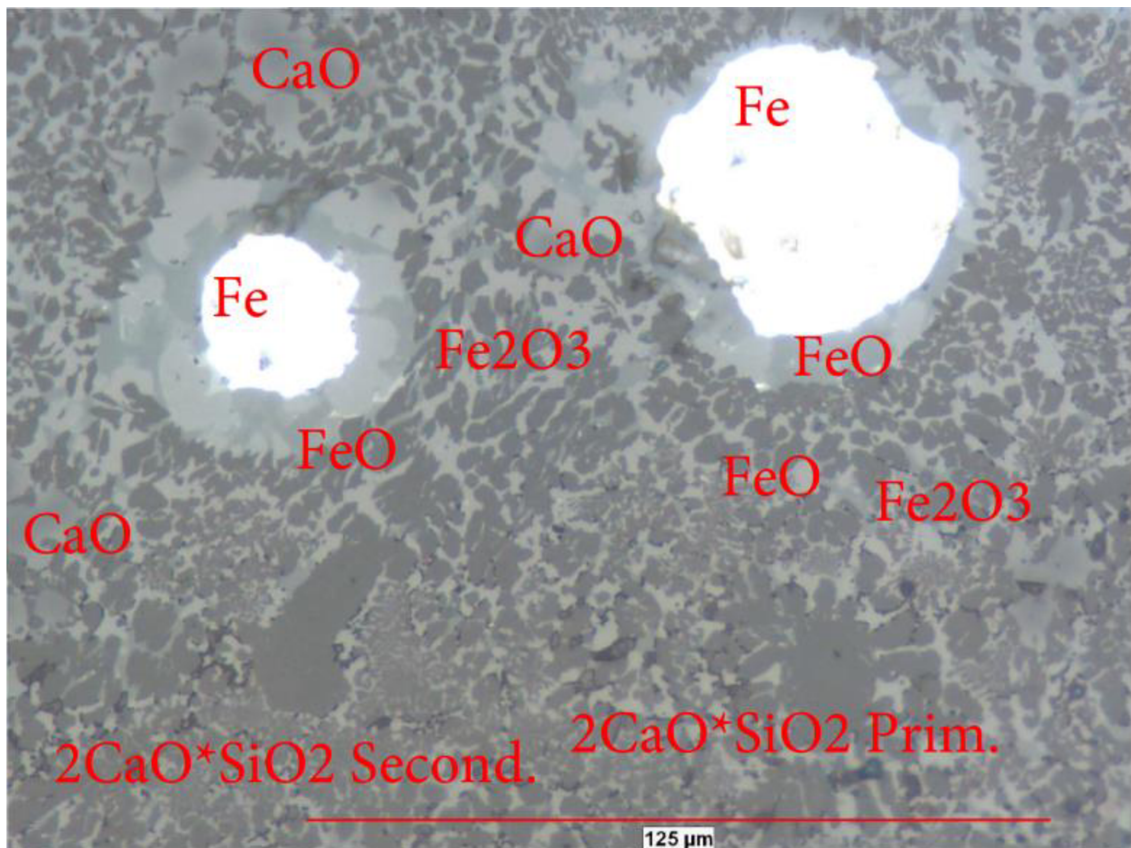


Figure 5-5: Microscopic investigation of LD slag phases

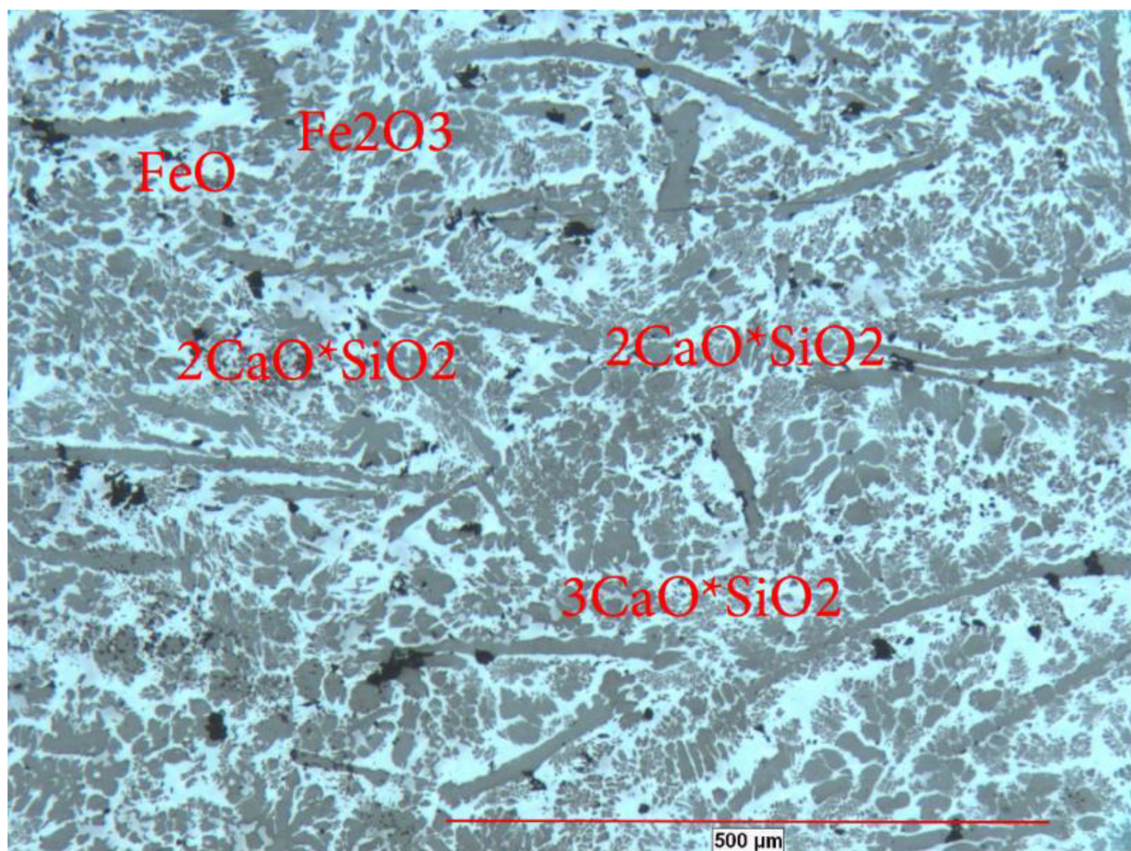


Figure 5-6: Microscopic investigation of LD slag phases

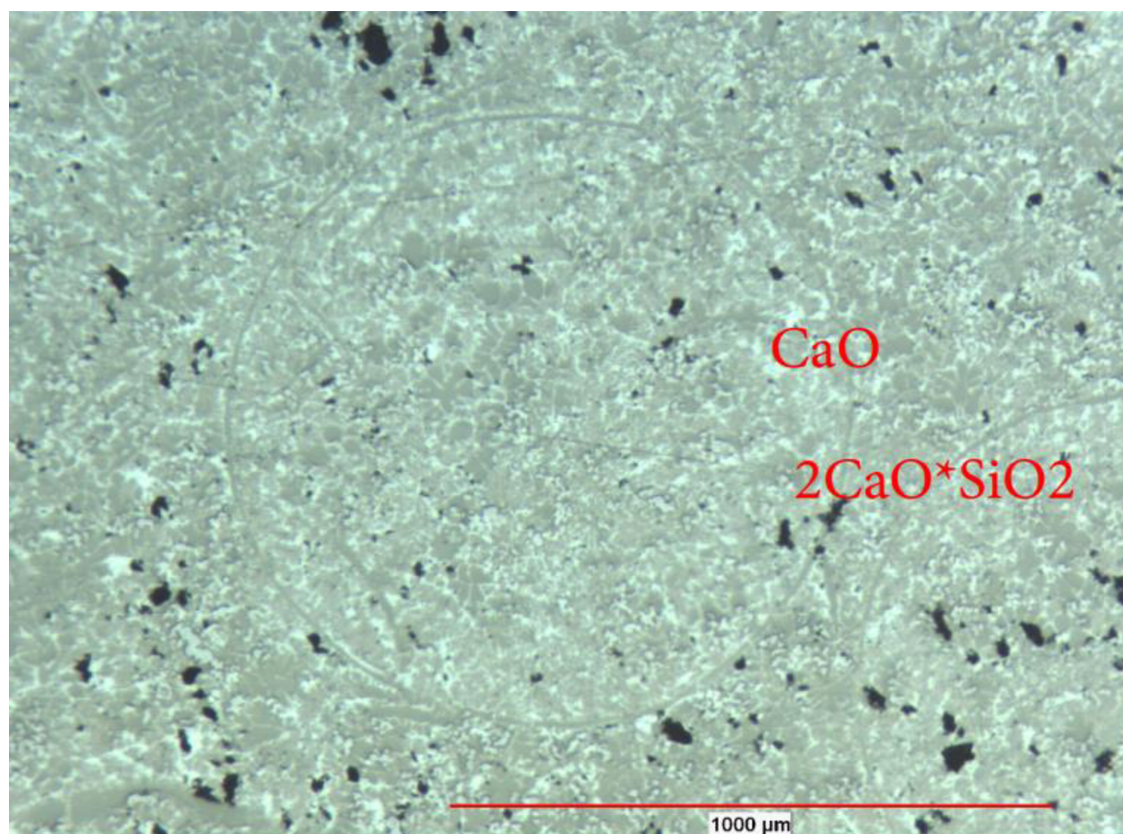


Figure 5-7: Microscopic investigation of LD slag phases

6 The methodology of the experiment

6.1 The research methodology for the selection of crucible material

Considering the complexity of the slag analysis and the presence of several components, first stage of experiments for the selection of crucible material was carried out with model slag containing: FeO, SiO₂ and CaO.

Samples of model slag were prepared from 99.99% pure reagents. Oxides of the elements were dried at the temperatures of 150-200 °C for 1.5-2 hours and placed in a desiccator. After drying samples were triturated and mixed in a predetermined ratio. Composition of model slag with mass and percentage is given in Table 6-1.

Table 6-1: The composition of model slag

Chemical composition	Mass, g	Content, mass. %
FeO	18	45
Fe ₂ O ₃	5	12.5
Fe ₃ O ₄	2	5
CaO	4	10
SiO ₂	4	10
H ₂ SiO ₃ , or (SiO ₂ ·H ₂ O)	6 (4.6 of SiO ₂)	15 (11.5 of SiO ₂)
Fe	1	2.5
Sum	40	100

The basicity of slag was defined as follows: $\text{CaO/SiO}_2=10/(10+11.5)=0.47$.

Tablets of 15 mm in diameter and 2 mm in height were made from powdered and stirred mixture of slag components by compression method under a pressure of 10 tons/cm² for 2 minutes. Samples were placed in crucibles and heated up to a desired temperature.

Experiment was carried out at various temperatures to reveal the effect of temperature on the process of interaction between the crucible material and slag: 1200°C, 1300°C, 1400°C, 1500°C and 1600 °C and held for 30 minutes after the desired temperature was reached. Samples were cooled down to the room temperature and extracted from the crucibles after melting process.

The inertness of crucible material in the process of slag melting was examined by X-ray fluorescence analysis, comparing the spectra of the characteristic radiation source of initial slag samples without heat treatment and slag samples melted in crucibles of SiO₂, MgO and BN.

6.2 Methods for determination of phase transformations in model slag

The study of slag phase composition was carried out to investigate and compare identified phases with literature data and to find possible chemical reactions of basic chemical compounds formation between the initial components of slag. Samples of 99.98% pure calcium, silicon and iron (II) oxides were selected in a specific stoichiometric ratio using the analytical balance. The quantitative composition of model slag is presented in Table 6-2.

Table 6-2: The quantitative composition of model slag

N^o of sample	CaO %	SiO₂ %	FeO %
1	40	35	25
2	30	35	35
3	40	25	35

Selected samples of the following oxides were mixed thoroughly, placed in a porcelain mortar and triturated to achieve a homogeneous state. After triturating 3g of the homogenized mixture of oxides in powder form was placed in a quartz crucible with dimensions of 2cm in diameter and 3cm in height. The choice of quartz crucibles for slag melting is explained in Chapter 7.1.

Quartz crucibles containing prepared mixture of oxides in a larger protective quartz crucible were placed in a high temperature vertical furnace Gero HTRV 200-250/17. The furnace setup is shown in Figure 6-1. The melting process was carried out under inert gas atmosphere, argon or nitrogen with a heating rate of 400°C per hour. The process was carried out until the desired temperature was reached (1400, 1500, 1600°C) and held at the target temperatures for 30 min. After the furnace was shut down crucibles with slag were removed from the heating zone and cooled down to room temperature. The walls of the crucible were removed using hammer and slag pieces were carefully separated from quartz crucible to analyze slag phase composition.

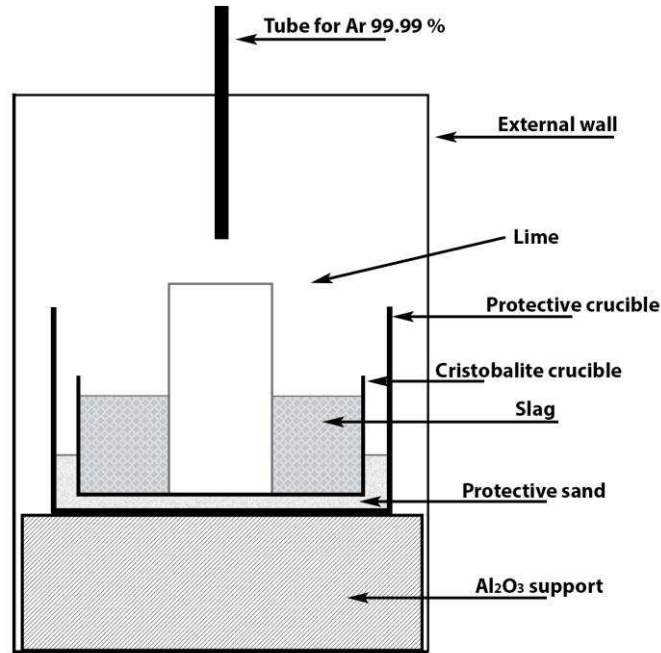


Figure 6-1: The principle setup of the Gero furnace

The investigation of model slag phase composition was performed by X-ray diffractometer Difrey-401 (see Figure 6-2).

Diffractometer is a desktop device which has an X-ray source and is equipped with a path for recording spectra and personal computer with the software package. Method of powder X-ray analysis is applied to obtain the diffractogram and a scheme of rays which focusing according to Bragg-Brentano. The device uses a coordinate-sensitive detector which provides high-speed recording of the spectrum. The device has consoles for powder samples including micro-objects with mass from 10^{-3} g and an automatic sample changer.



Figure 6-2: The principle of the device structure

The program "Phase Analysis" was used to decrypt the spectra obtained. "Phase Analysis" program allows conducting a qualitative X-ray analysis of the powdered samples, to specify parameters of the crystal lattice, to carry out a semi-quantitative analysis (by the ratio of 100% peaks) and compare diffractograms by superposition method. The position of the diffraction lines characterizes the geometry of the unit

cell and their intensity specifies the location of atoms in it. Thus, the summarized data can be considered as "X-ray sheet" of the crystalline phase. The analysis of various phases present in the sample can be achieved by a comparison of the experimental diffractograms with the standards from the database. The most comprehensive and regularly updated database with the diffraction standards is PDF2 ICDD (previously known as PDF JCPDS), which contains information about nearly a hundred thousand inorganic and organic crystalline phases.

Database contains information about the chemical composition of the substances, size and symmetry of the unit cell of the crystal, the conditions for "picturing" and "obtaining" a substance and some of its physical properties such as (optical parameters, phase transformation temperatures, etc.), the degree of reliability of the data and the position of the diffraction minimums in the system of coordinates.

6.3 The methodology of the Kinetic investigations

The investigation of lime dissolution kinetics in steelmaking slags was performed with samples of industrial slag №1 and model slag with the following composition: 20% CaO, 35% SiO₂, 45% FeO. Mass transfer coefficients were determined by the mass loss of cylindrical samples of industrial lime or pure CaO after the dissolution in the slag. The composition of industrial limes is shown in the Table 6-3.

Table 6-3: The composition of the industrial limes provided by Voestalpine Linz

№ of sample	Quantity, mass.%			True density, g/cm ³
	CaO	MgO	Other	
A	97.00	2.00	1.00	3.152
B	90.10	4.30	5.60	3.150
C	91.40	4.30	4.30	3.204
D	91.10	5.60	3.30	3.161
E	91.60	6.20	2.20	3.156
F	90.10	7.60	1.30	3.184

The composition of other elements for lime samples C, D, E and F is shown in Table 6-4.

Table 6-4: The composition of other elements for lime samples

Sam ple	Fe	SiO ₂	Mn	Al ₂ O ₃	P	TiO ₂	K ₂ O	LO I
C	0.03	0.35	0.04	0.18	0.005	0.008	0.022	2.39
D	0.02	0.20	0.04	0.10	0.002	0.003	0.019	4.03
F	0.03	0.16	0.01	<0.10	0.003	0.005	0.021	5.82
E	0.04	0.13	0.30	0.10	0.004	0.007	0.017	1.63

Samples of "chemically pure" calcium, silicon and iron (II) oxides in a predetermined stoichiometric ratio were prepared to make model slag using the analytical balance. Oxides of the following elements were dried at 150-200°C for 1.5-2 hours and placed in a desiccator. After drying samples were mixed thoroughly, placed in an agate mortar and mixed to achieve a homogeneous state.

The homogenized mixture of oxides with a mass of 2 g was placed in a quartz crucible. The decision to use quartz crucibles for slag melting is explained by the satisfactory material inertness of the crucible with respect to the slag composition in the range of the given temperatures, and the option of extracting, the crystallized fused slag without requiring special equipment. Crucibles were placed in a high temperature vertical furnace Gero HTRV 200-250/17. The melting process was carried out under inert gas, argon or nitrogen atmosphere at a predetermined temperature (1300, 1400, 1500 and 1600°C). The maintained heating rate was 400°C per hour. The desired temperature of the process was reached and held for 30 minutes, and lime samples heated up to the same temperature, respectively, were added to limit the thermal buoyancy.

Samples from calcium oxide and lime were prepared in the form of cylinders using Carl Zeiss press machine with the pressure of 7 tons per cm². To improve strength and reduce porosity of the material all samples were calcined at 1400°C for 20 min before the experiment. In order to eliminate the temperature gradient, lime samples were heated up to chosen temperatures (1300, 1400, 1500 and 1600°C) and immersed into molten slag of same temperature. By limiting the working crucible with protective shell - large size crucible, a stable state of the melt was maintained to avoid temperature fluctuations in the process.

Calcium oxide and lime samples with mass ranging from 1.2725 to 1.6482 g, height 7-10 mm and diameter 22-24 mm were immersed in the molten slag. After predetermined time intervals samples were removed, cooled down to the room temperature and weighed on an analytical balance. After removing lime sample from the melt, content of the crucible was quenched; slag saturated with CaO was removed, triturated and analyzed to determine the content of CaO, MgO and other elements. The concentration of calcium and magnesium in the slag samples was investigated by X-ray fluorescence method using energy-dispersive X-ray fluorescent spectrometer PANalytical Epsilon 3. By measuring the mass of dissolved lime in the slag, a change in sample dimensions and the measurement of the concentration of calcium and magnesium oxides in the slag, mass transfer coefficients were calculated.

7 Refractory materials used in the metallurgical experiment

Refractory materials of crucibles must be chemically stable and chemically inert. Most thermodynamically stable compounds are characterized by the minimum value of isobaric thermodynamic potential change (Gibbs energy). These oxides include [55]:

- MgO, $\Delta_f G = -710$ KJ
- Al₂O₃, $\Delta_f G = -718$ KJ
- ZrO₂, $\Delta_f G = -745$ KJ
- BeO, $\Delta_f G = -842$ KJ
- CaO, $\Delta_f G = -845$ KJ
- ThO₂, $\Delta_f G = -895$ KJ

where $\Delta_f G$ – is Gibbs energy of oxide formation at T = 1873 K per 1 mole of oxygen for the reaction of oxide formation:

- 2Mg+O₂= 2MgO sol
- 2Al + O₂=0.5 Al₂O₃ sol
- Zr+O₂=ZrO₂ sol
- 2Be+O₂= 2BeO sol
- 2Ca+O₂=2CaO sol
- Th+O₂=ThO₂ sol

Properties of the most commonly used refractory materials are presented in Table 7-1. [55]

Table 7-1: Properties of the refractory materials [55]

Refractories composition, %	T, °C melting, and max operation		Real density, g/cm ³	Specific heat capacit, J/(g·K) 20-1000 °C	Specific electrical resistance, Ohm·cm at 20 °C 1000 °C		Thermal resistance
Sintered Al ₂ O ₃ , 99.9	2030	1950	3.97	1.09	>10 ¹⁴	10 ⁸	very good
Sintered MgO, 99.8	2800	1900	3.58	1.05	>10 ¹⁴	10 ⁷	low
Sintered CaO, 99.8	2600	2000	3.32	0.96	>10 ¹⁴	10 ⁶	low
Sintered BeO, 99.8	2570	1900	3.03	2.10	>10 ¹⁴	10 ⁸	very good

Sintered TiO_2 , 99.5	1840	1600	4.24	0.84	$5 \cdot 10^{-6}$	$25 \cdot 10^{-6}$	excellent
Sintered ZrO_2 92; HfO_2 4; CaO 4	2550	2200	5.61	0.59	$>10^8$	500	satisfactive
Sintered mullite Al_2O_3 72; SiO_2 28	1810	1750	3.03	1.05	$>10^{14}$	-	good
Sintered forsterite Mg_2SiO_4 , 99.5	1885	1750	3.22	0.96	$>10^{14}$	10^6	low
Sintered ThO_2 , 99.8	3050	2500	10.0	0.25	$>10^{14}$	10^5	low
High-alumina porcelain 95 Al_2O_3 , SiO_2 5	1750	1500	3.75	1.09	$>10^8$	10^4	very good
High quality fireclay Al_2O_3 45, SiO_2 55	1750	1650	2.1	1.09	10^8	10^4	low
Magnesia bricks MgO 83-93, FeO 2-7	2100	1750	3.2	1.05	10^8	10^5	excellent

In the laboratory practice pure alumina as well as alumina based refractories are often used. Laboratory crucibles are often made from different pure oxides or mixtures of oxides: Al_2O_3 , BeO , MgO , SiO_2 , CaO , ZrO_2 and ThO_2 .

Al_2O_3 is stable in the air at the temperatures up to 1700°C and in atmosphere of water vapor, hydrogen, argon, carbon monoxide, nitrogen and in vacuum. Al_2O_3 reacts with hydrogen sulfide.

BeO is stable when heated in the air, in vacuum and is unstable in the atmosphere of water vapor in the presence of halogens or sulfides.

MgO is stable in the air, nitrogen, CO , in vacuum, Ar , H_2 , NH_3 atmosphere and is unstable in the halogen atmosphere and in the presence of sulfur or carbon.

ZrO_2 and ThO_2 are stable in oxidizing atmospheres and unstable in the presence of halogens, sulfur, and carbon or at high temperatures.

CaO is a stable oxide but due to the absorption of moisture from the air quickly becomes unstable.

Refractories containing SiO_2 are stable in an oxidizing atmosphere, however in a reducing atmosphere or in a carbon atmosphere volatile silicon monoxide SiO is generated.

Industry offer wide variety of refractories that can be applied in laboratory practice. The most frequently used is chamotte which has a good resistance to the liquid metals and has high thermal insulating properties.

For laboratory practice it is also recommended to use fireclay bricks containing from 46 to 60 % of alumina. Heat resistance of these materials is up to 1600°C - 1800°C .

Magnesite bricks consisting of 6-7% of technical alumina and 93-94% of sintered magnesite powder including MgO up to 89-92% and they are used very often.

Crucibles made of magnesium oxide or electrofused magnesite are suggested for liquid melts containing FeO. Such crucibles are well resistant against liquid slags and metals. Fused magnesia is produced by melting of sintered magnesite in electric arc furnaces.

Electrofused magnesite has high resistance to heat and slag at high temperatures. For instance, it is used to manufacture crucibles for estimating mass transfer properties in melts at 1200-1600°C. The crucibles containing minimum 97 % of MgO have a low porosity of 5 % and are stable at temperatures above 2000 °C.

Fused magnesite is resistant towards slags containing iron. Solubility of MgO in slag systems FeO-SiO₂ and FeO-P₂O₅ is only 0.5-1.11 %.

For liquid melts containing FeO it is also advised to utilize platinum alloy crucible with rhodium.

Crucibles prepared from pure oxides, such as alumina, ZrO₂ and ThO₂ are often used in the laboratory. Such refractory materials can withstand temperatures up to 2000 °C and be in the operation up to 2300 °C. Manufactured ZrO₂ crucibles contain 90 % of ZrO₂, 7 % CaO and 0.1% FeO. Crucibles of ZrO₂ and ThO₂ are recommended for the acidic slags.

In metallurgical practice corundum crucibles and lime crucibles are also used. However, good adhesion of lime particles is required in the manufacture process of lime crucibles. Therefore, very pure lime and 1 % of Cr₂O₃ should be used to produce crucibles resistant to the temperatures up to 2000 °C.

For metallurgical experiments boron nitride crucibles can be employed. Crucibles from boron nitride have high thermal stability and resistance to thermal shock, which makes these crucibles most suitable materials for use in the heat treatment processes.

Tungsten nitride crucibles are also introduced in the laboratory practice. Tungsten nitride crucibles do not contain moisture and organic impurities; cannot be wetted by most of molten metals. In addition, tungsten nitride crucibles are chemically resistant to halides and other reagents. A number of these properties make them ideal for use in the process of melting a variety of metals and alloys. [55, 56]

7.1 The results of experimental studies for the crucible material choice

The choice of the crucible material was based on the following requirements:

- Inertness of the material and absence of chemical reactions with slag components
- The availability of heat-resistant materials in the retail
- The cost of heat-resistant materials

- The possibility of the destruction of crucible after cooling and extraction of the components without requiring special equipment
- The operational ability for the required time

The following materials were selected to investigate the chemical inertness of crucible materials for slag melting process: corundum, boron nitride, quartz with modification of cristobalite and fused magnesia crucibles (see Figure 7-1). Pictures of crucibles after slag melting are presented in figures 7-2, 7-3 and 7-7.



Corundum crucible



Boron nitride crucibles



Quartz crucibles



Fused magnesia crucibles



Figure 7-1: General view of crucibles subjected for the study of the interaction of crucible material with slag



Figure 7-2: Pictures of broken BN crucible after test with LD slag at 1500°C

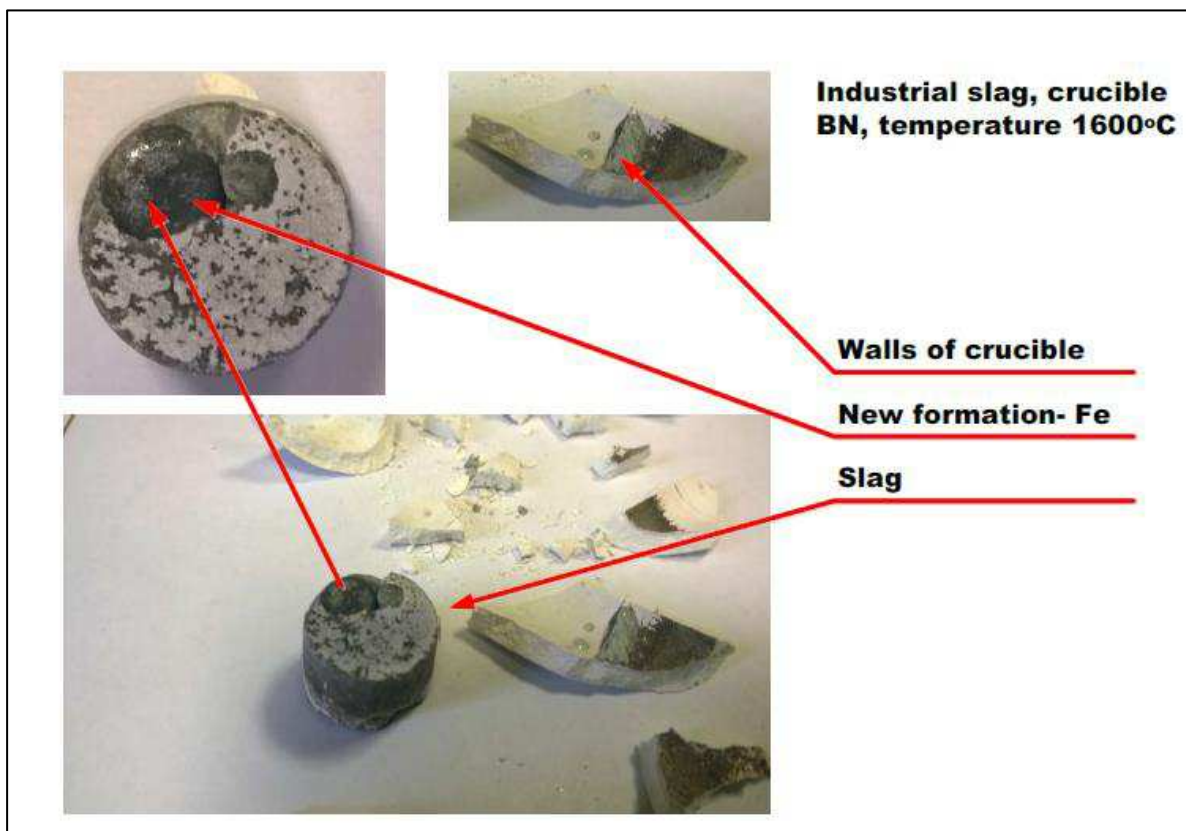


Figure 7-3: Pictures of broken BN crucible after test with LD slag at 1600°C

In the process of melting of industrial slag in the corundum and in boron nitride crucible chemical reaction occurred between the components of slag and crucible material.

In the boron nitride crucible after heat treatment the damage is not observed, however, the extraction of slag requires special equipment. The destruction of crucible walls using laser with a power of 20 W did not allow the complete removal of the crucible content in order to carry out the analysis. A pressure of 20 ton/cm² was applied to break the crucible after laser operation. During visual inspection of boron nitride crucible after the experiment a new formation which looked like elemental iron was found and diagnosed by X-ray analysis method. Figure 7-4 shows the spectrum of the slag after heat treatment without new formation.

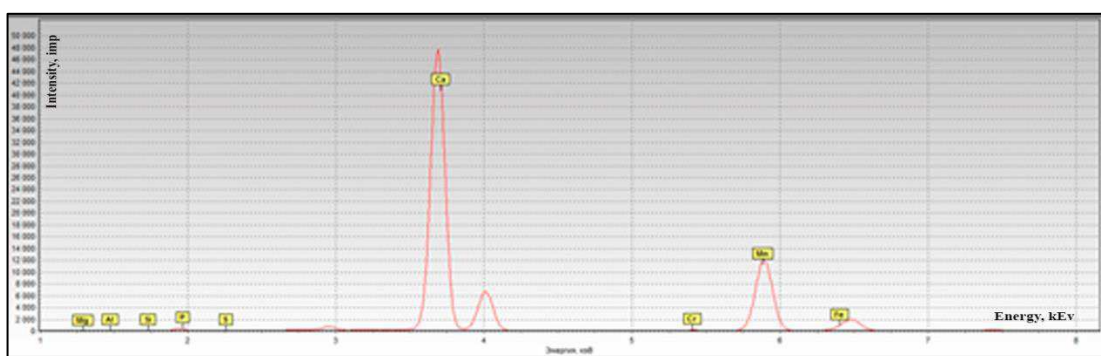


Figure 7-4: Characteristic X-ray spectrum of industrial slag after heat treatment in the BN crucible without new formed structure

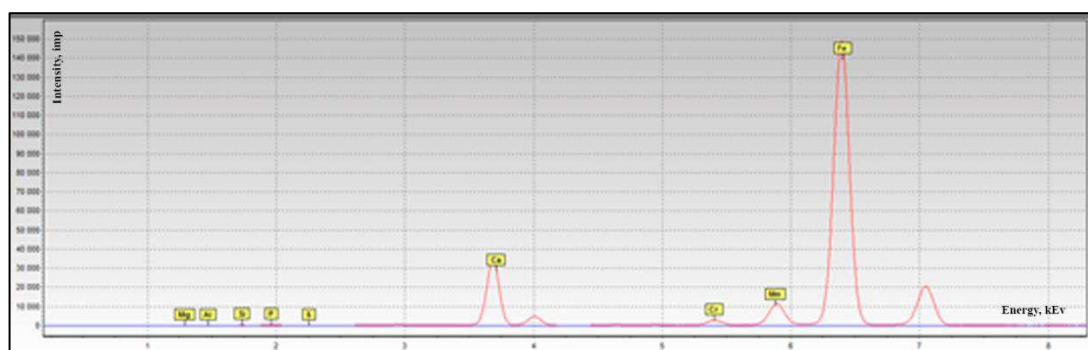


Figure 7-5: Characteristic X-ray spectrum of new structure formed after heat treatment of industrial slag in the BN crucible

According to the results of X-ray analysis in the sample of fused slag iron content has decreased, while in the new formed structure iron concentration increased significantly.

After examination of magnesia crucible partial insignificant diffusion of molten slag in the crucible material can be visually observed. It was not possible to remove the slag from the crucible without involvement of laser and cutting equipment. The operation of the extraction of solid crystallized slag was hard to implement and faced

number of difficulties. Figure 7-6 shows the spectrum of the slag sample after melting in MgO crucible.

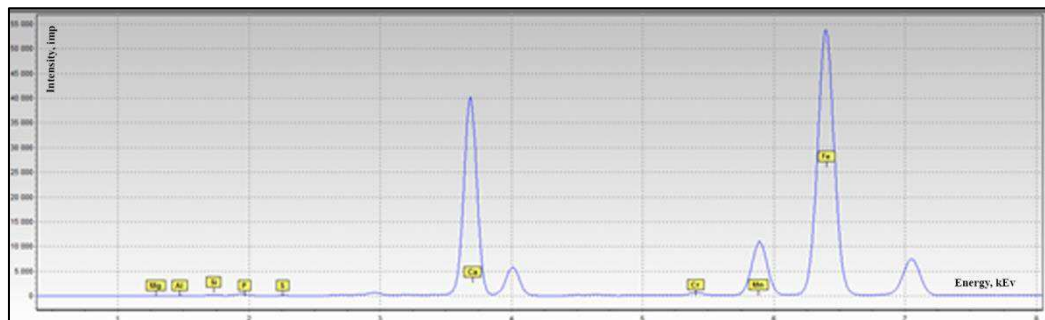


Figure 7-6: Characteristic X-ray spectrum of industrial slag after heat treatment in magnesia crucible

An increase in the silicon content in samples is not observed on the radiographs compared to the initial concentrations, and at the same time there is no raise in the magnesium, phosphorus and sulfur contents in the samples of fused slag.



Figure 7-7: Parts of MgO crucible with industrial slag at 1500°C and 1600°C

Figure 7-8 shows photographs of quartz crucibles after melting of slag at the range of temperatures. According to the visual inspection the interaction of crucible material with slag starts at temperature of 1600°C.



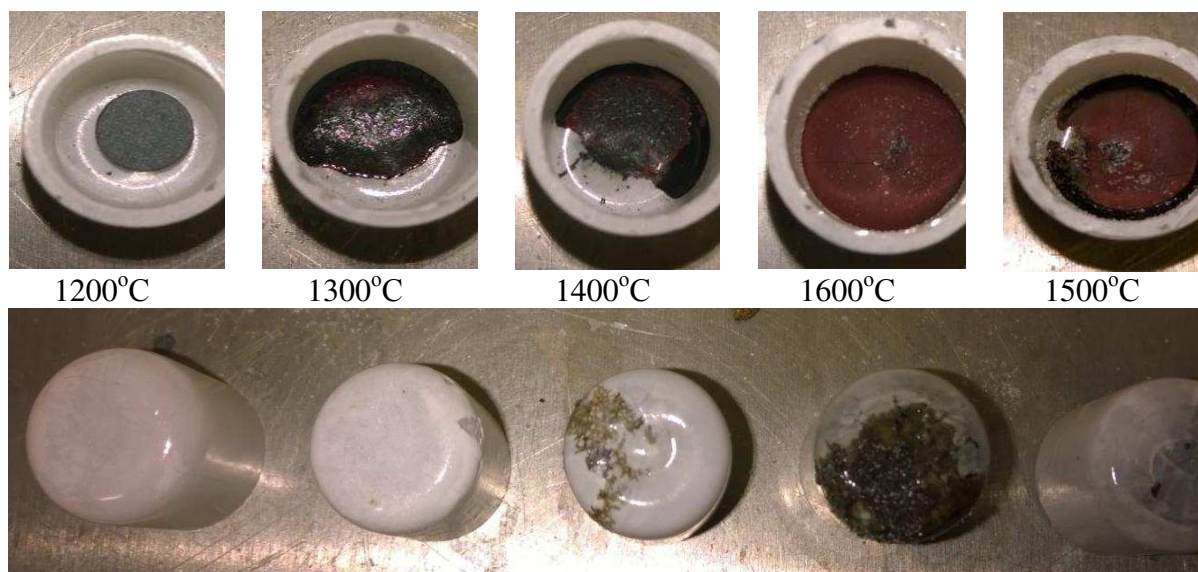


Figure 7-8: Visual control of interaction between slag and crucible at different temperatures and defect of crucible after melting

Cristobalite phase in slag after melting process in cristobalite crucibles was detected by X-ray analysis method only at the melting temperature above 1600°C.

Figure 7-9 presents the comparison of XRD spectrums of slag melted at 1500°C in MgO and in SiO₂ crucibles. The spectrum shows no MgO or cristobalite phases. Figure 7-10 demonstrates the results of qualitative XRD analysis on the presence of SiO₂ in the slag samples in the form of cristobalite which has transited into the slag at temperatures above 1600°C.

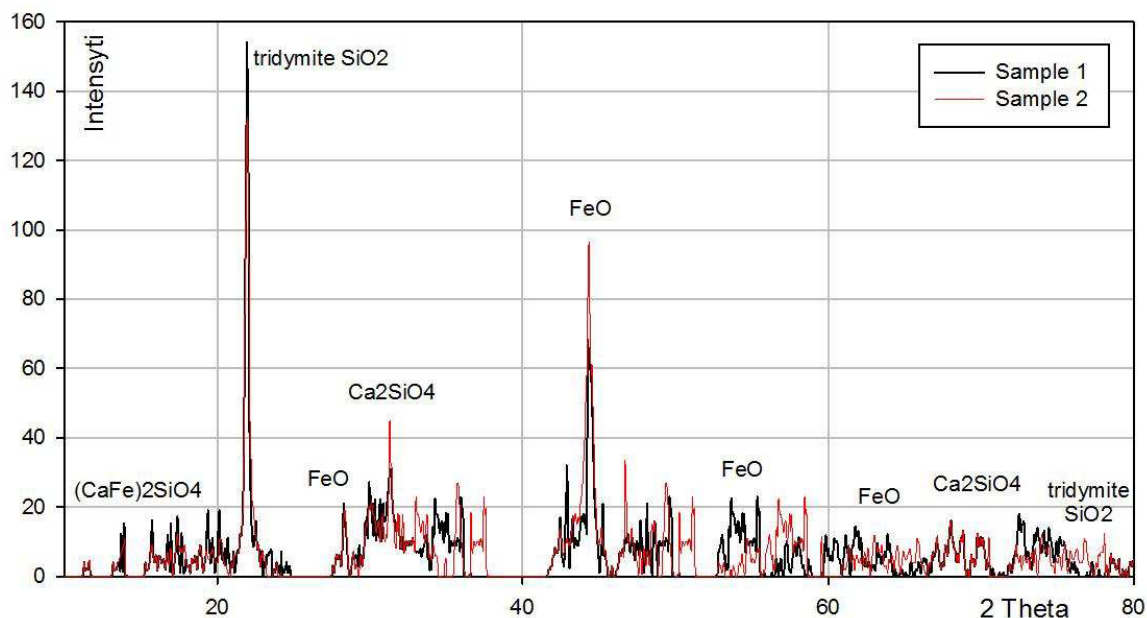


Figure 7-9: Crucible from electrofused magnesite, 2 –Crucible from silica modified to cristobalite

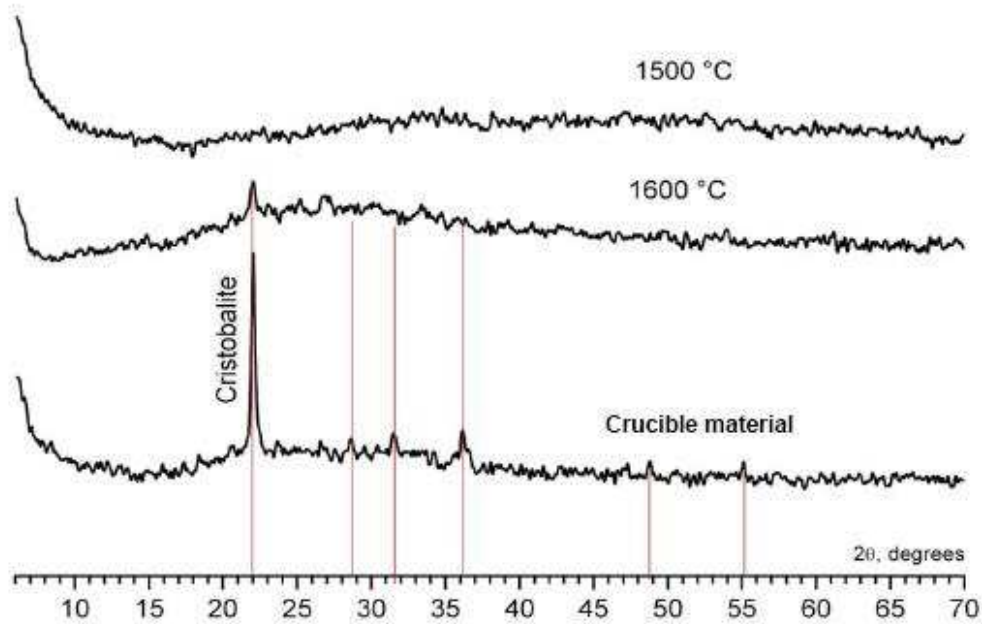


Figure 7-10: The results of qualitative XRD on the presence of cristobalite in the samples of industrial slag

Samples of slag melted in quartz crucibles were thoroughly grinded and analyzed by X-ray fluorescence method in order to support the results derived.

Figure 7-11 shows the spectrum in the range of light elements of the industrial slag without heat treatment and in Figure 7-12 spectrum of slag after heat treatment in Quartz crucibles at 1500°C is presented.

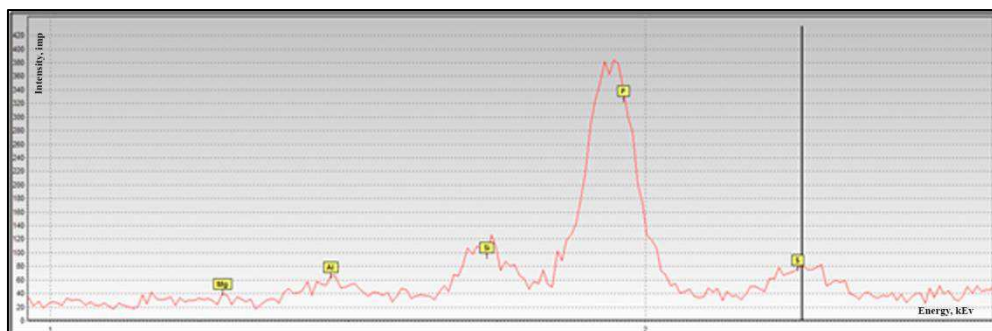


Figure 7-11: Characteristic X-ray spectrum of industrial slag without heat treatment

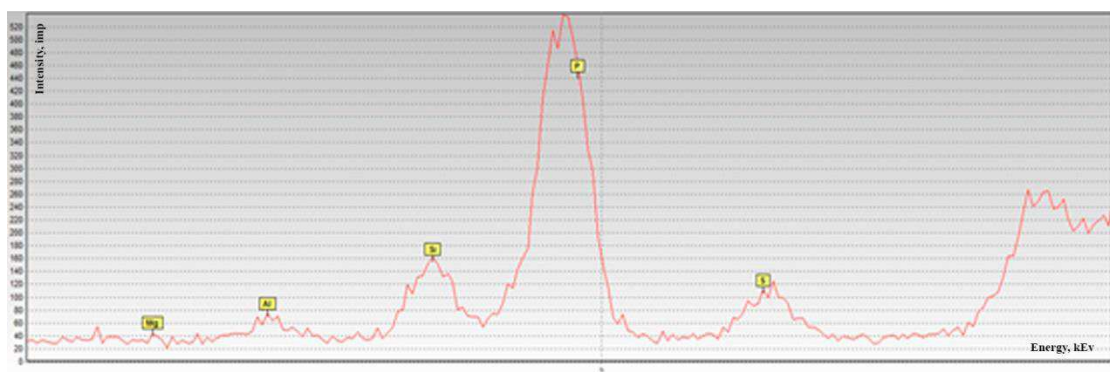


Figure 7-12: Characteristic X-ray spectrum of industrial slag after melting at 1500°C in a quartz crucible

According to the RFA results, silicon content in slag samples after melting in quartz crucibles match with its original content in slag and is consistent with the results of X-ray diffraction analysis.

The summarized intensities of slag samples melted in various crucibles are presented in the Table 7-2.

Table 7-2: Intensities of slag melted in various crucibles at 1500°C

Name of the sample	Intensity of Ka series								
	Mg	Al	Si	P	S	Ca	Cr	Mn	Fe
Industrial slag № 1, before heat treatment	46	110	520	460	90	37500	530	8100	37600
Quartz crucible	88	105	1684	130	70	35100	200	520	29920
MgO crucible	40	75	180	440	110	40000	700	11000	54000
Boron Nitride crucible	50	75	150	540	100	48000	210	12100	2000
New formed structure	40	90	130	400	80	34240	2760	11200	150000
Cruciblewalls	60	50	50	30	30	40	30	60	60
Other slag parts	50	75	190	530	110	49900	160	9800	1700

Figure 7-13 presents the distribution of elements with respect to the intensity. According to the results it is evident from the graph, the new formed structure in the BN crucible conforms to pure iron, which occurred due to the chemical reaction between crucible and slag.

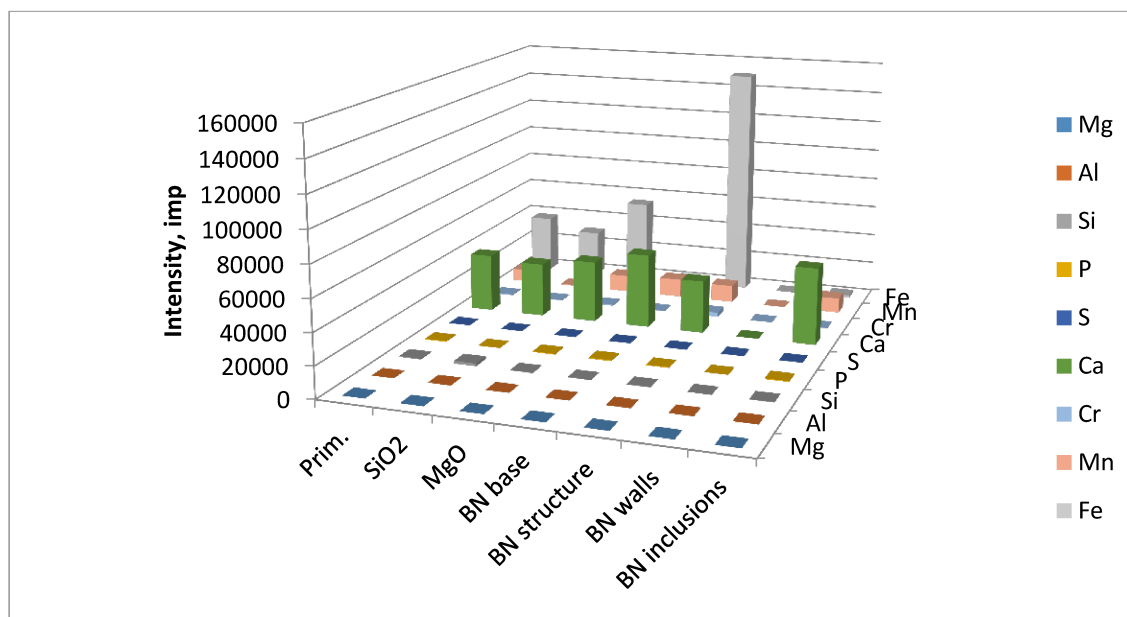


Figure 7-13: The distribution of elements according to the intensity

Table 7-3 presents the comparison of all phases detected by XRD method in the industrial slag after melting in SiO₂, MgO and BN crucibles. Phase composition of slag after melting in quartz crucible matches with its composition after melting in magnesia crucible. However, after test in BN crucible a large number of different phases occurred.

Table 7-3: Detected phases of industrial slag after melting at 1500°C in different crucibles: quartz, magnesia and boron nitride

Detected phase after melting in quartz crucible	Detected phase after melting in magnesia crucible	Detected phase after melting in Boron nitride crucible	The name of the phase
$\text{Ca}_2\text{Fe}_2\text{O}_5$	$\text{Ca}_2\text{Fe}_2\text{O}_5$	-	Brownmillerite
Mg_2SiO_4	Mg_2SiO_4	Mg_2SiO_4	Magnesium Silicate
Fe_2O_3	Fe_2O_3	Fe_2O_3	Hematite
$\text{CaMn}_6\text{SiO}_{12}$ ($\text{CaO} \cdot 3\text{Mn}_2\text{O}_3 \cdot \text{SiO}_2$)	$\text{CaMn}_6\text{SiO}_{12}(\text{CaO} \cdot 3\text{Mn}_2\text{O}_3 \cdot \text{SiO}_2)$	$\text{CaMn}_6\text{SiO}_{12}$ ($\text{CaO} \cdot 3\text{Mn}_2\text{O}_3 \cdot \text{SiO}_2$)	Calcium Manganese Silicon Oxide Neltnerite
$\text{MnMn}_6\text{SiO}_{12}$ ($\text{MnO} \cdot 3\text{Mn}_2\text{O}_3 \cdot \text{SiO}_2$)	$\text{MnMn}_6\text{SiO}_{12}$ ($\text{MnO} \cdot 3\text{Mn}_2\text{O}_3 \cdot \text{SiO}_2$)	$\text{MnMn}_6\text{SiO}_{12}$ ($\text{MnO} \cdot 3\text{Mn}_2\text{O}_3 \cdot \text{SiO}_2$)	Manganese Silicate Braunite-1 Q

Ca Mn_{11.62} Fe_{2.38}Si O₂₄(CaO·xMn₂O₃· yFe₂O₃·SiO₂)	Ca Mn_{11.62}Fe_{2.38}Si O₂₄ (CaO·xMn₂O₃· yFe₂O₃·SiO₂)	Ca Mn_{11.62} Fe_{2.38}Si O₂₄ (CaO·xMn₂O₃· yFe₂O₃·SiO₂)	Calcium Manganese Iron Silicate Braunite
Mn₂O₃	Mn₂O₃	Mn₂O₃	Manganese Oxide
-	MgO	-	Magnesium oxide
Ca₅(PO₄)₂(SiO₄)	Ca₅(PO₄)₂(SiO₄)	-	Calcium Phosphate Silicate
FeMnO₃	FeMnO₃		Iron Manganese Oxide Bixbyite
	Ca₂SiO₄		Calcium Silicate
-	-	Fe (after breaking the crucible pure iron formation was found)	
-	-	FeSiO₃	Iron Silicate Nontronite
-	-	MnSi	Manganese Silicon
-	-	Ca₂P₂O₇	Calcium Phosphate
-	-	FePO₄·FeO	Iron Phosphate
-	-	Fe₂SiO₄	Iron Silicate Fayalite
SiO₂	-	-	Cristobalite

Based on the laboratory experimental research carried out in this thesis, the following conclusions can be made:

1. The material of magnesia crucibles does not affect the thermal treatment of industrial slag at 1500°C, but it requires special equipment for breaking the crucible. Considering the high cost of magnesia crucible (about 200 euros per piece), the complexity of extracting slag and only single use of crucible, it is not reasonable to use it for kinetic studies.
2. It is observed that after heat treatment in a crucible made of boron nitride new structure of pure iron was formed. The disadvantages of the use of this material should also include the complexity of slag extraction from the crucible and high cost (around 200 euros per piece).
3. Due to the absence of cristobalite phase in the composition of slag samples melted at temperatures 1300-1500°C it is reasonable to use quartz crucibles for the metallurgical experiment and kinetic studies. The advantages of quartz crucibles include the low cost of the material, the availability of purchase, easy extraction and separation of the crystallized slag from the crucible. Crucibles made of SiO₂, can be utilized to study the dissolution kinetics of calcium oxide, lime and magnesium in slags.

8 Experimental results of the study of slag phase transformations

The change in phase composition of model slag is studied here in order to investigate the formation of chemical compounds that influence the mass transfer coefficient value of lime dissolution in slag. Methods for determining the phase composition described in Chapter 6.2.

The experimental results are compared with calculations of ternary phase diagram FeO - CaO - SiO₂ (see Figure 8-1) and literature data. [57]

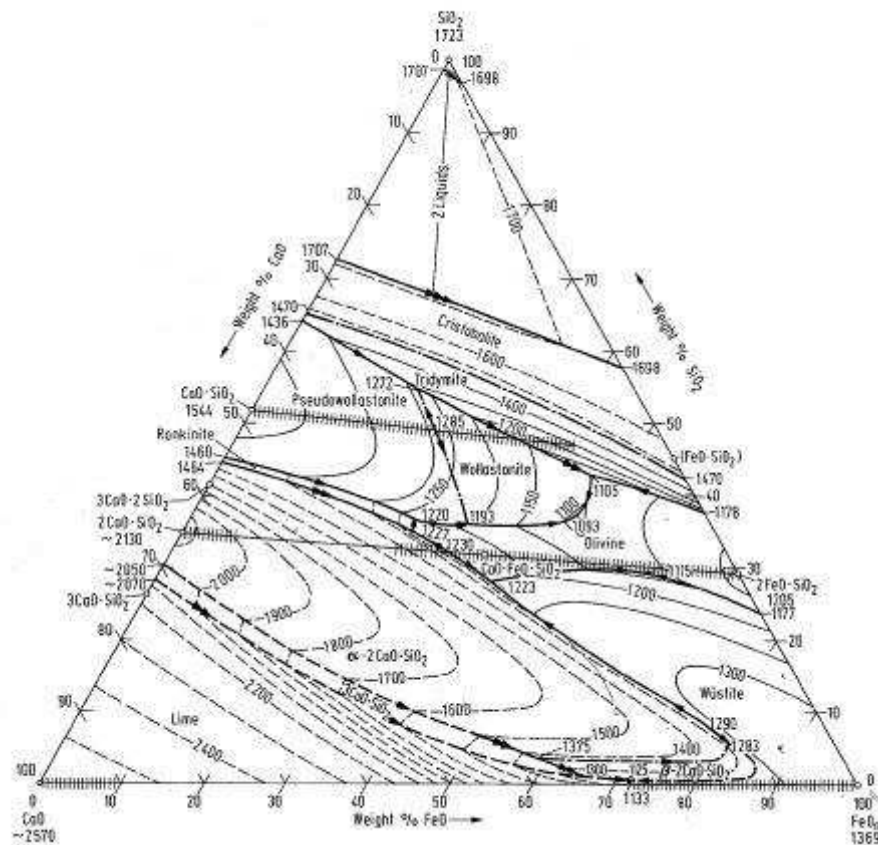


Figure 8-1: Ternary diagram of the system CaO - FeO - SiO₂ [57]

Model slag №1 has the following composition: 40% CaO, 25% FeO; 35% SiO₂. The X-ray spectrums of model slag №1 are presented in Figures 8-2, 8-3 and 8-4.

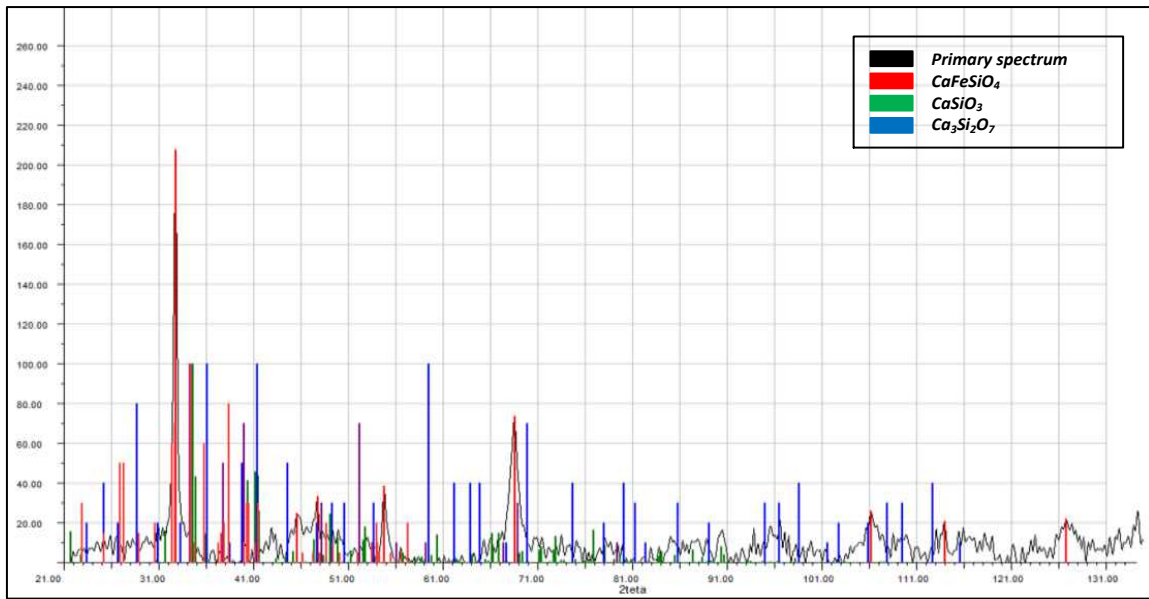


Figure 8-2: The X-ray spectrum of model slag №1 melted at 1400°C for 30 min

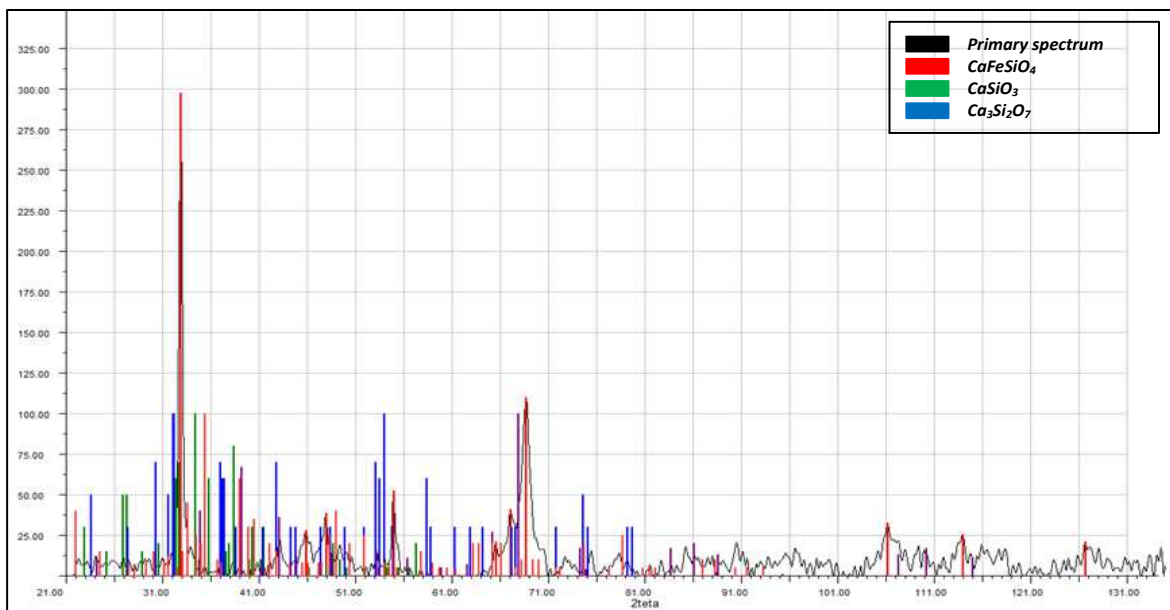


Figure 8-3: The X-ray spectrum of model slag №1 melted at 1500°C for 30 min

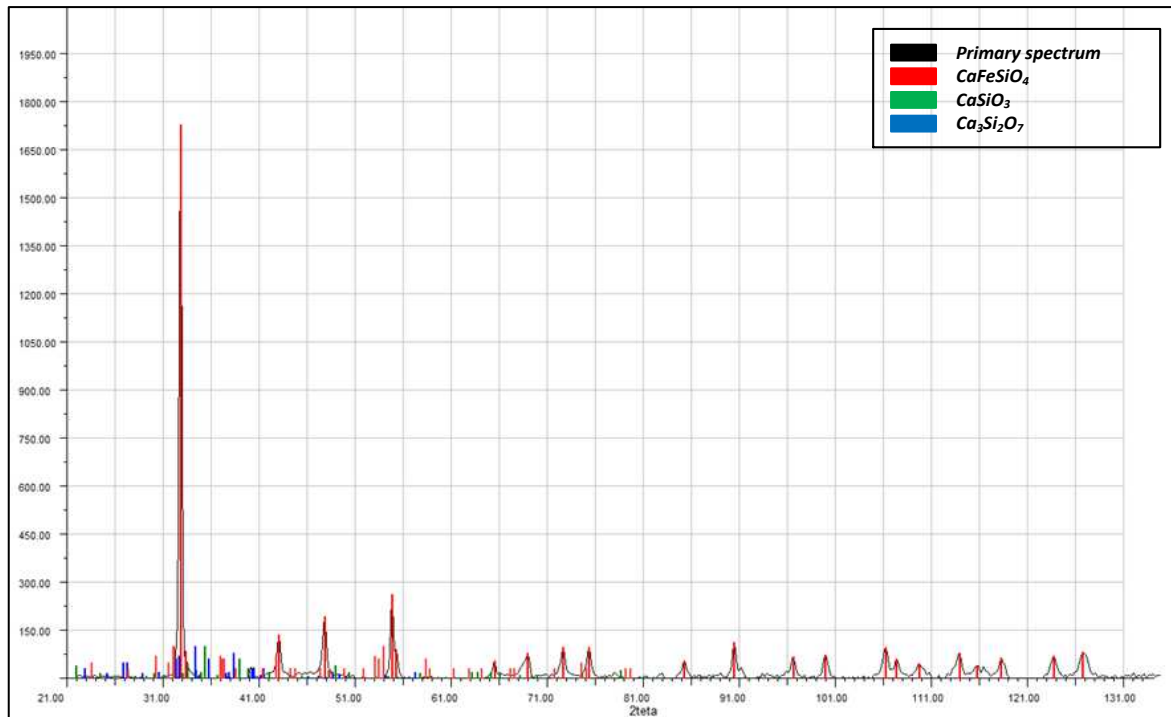


Figure 8-4: The X-ray spectrum of model slag №1 melted at 1600°C for 30 min

Three phases were identified according to the specified values of the reflection angles θ : $3\text{CaO}\cdot 2\text{SiO}_2$, $\alpha\text{CaO}\cdot\text{SiO}_2$, $\text{CaO}\cdot\text{FeO}\cdot\text{SiO}_2$ (see Table 8-1)

Table 8-1: Identified phases of model slag №1

№ of slag	Identified phase	Phase quantity, % by X-ray analysis		
		1400°C	1500°C	1600°C
1	$3\text{CaO}\cdot 2\text{SiO}_2$	9.07	9.88	16.1
	$\alpha\text{CaO}\cdot\text{SiO}_2$	15.12	37.77	67.6
	$\text{CaO}\cdot\text{FeO}\cdot\text{SiO}_2$	75.6	52.33	16.3

Analysis of the phase diagram of the system $\text{CaO} - \text{FeO} - \text{SiO}_2$:

A point of a given composition ($\text{CaO} \%$, 40; $\text{FeO} \%$, 25; $\text{SiO}_2 \%$, 35) corresponds to a melt containing components without the presence of solid phases in the range of the temperatures 1400 -1600°C. The given point is located in the area of elementary triangle: $2\text{CaO}\cdot\text{SiO}_2 - \text{CaO}\cdot\text{FeO}\cdot\text{SiO}_2 - \text{CaO}\cdot\text{SiO}_2$, where the crystallization of the solid phase starts at temperature of 1220°C in the eutectic point of the following composition: $\text{SiO}_2 - 37.0\%$; $\text{FeO} - 27.0\%$; $\text{CaO} - 36.0\%$. Three following phases crystallize from the melt of eutectic composition: $2\text{CaO}\cdot\text{SiO}_2$, $\text{CaO}\cdot\text{FeO}\cdot\text{SiO}_2$ and $\text{CaO}\cdot\text{SiO}_2$ according to the following phase reaction:

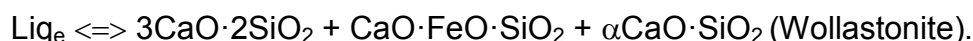


Table 8-2 presents the composition and number of phases of model slag №1 melted at 1400°C, 1500°C, and 1600°C obtained experimentally, calculations of the ternary diagrams and comparison with literature data.

Table 8-2: Identified phases of model slag №1 compared with phase diagram and literature

№ of slag	Identified phase	Phase quantity, % X-ray analysis			Phase quantity, % Ternary diagram calculations for 1600°C FeO - CaO - SiO ₂	Phase quantity in the literature, % [58]
		1400°C	1500°C	1600°C		
1	3 CaO·2 SiO ₂	9.07	9.88	16.10	21	-
	αCaO·SiO ₂	15.12	37.77	67.60	65	-
	CaO·FeO·SiO ₂	75.60	52.33	16.30	14	-
	2FeO·SiO ₂ olivin	-	-	-	-	42

Model slag №2 was prepared with the following content: CaO %, 30; FeO %, 35; SiO₂ %, 35.

The X-ray spectrums of model slag №2 are presented in Figures 8-5, 8-6 and 8-7.

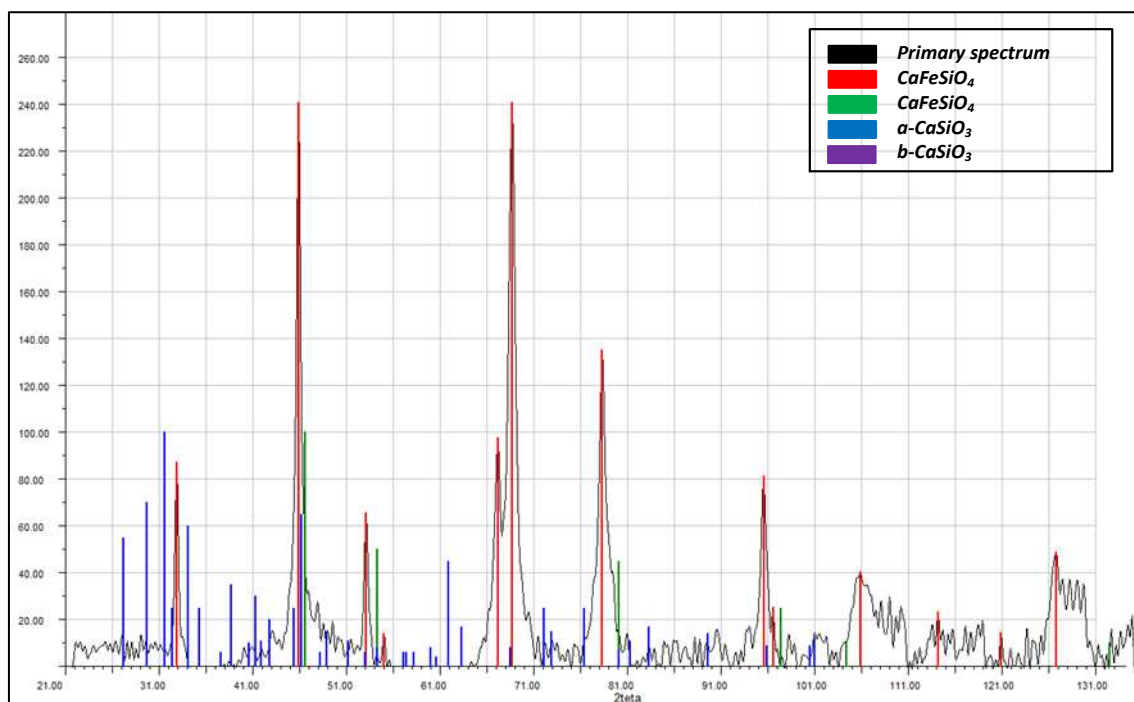


Figure 8-5: The X-ray spectrum of model slag №2 melted at 1400°C for 30 min

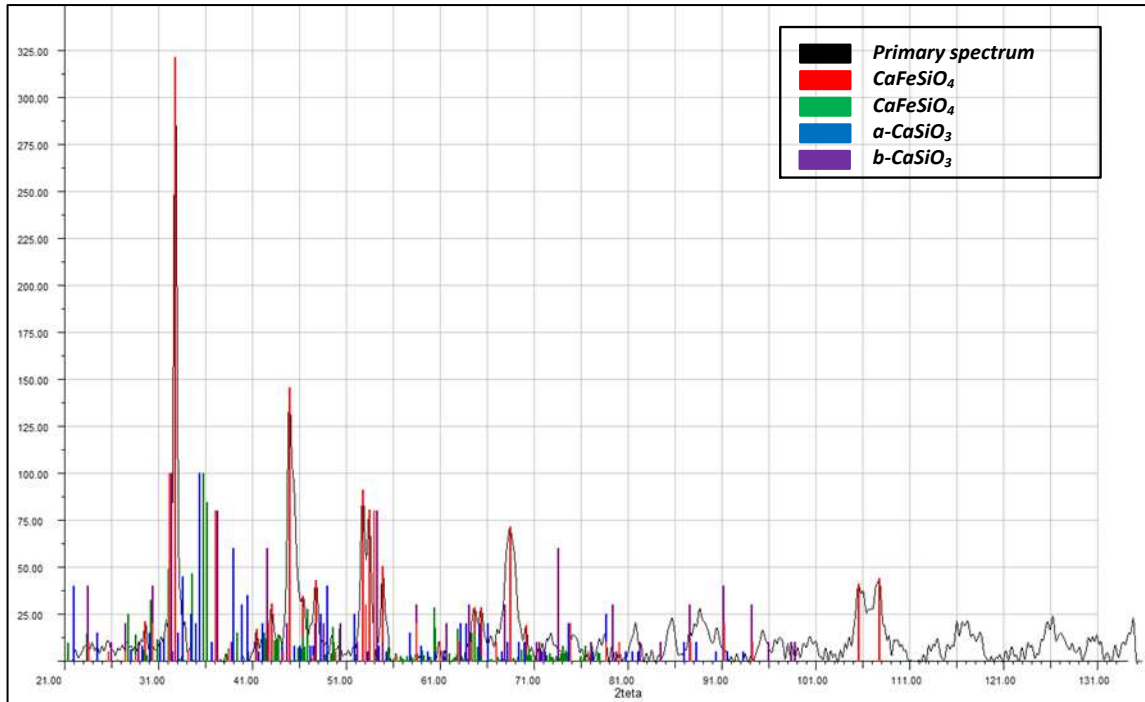


Figure 8-6: The X-ray spectrum of model slag №2 melted at 1500°C for 30 min

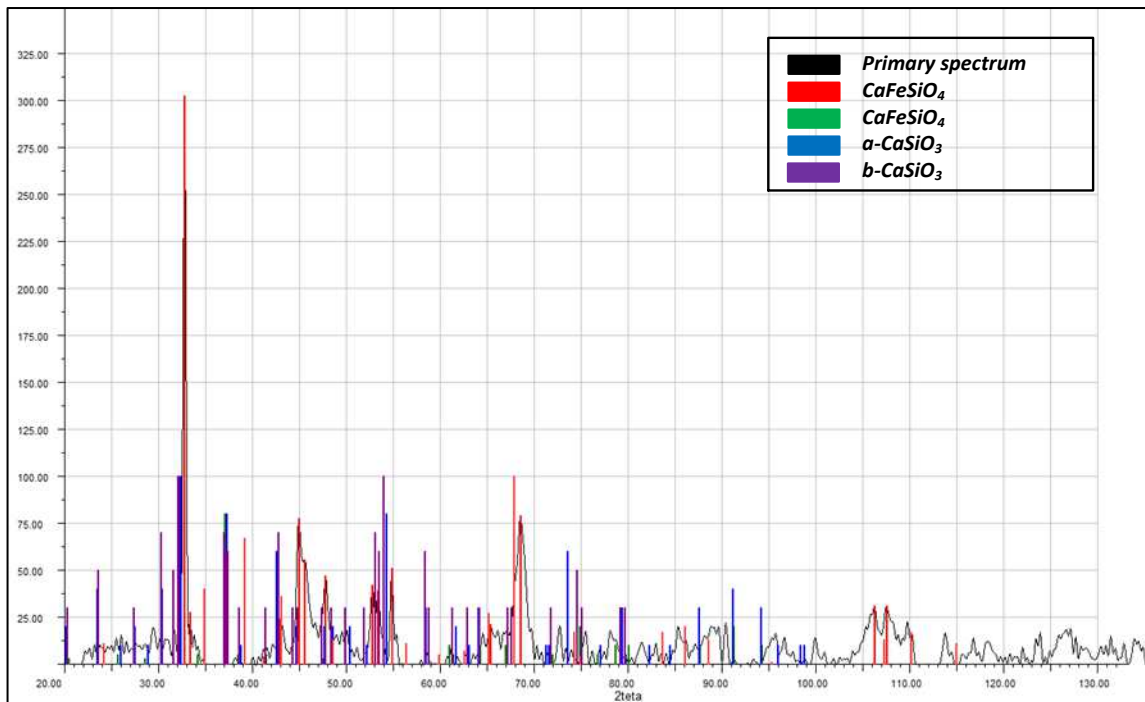


Figure 8-7: The X-ray spectrum of model slag №2 melted at 1600°C for 30 min

Three phases were identified according to the specified values of the reflection angles θ : $3 \text{ CaO} \cdot 2\text{SiO}_2$, $\alpha\text{CaO} \cdot \text{SiO}_2$, $\text{CaO} \cdot \text{FeO} \cdot \text{SiO}_2$ (see Table 8-3).

Table 8-3: Identified phases of model slag №2

№ of slag	Identified phase	Phase quantity, % X-ray analysis		
		1400°C	1500°C	1600°C
2	CaO·FeO·SiO ₂	66.2	66.4	66.9
	αCaO·SiO ₂	33.8	33.6	33.1
	βCaO·SiO ₂			

A point of a given composition (CaO %, 30; FeO %, 35; SiO₂ %, 35) is located in the area of crystallization from the melt of ternary chemical compound CaO·FeO·SiO₂ with a melting point at 1230°C. In the range of temperatures 1400°C-1600°C the melt containing 30% CaO, 35% FeO and 35% SiO₂ without solid phases. The given point is located in the area of elementary triangle: 2CaO·SiO₂ - CaO·FeO·SiO₂ - 2FeO·SiO₂, where the crystallization of the solid phase starts at temperature of 1193°C in the eutectic point of the following composition: SiO₂ - 36,0%; FeO - 34,0%; CaO - 30,0%. Three following phases crystallize from the melt of eutectic composition: 2CaO·SiO₂, CaO·FeO·SiO₂ and FeO according to the following phase reaction:



Table 8-4 presents the composition and number of phases of model slag №2 melted at 1400°C, 1500°C, and 1600°C obtained experimentally, calculations of ternary diagrams and literature data.

Table 8-4: Composition of model slag №2 compared with phase diagram and literature

№ of slag	Detected phase	Phase quantity, % X-ray analysis			Phase quantity, % Diagram calculations FeO - CaO - SiO ₂ at 1600°C	Phase quantity, % [58]
		1400°C	1500°C	1600°C		
2	CaO·FeO·SiO ₂	66.2	66.4	66.9	94	-
	αCaO·SiO ₂	33.8	33.6	33.1	6	Solid solution on the base of 97% CaO·SiO ₂
	βCaO·SiO ₂					
	2FeO·SiO ₂ olivin	-	-	-	-	57

Model slag №3 was prepared with the following content: CaO %, 40; FeO %, 35; SiO₂ %, 25. The X-ray spectrums of model slag №3 presented in Figures 8-8 and 8-9.

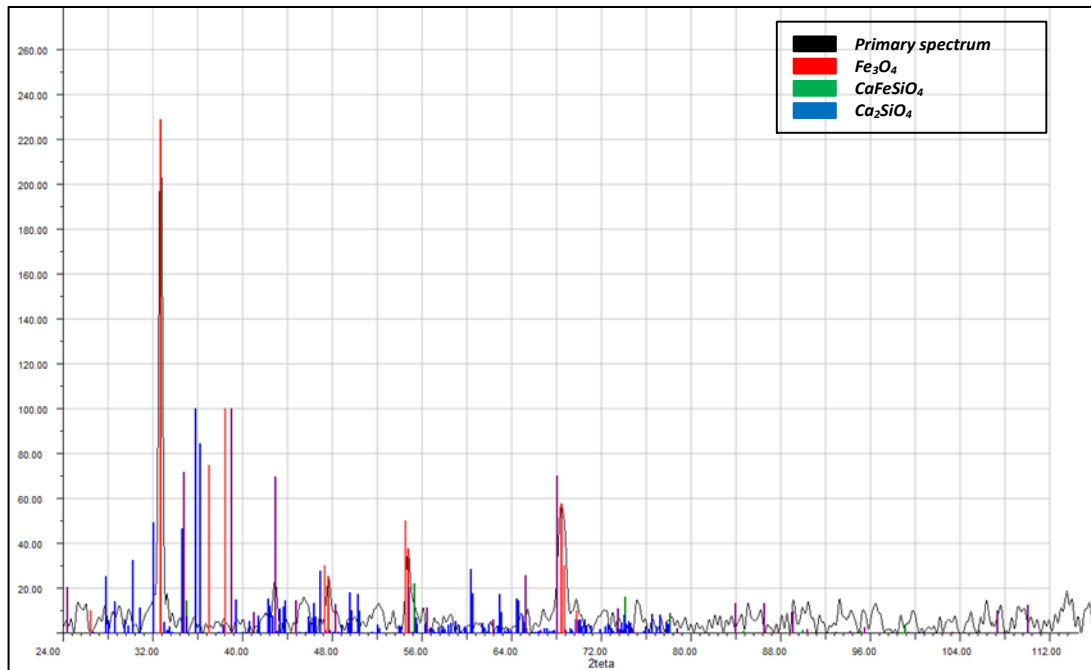


Figure 8-8: The X-ray spectrum of model slag №3 melted at 1500°C for 30 min

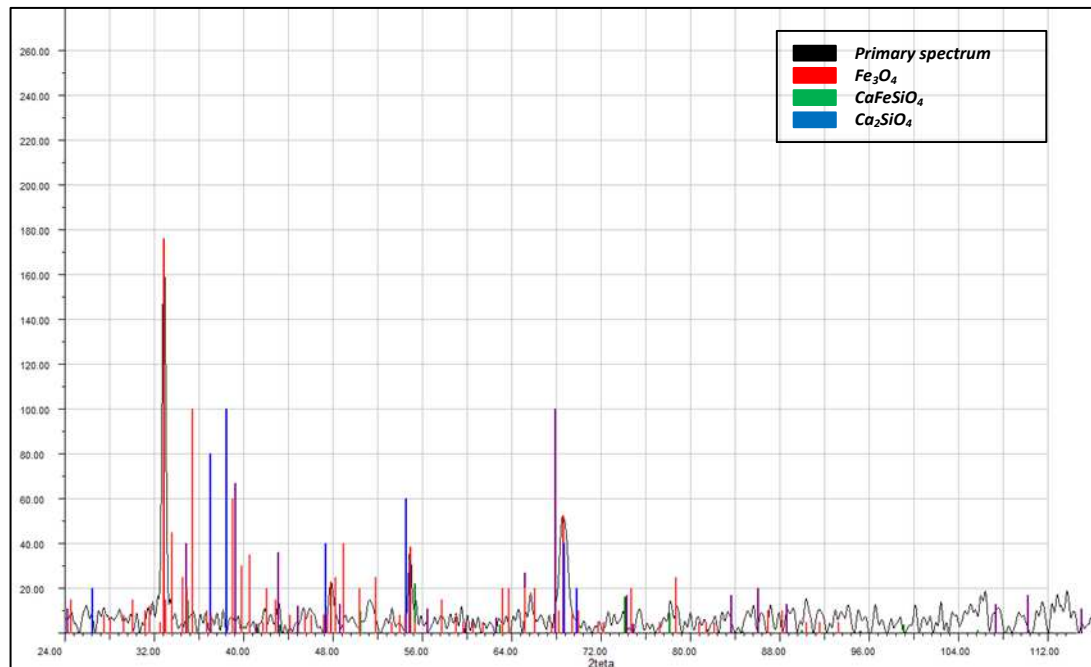


Figure 8-9: The X-ray spectrum of model slag №3 melted at 1600°C for 30 min

The analysis of the phase diagram of the system CaO - FeO - SiO₂:

A point of the following composition (CaO%, 40; FeO%, 35; SiO₂%, 25) is located in the area of crystallization from the melt of dicalcium silicate with a melting point at 2130°C. At the temperature of 1400°C the melt contains 35% CaO·SiO₂, at 1500°C content of CaO·SiO₂ in the melt decreases to 22% and at 1600°C – to 11%. Since the figurative point located in the area of elementary triangle: 2CaO·SiO₂ - CaO·FeO·SiO₂ – FeO, crystallization of the solid phase starts at temperature of 1223°C in the eutectic point of the following composition: SiO₂ - 30,0%; FeO - 40,0%; CaO - 30,0%. Three following phases crystallize from the melt of eutectic composition: 2CaO·SiO₂, CaO·FeO·SiO₂ and FeO according to the following phase reaction:

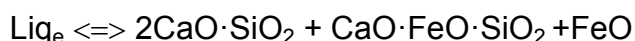
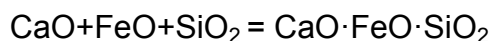
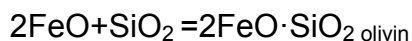
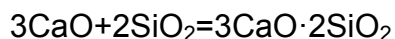
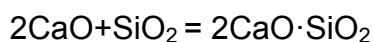
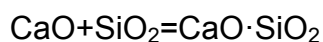


Table 8-5 presents the composition and number of phases of model slag №3 obtained experimentally, calculations of ternary diagram and literature data.

Table 8-5: Composition of model slag №3 melted at 1400°C, 1500°C, 1600°C compared with phase diagram and literature

№ of slag	Identified phase	Phase quantity, % X-ray analysis		Phase quantity, % Diagram calculations FeO - CaO - SiO ₂ at 1600°C
		1500°C	1600°C	
3	2CaO·SiO ₂	45.2	55.5	47
	CaO·FeO·SiO ₂	25.0	22.3	30
	FeO	25.8	22.2	22

Based on the experimental results, phase transformations take place between the main components of slag by the following chemical reactions during melting process:



Calcium and iron silicates are compounds with high melting point. However, the temperature of phase transformation is outside the experimental temperature range at which the kinetics of lime dissolution in the industrial slag is studied (1300°C - 1600°C).

The number of identified chemical compounds is in satisfactory agreement with the calculations of ternary phase diagram: CaO-FeO-SiO₂. Since calcium, iron and

silicon oxides are the main components of the industrial slag, silicates which are formed with melting points above 1500°C in the process of slag melting will affect the value of mass transfer coefficients of lime dissolution.

9 Experimental results of the study of CaO and lime dissolution in slags

In this Chapter the dissolution of pure calcium oxide and industrial lime in model and in industrial slag systems is studied.

The results of experimental study on the dissolution behavior of cylindrical samples of pure CaO in the model slag are presented in Table. 9-1. Figure 9-1 shows the dependence of the amount of the dissolved CaO sample on the contact time of sample with slag.

Table 9-1: The experimental results of the dissolution process of CaO samples in the model slag

№ of test	1300°C		1400 °C		1500 °C	
	Time, s	Mass of CaO dissolved in the slag phase, g	Time, s	Mass of CaO dissolved in the slag phase, g	Time, s	Mass of CaO dissolved in the slag phase, g
1	20	0.1859	20	0.1192	20	0.3778
2	30	0.1800	30	0.2124	30	0.5783
3	30	0.1967	30	0.2216	30	0.5744
4	45	0.2646	45	0.3017	45	1.0010
5	60	0.3529	45	0.3577	60	1.3011
6	60	0.3852	60	0.5185	60	1.3445
7	90	0.6554	60	0.7678	90	1.3889
8	120	0.7871	60	0.5795	120	1.4778
9	150	0.8843	90	0.8587	150	1.5045
10	180	0.9797	90	0.8735	180	1.5673
11	200	1.0248	120	1.1748	300	1.5334
12	300	1.0280	150	1.3085	-	-
13	-	-	180	1.2991	-	-
14	-	-	300	1.2557	-	-

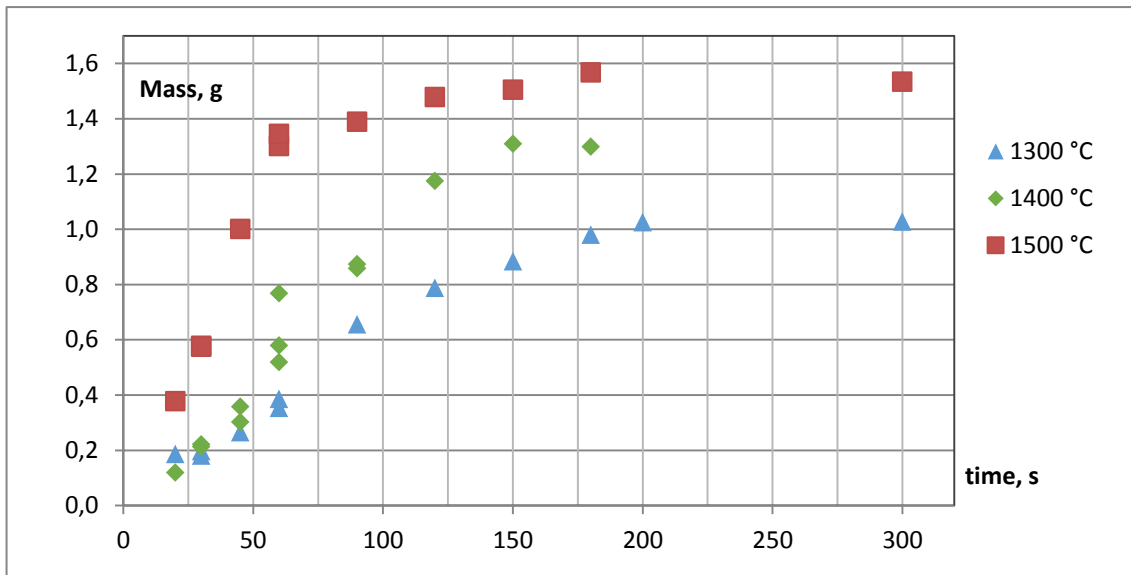


Figure 9-1: Dependence of the amount of dissolved CaO on the contact time of sample with the slag

According to experimental data derived the amount of dissolved CaO ceases to change after time interval of 150-160 seconds, which characterizes the saturation of the slag with calcium oxide. Equilibrium concentration of calcium oxide in the slag phase at 1300°C is 46-47%, 50-51% at 1400°C and 54-55% at 1500°C. This is close to the theoretic saturation values: 40-42% at 1300°C, 48-50% at 1400°C and 50-53% at 1500°C [57].

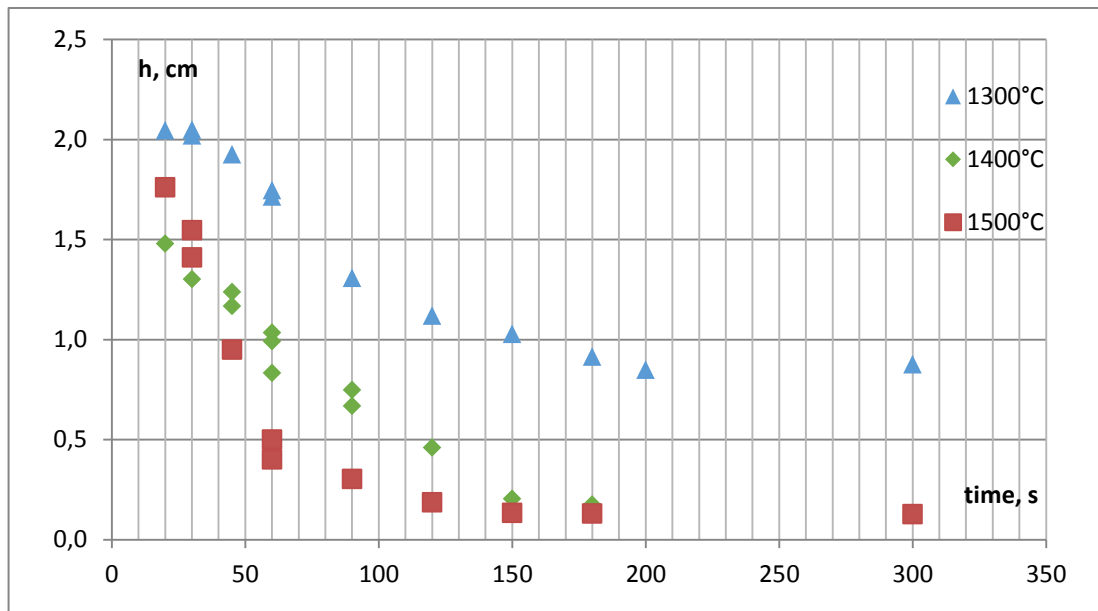


Figure 9-2: The dependence of Calcium oxide sample's height on time

It is evident from the experiment that with a contact time of more than 150 seconds there is no change in the linear dimensions of CaO samples. The relation between the linear rate of samples dissolution $\frac{\Delta h}{\Delta \tau}$ and the saturation concentration of CaO in slag derived (see Figure 9-3) indicates the diffusion regime of CaO dissolution process in the melt. With the increasing concentration of CaO in the slag the dissolution rate of samples drops which agrees with the main kinetic equation (4-34) and is explained by the decrease in the concentration gradient $(CaO\%)_{sat} - (CaO\%)$.

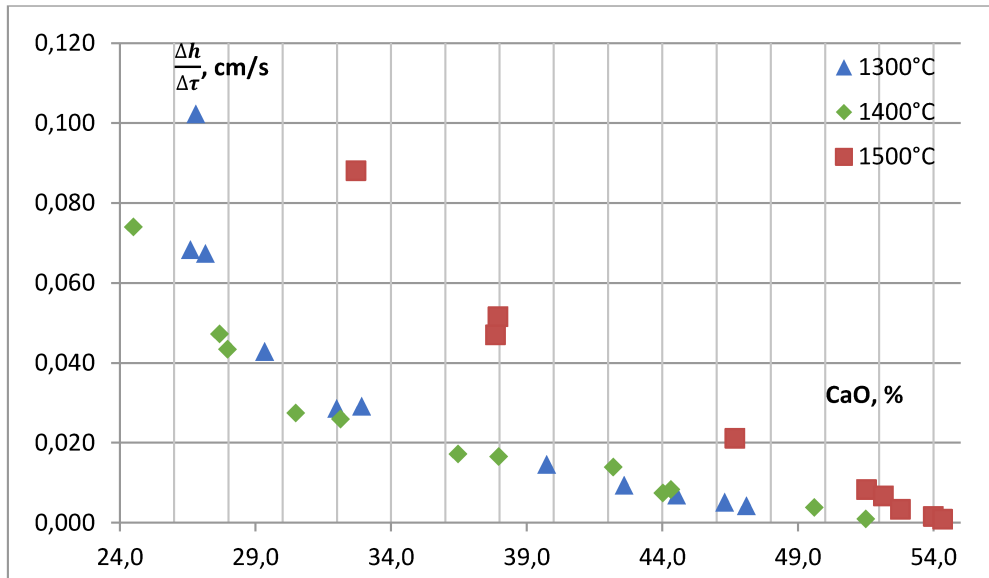


Figure 9-3: The dependence of the linear rate of CaO samples dissolution on the saturation of slag with calcium oxide

In the process of lime dissolution in slag the determination of dissolution kinetics is based on the measurement of the mass transfer coefficient. Figure 9-4 shows calculated values of mass transfer coefficients of CaO dissolution in the model slag using the experimental data and the kinetic equation (4-34) presented in Chapter 4.1.2.

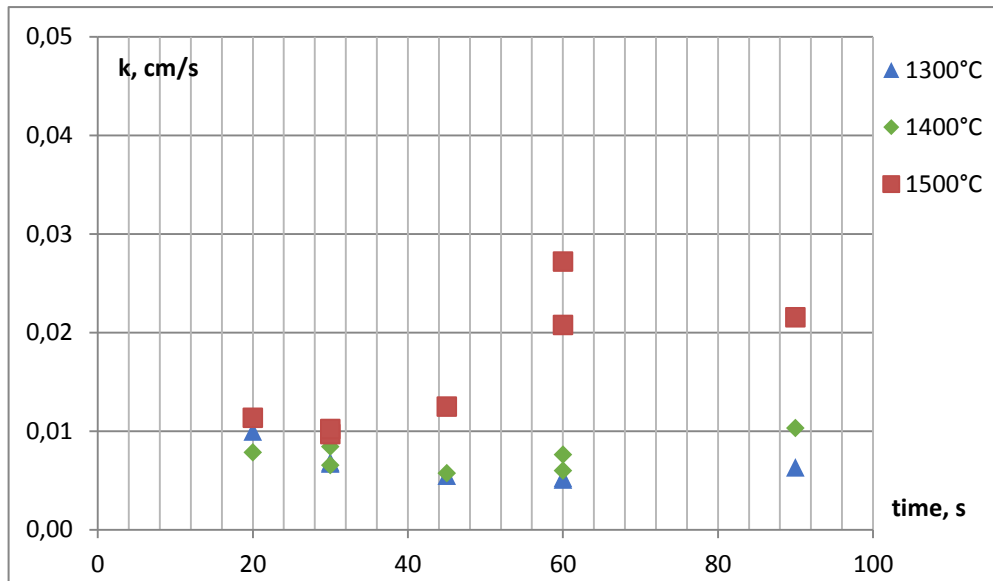


Figure 9-4: The dependence of the mass transfer coefficient values of CaO dissolution in model slag on the dissolution time

According to the results derived, in the dissolution process of CaO in the model slag the mass transfer coefficient raises with the decreasing sample size.

This behavior is explained by the two following factors: the decrease in the thickness of the boundary layer and the formation of chemical compounds between the components of model slag and calcium oxide. The mass transfer coefficient value depends on the particle size of lime, thus, during the dissolution of samples the thickness of the boundary layer drops leading to the raise in mass transfer coefficient.

Calculated average effective k values are: 0.0066 ± 0.0007 cm/s at 1300°C , 0.0078 ± 0.0009 cm/s at 1400°C and 0.0162 ± 0.0011 cm/s at 1500°C . The calculated apparent activation energy value of CaO dissolution in model slag is 71.5 ± 8.6 kJ/mol using equation (4-29) and characterizes the diffusion limiting step in the process.

Accordingly, the dissolution of CaO in the industrial slag is followed by lower values of mass transfer coefficients due to complexity of the slag composition.

Experiment with cylindrical CaO samples has been carried out to determine mass transfer coefficients of CaO dissolution in the industrial slag, according to the methodology described in Chapter 6. Elemental and phase composition of slags is presented in Tables 5-1, 5-2 and 5-4 in Chapter 5.

The mass of calcium oxide dissolved in the industrial slag is shown in Table 9-2 and is presented as a function of contact time of CaO with the slag in Figure 9-5.

Table 9-2: The results of experimental studies of CaO dissolution in the industrial slag

№ of test	1300 °C		1400 °C		1500 °C	
	Time, s	Mass of CaO dissolved in the slag phase, g	Time, s	Mass of CaO dissolved in the slag phase, g	Time, s	Mass of CaO dissolved in the slag phase, g
1	20	0.0122	20	0.0038	20	0.0254
2	30	0.0058	30	0.0067	30	0.0298
3	45	0.0076	45	0.0183	45	0.0237
4	60	0.0075	60	0.0217	60	0.0725
5	90	0.0231	90	0.0470	90	0.1900
6	120	0.0343	120	0.0741	120	0.2760
7	150	0.0420	150	0.1789	150	0.4491
8	180	0.0700	180	0.2240	180	0.8378
9	300	0.2090	300	0.4283	300	1.3604
10	400	0.2000	400	0.5715	400	1.4371
11	600	0.2324	600	0.6150	600	1.4704

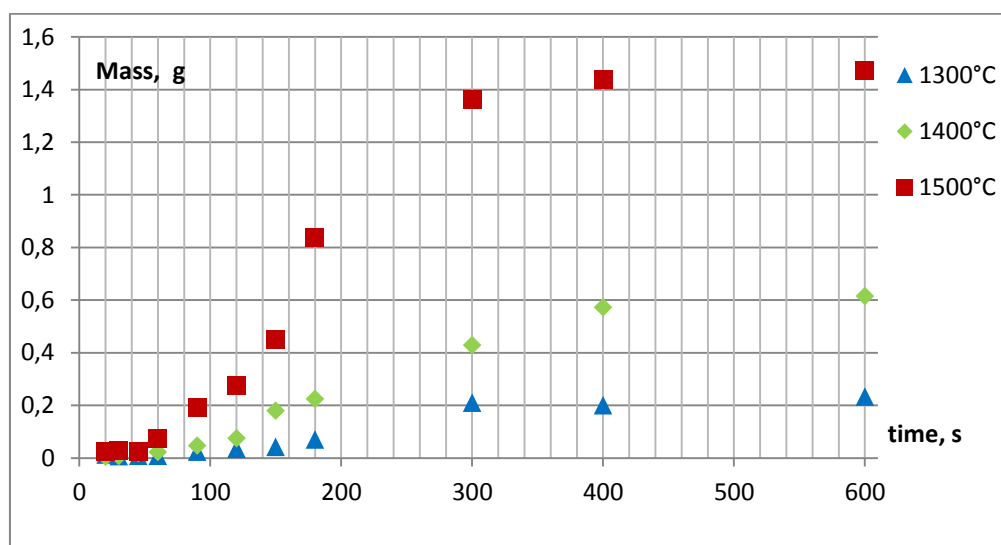


Figure 9-5: The dependence of the amount of dissolved CaO sample on contact time of sample with the slag

The time interval until mass of CaO ceases to change defining the saturation of industrial slag with CaO is increased to 300-350 seconds in comparison with model slag. The saturation concentration of calcium oxide in the slag is 47-48% at 1300°C, 54 -55% at 1400°C and 65-66% at 1500°C. On Figure 9-6 the relationship between the linear dimensions of calcium oxide cylindrical samples on the contact time of CaO with the industrial slag is presented.

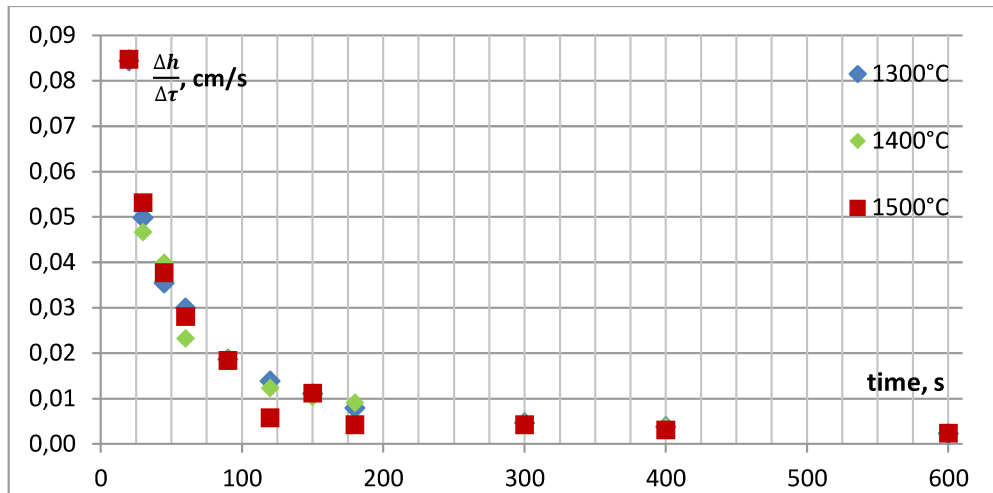


Figure 9-6: The dependence of calcium oxide sample linear dimensions (height of the cylinder) change on time

As it is evident from the experiment with a contact time above 300 seconds the dissolution of CaO samples does not progress which characterizes the equilibrium state of the system - the saturation of model slag with lime.

The relation between the linear rate of sample's dissolution $\frac{\Delta h}{\Delta \tau}$ and the saturation concentration of CaO in slag indicates the diffusion regime of CaO dissolution process (see Figure 9-7), similar to that in the experiment with the model slag.

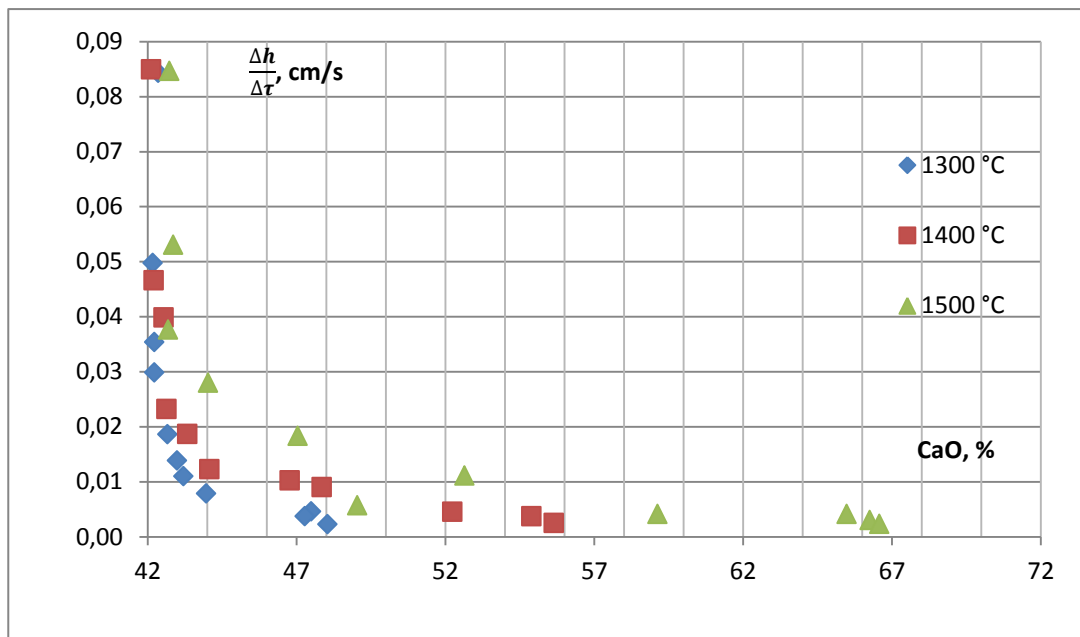


Figure 9-7: The dependence of the dissolution rate of CaO samples on the calcium oxide concentration in slag

The mass transfer coefficient values of CaO dissolution in industrial slag calculated on the basis of the experimental data using the equation (4-34) are presented in Figure 9-8.

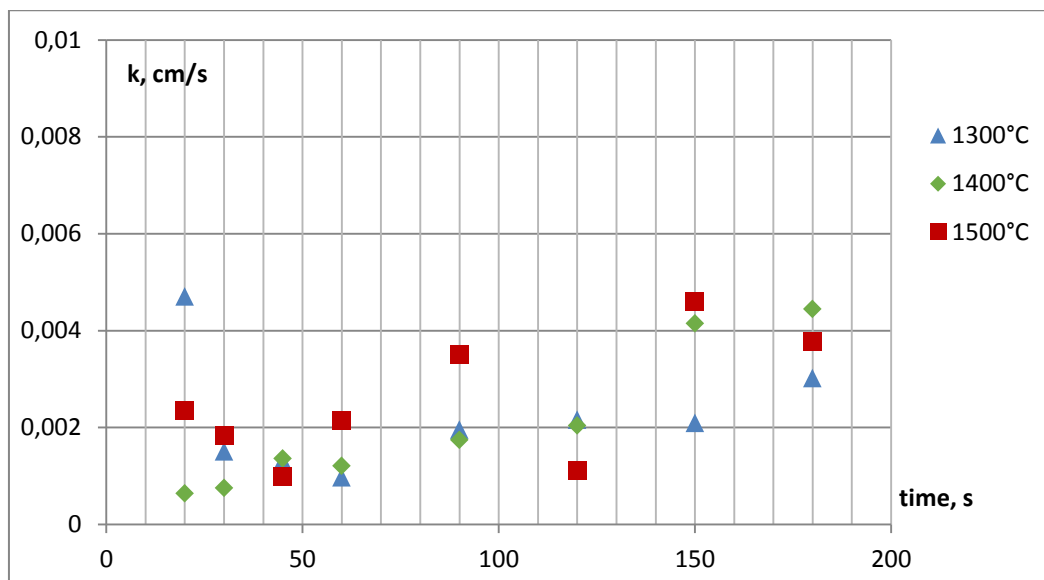


Figure 9-8: The dependence of mass transfer coefficient values of CaO dissolution in the industrial slag on the dissolution time

An increase in the mass transfer coefficient values is observed due to the reduced size of the dissolved solids. The decrease in the linear dimensions of the dissolving

solid body and as the result the decrease in thickness of the boundary layer explains the raise in mass transfer coefficients up to a certain value.

The lower values of CaO mass transfer coefficients in the system of industrial slag in comparison with model slag is due to the formation of different chemical compounds between industrial slag components and calcium oxide. Calculated average effective values of k : 0.0022 ± 0.0004 cm/s at 1300°C , 0.0030 ± 0.0006 cm/s at 1400°C and 0.0053 ± 0.0008 cm/s at 1500°C accordingly. The value of the apparent activation energy of the dissolution process of calcium oxide in the industrial slag is 70.6 ± 8.1 kJ/mol.

In steelmaking processes industrial lime is used instead of pure calcium oxide, therefore in the following work kinetics of technical lime dissolution in the industrial slag was also investigated.

Experimental results of the dissolution of industrial lime cylindrical samples in the industrial slag are presented in Table 9-3. In Figure 9-9 the amount of lime dissolved is presented as a function of time. Industrial lime composition is presented in Table 6-3 and refers to sample B.

Table 9-3: Experimental results of the dissolution of cylindrical lime samples in the industrial slag

№ of the test	1300 °C		1400 °C		1500 °C	
	Time, s	Mass of lime dissolved in the slag phase, g	Time, s	Mass of lime dissolved in the slag phase, g	Time, s	Mass of lime dissolved in the slag phase, g
1	20	0.0047	20	0.0023	20	0.0041
2	30	0.0028	30	0.0010	30	0.0070
3	45	0.0050	45	0.0053	45	0.0091
4	60	0.0040	60	0.0111	60	0.0402
5	90	0.0034	90	0.0208	90	0.0544
6	120	0.0192	120	0.0531	120	0.0596
7	180	0.0377	180	0.1001	180	0.3325
8	300	0.1034	300	0.3436	300	0.6706
9	400	0.1223	400	0.4107	400	0.8890
10	600	0.1135	600	0.4380	600	0.8647
11	900	0.1157	900	0.4230	900	0.8978
12	1200	0.1095	1200	0.4390	1200	0.9489
13	2400	0.1195	2400	0.4331	2400	0.9438

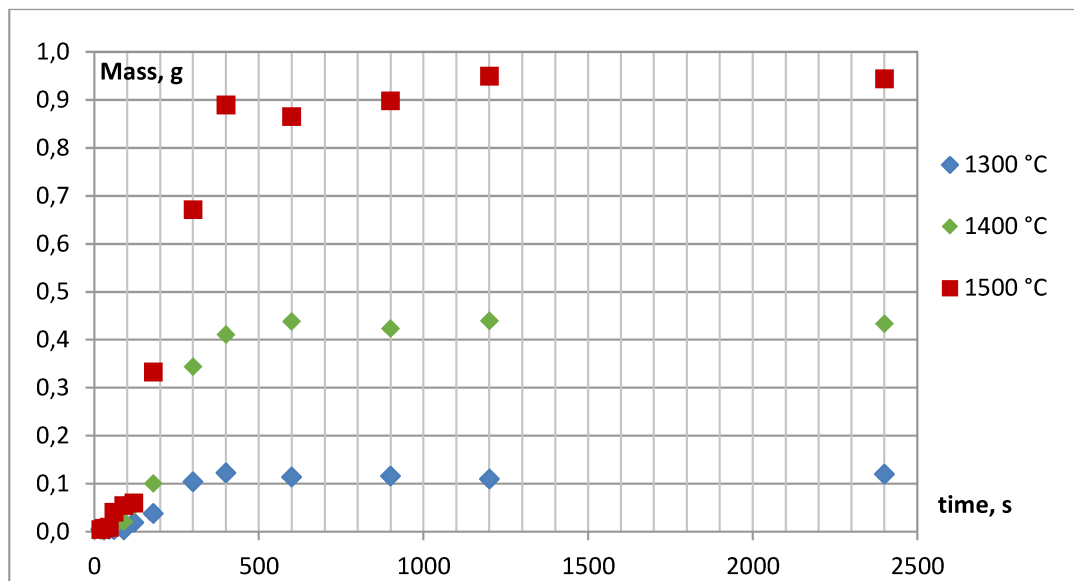


Figure 9-9: The dependence of the amount of the lime dissolved in the industrial slag on time

Time to reach equilibrium concentration when technical lime dissolves in the melt increases from 300 to 400 seconds compared to the dissolution of pure CaO. Solubility of CaO in the system of technical lime - industrial slag is dropped to 44-45% at 1300°C, 50-51% at 1400°C and 57-58% at 1500°C.

In the case of lime dissolution, the "salting out" effect - the decrease in the solubility of CaO compound in the presence of the MgO compound was observed.

The linear dissolution rate of lime samples is presented as a function of CaO concentration in the slag in Figure 9-10, and the dependence of mass transfer coefficients on the duration of the dissolution process is presented in Figure 9-11.

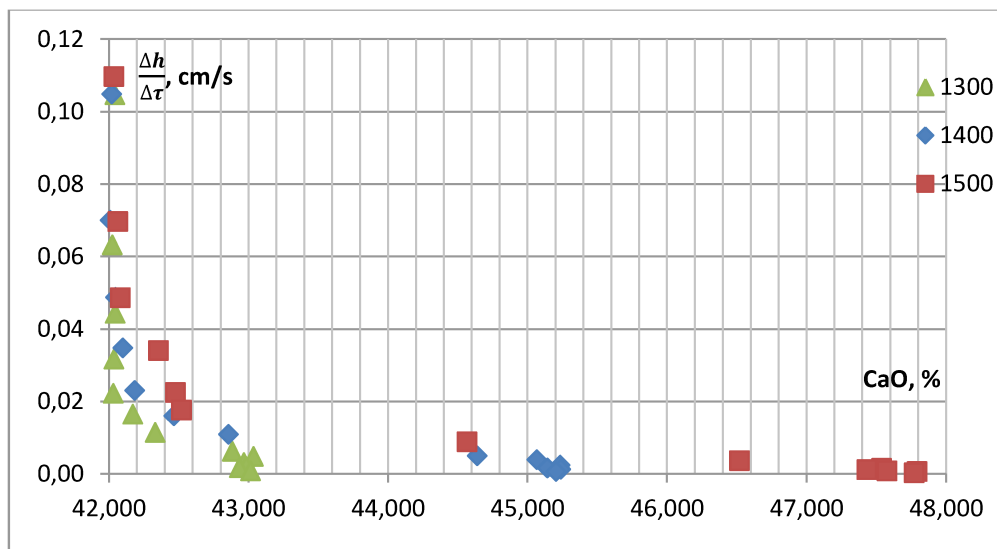


Figure 9-10: The dependence of the linear rate of lime dissolution on the CaO concentration in the industrial slag

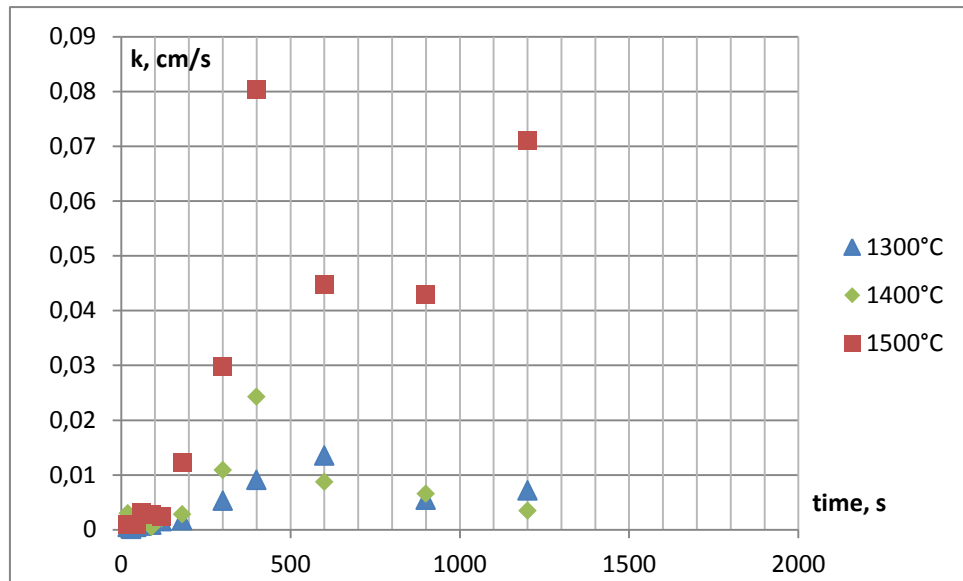


Figure 9-11: The values of calculated mass transfer coefficients of lime in the industrial slag

In the process of lime dissolution in the melt mass transfer coefficient is continuously increases due to the reduced size of the sample, which causes a decrease in the thickness of the boundary layer. However, after reaching the saturation, the decrease in mass transfer coefficients is observed, which is explained only by the decrease of the diffusion coefficient when a certain minimum value of δ has been reached. The decrease in the diffusion coefficient is possible due to the braking effect that occurs during the formation of the solid phase.

Dogan et al [1] reported that the dissolved lime particles enveloped by a layer of dicalcium $2\text{CaO}\cdot\text{SiO}_2$ and tricalcium silicate $3\text{CaO}\cdot\text{SiO}_2$.

Analysis of the phase composition of slag saturated with CaO performed in this work showed the presence of these compounds (Chapter 8 Figures 8-8 and 8-9).

Calculated mean values of the effective mass transfer coefficient until the saturation are in the satisfactory agreement with the values of k in the dissolution process of pure calcium oxide in the industrial slag at 1300°C resulted in 0.0017 ± 0.0004 cm/s, at 1400°C – 0.0023 ± 0.0006 cm/s, at 1500°C – 0.0066 ± 0.0007 cm/s. The value of the apparent activation energy is 103.8 ± 10.0 kJ/mol.

The mass transfer coefficient of MgO dissolution from technical lime in the slag has been calculated using equation (4-35). According to the experimental data, the saturation concentration of industrial slag with MgO was 6.5-6.6% at 1300°C, 6.7-6.8% at 1400°C and 6.9-7.0% at 1500°C which agrees with literature. [58,59] The saturation concentration of magnesium oxide in slag is mainly influenced by the temperature and the content of CaO, which is consistent with the literature about the dominant effect of temperature and basicity of slag. [1,3,60]

The values of derived mass transfer coefficients of MgO in the process of lime dissolution in the slag at 1300°C are 0.00033 cm/s, at 1400°C – 0.00060 cm/s, and at

1500°C – 0.0028 cm/s. An increase in mass transfer coefficients is observed until the saturation and after saturation values of k drop (See Figure 9-11). The decrease in the values of k is due to the envelopment of lime particles with solid chemical compounds of MgO with slag components such as merwinite $\text{Ca}_3\text{Mg}(\text{SiO}_4)_2$. Low values of MgO mass transfer compared to CaO, characterize the limitation of lime dissolution process by MgO diffusion in the bulk slag.

Similar results were reported in the literature by Dogan. et. al. [1] Authors indicated a limiting step by the diffusion of MgO in the case FeO content in slag is above 20%, which corresponds to the FeO content in the industrial and model slags used.

The following conclusions are summarized below:

1. The kinetics of calcium oxide and lime dissolution in a non-steady- state diffusion at temperatures ranging from 1300-1500°C has been studied. Effective mass transfer coefficients were calculated by a differential equation of the mass change over time and linear rate of dissolution of solids in the liquid phase, considering the total mass balance of the dissolving agent: its transition into the melt phase and accumulation in the sequentially soluble layers of solid.
2. The dependence of the linear rate of samples dissolution on the saturation concentration of CaO in the slag has been derived, indicating the diffusion regime of CaO dissolution in the melt. When the concentration of CaO in the slag increases the dissolution rate of samples drops, due to the decrease in the diffusion concentration gradient $(\text{CaO}\%)_{sat} - (\text{CaO}\%)$.
3. In the process of solid body dissolution it has been revealed that the mass transfer coefficient increases due to the reduced size of the dissolving CaO or lime sample, which is explained by the decrease in the thickness of the boundary layer δ . The values of the apparent activation energy were calculated.
4. It was found that after reaching the saturation the values of mass transfer coefficient of CaO dissolution drop due to the formation of solid phases, such as (dicalcium $2\text{CaO}\cdot\text{SiO}_2$ and tricalcium silicate $3\text{CaO}\cdot\text{SiO}_2$), enveloping dissolved lime particles.
5. Mass transfer coefficients of MgO dissolution in slag have been calculated. Low values of the effective mass transfer coefficients of MgO dissolution in comparison with CaO characterize the limitation of the dissolution process of lime in slag containing of FeO above 20% by the diffusion of MgO
6. The value of the apparent activation energy for the dissolution of lime in the slag (less than 200 kJ/mol) has been calculated and characterizes the diffusion limiting step in the dissolution process.

10 Experimental results of the study of lime dissolution containing various amounts of MgO in model slag

In this Chapter the kinetics of lime dissolution containing various amounts of magnesium oxide (2, 4.3, 5.6, 6.2 and 7.6%) in model slags with the composition 20%CaO, 45%FeO and 35%SiO₂ is studied in a non-stationary diffusion, at temperatures ranging from 1300-1600°C, directly in the hot process. The description of lime samples is given in Tables 6-3 and 6-4. Phase analysis of lime sample containing 4.3% MgO in presented in Figure 10-1. Other samples had similar composition.

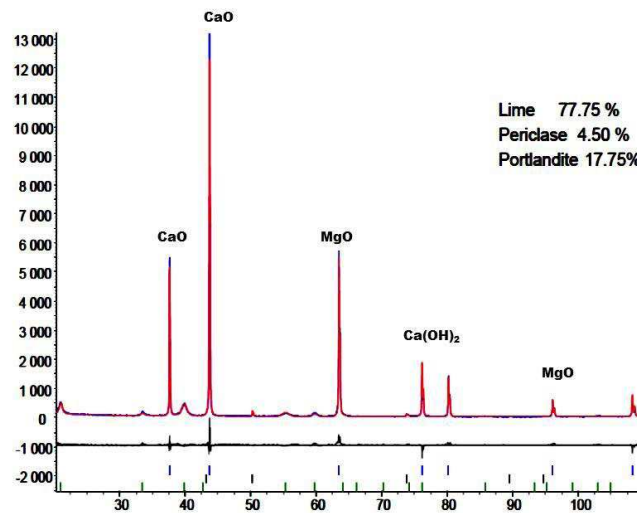


Figure 10-1: The X-Ray spectrum of the industrial lime containing 4.3% MgO

The experimental results of lime dissolution containing 2% of MgO in the model slag are presented in Table 10-1. The dependence of the amount of the dissolved lime sample on the contact time of sample with slag is presented in Figure 10-2.

Table 10-1: The experimental results of the dissolution process of lime samples containing 2% of MgO in the model slag

№ of test	1300°C		1400 °C		1500 °C		1600°C	
	Time, s	Mass of lime dissolved in the slag phase, g	Time, s	Mass of lime dissolved in the slag phase, g	Time, s	Mass of lime dissolved in the slag phase, g	Time, s	Mass of lime dissolved in the slag phase, g
1	30	0.01	30	0.01	30	0.005	30	0.004
2	60	0.005	60	0.02	60	0.005	60	0.015
3	90	0.01	90	0.03	90	0.05	90	0.07
4	120	0.02	120	0.04	120	0.08	120	0.08
5	180	0.05	180	0.09	180	0.13	180	0.18
6	300	0.06	300	0.12	300	0.19	300	0.29
7	600	0.14	600	0.21	600	0.49	600	0.67
8	900	0.18	900	0.27	900	0.50	900	0.87
9	1200	0.24	1200	0.39	1200	0.63	1200	0.94
10	1500	0.23	1500	0.43	1500	0.63	1500	0.97
11	1800	0.24	1800	0.44	1800	0.64	1800	0.98
12	2400	0.24	2400	0.45	2400	0.63	2400	0.99

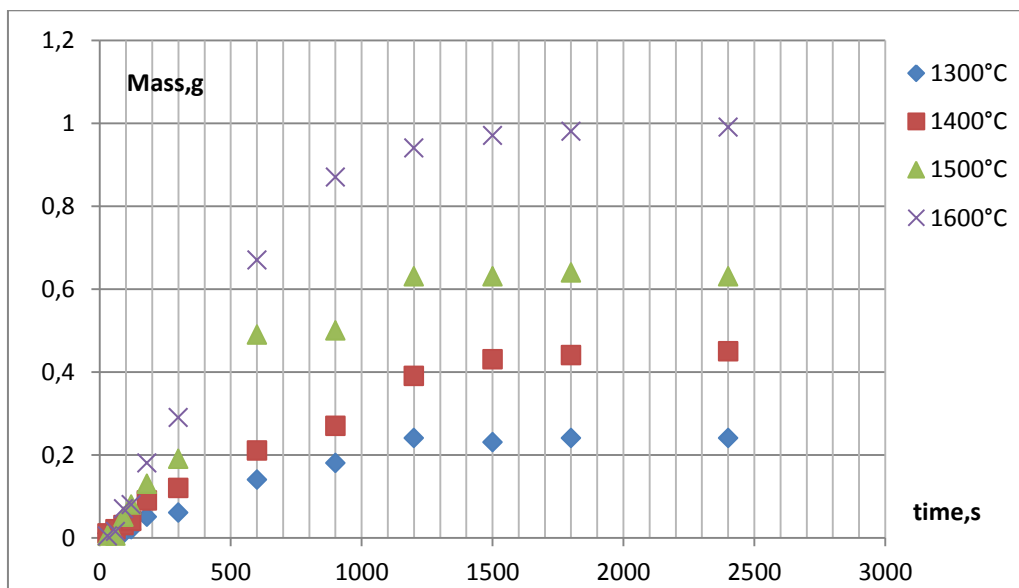


Figure 10-2: The dependence of the amount of dissolved lime containing 2% of MgO on time

As it is seen from experimental data the amount of the dissolved lime ceases to change after time interval of 800 seconds, which characterizes the saturation of the slag with lime. Equilibrium concentration of calcium oxide in the slag phase at 1300°C is 28.3%, 34.3% at 1400°C, 38.6% at 1500°C and 45.8 at 1600°C. The values derived are consistent with literature. [3,30,60] In comparison with pure CaO, lime dissolution containing 2% of MgO requires longer time to dissolve and to reach saturation. Furthermore, the amount of lime sample dissolved is relatively lower than that of pure CaO. As it is observed in the experiment with a contact time of more than 800 seconds there is no change in the linear dimensions of lime samples which also defines the saturation of slag.

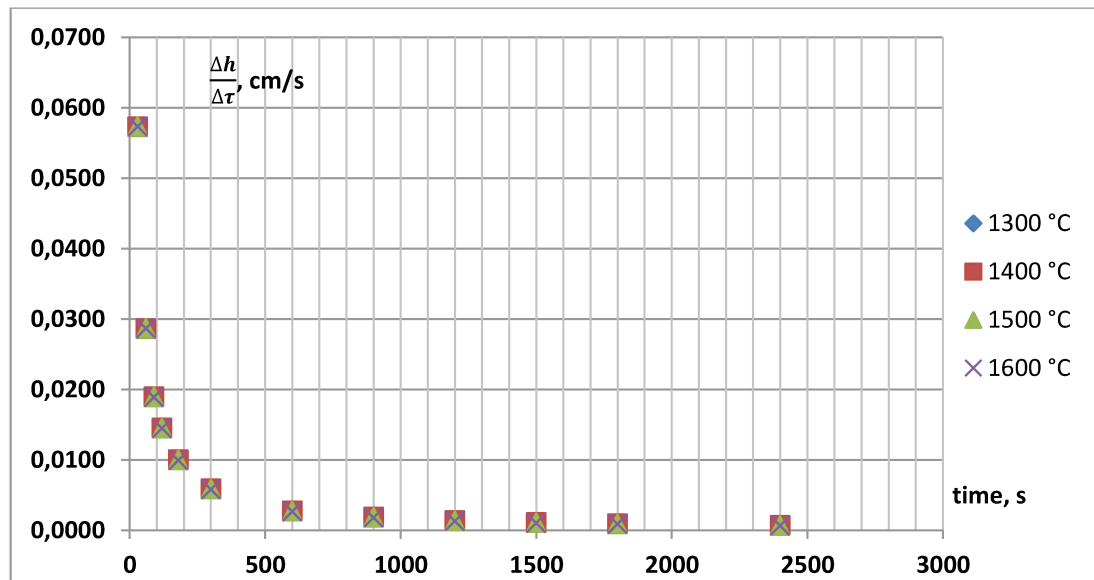


Figure 10-3: The dependence of the linear dimensions of lime samples containing 2% of MgO on the dissolution time

The relation between the linear rate of samples dissolution $\frac{\Delta h}{\Delta \tau}$ and the saturation concentration of CaO in slag has been derived (see Figure 10-4). With the increasing concentration of CaO in the slag the dissolution rate of samples drops which is due to the decrease in the concentration gradient $(CaO\%)_{sat} - (CaO\%)$.

The mass transfer coefficient values of lime containing 2% MgO dissolution in model slag calculated on the basis of the experimental data are presented in Figure 10-5. Based on differential equations of mass balance of the dissolving substance and taking into account its transition into the melt phase, and accumulation in the consistently dissolving layers of solid, values of mass transfer coefficients were calculated. The experiment showed an increase in mass transfer coefficients up to a certain value calculated by the equation (4-34) until the saturation of slag with lime was reached.

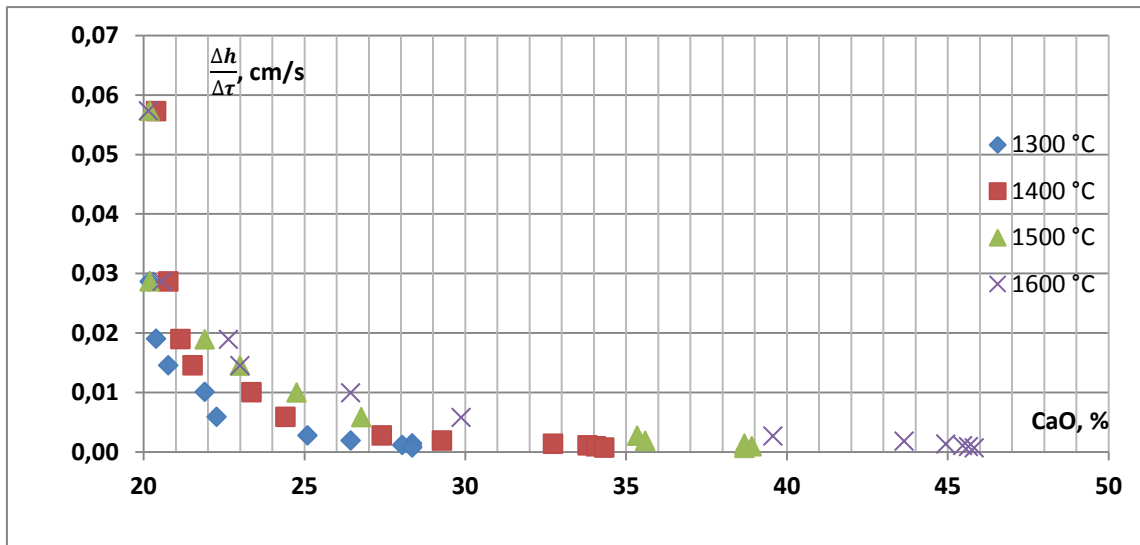


Figure 10-4: The dependence of the linear rate of dissolution of lime samples containing 2% of MgO on the CaO content in slag

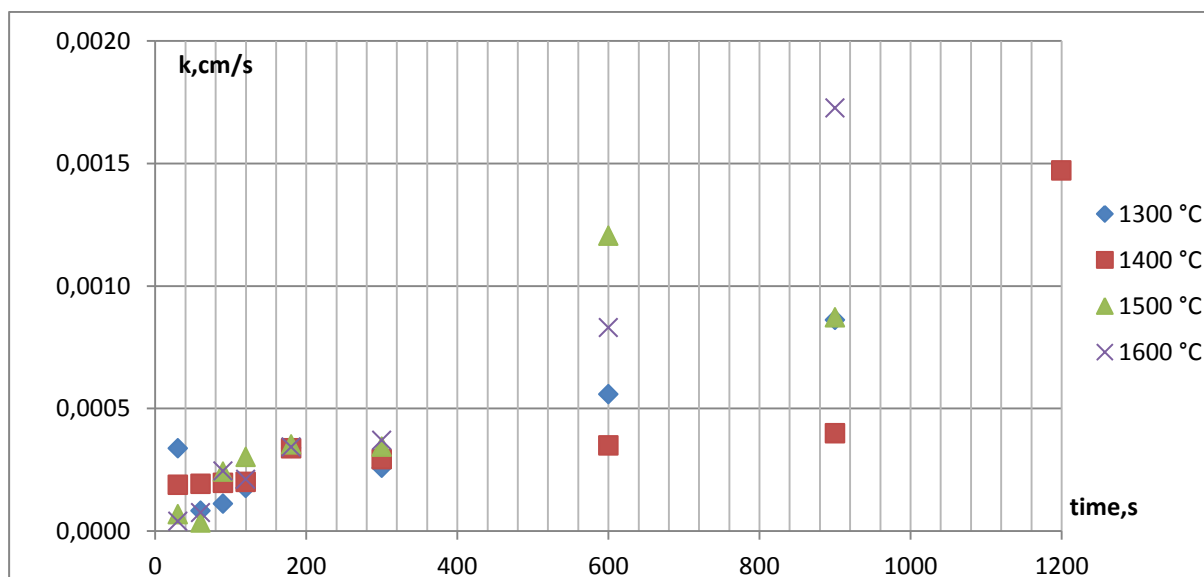


Figure 10-5: Calculated mass transfer coefficients of lime containing 2% MgO

In the experiment the results of the mass change of lime cylindrical samples containing 4.3, 5.6, 6.2 and 7.6% of MgO have been obtained as a function of the contact time with slag at temperatures between 1300-1600°C as shown in Figures 10-6 – 10-9 and are summarized in Tables 10-2 – 10-5. The following limes were provided by Voestalpine Linz with similar grain size distribution and preparation procedure (see Table 6-3).

10 Experimental results of the study of lime dissolution containing various amounts of MgO
in model slag

Table 10-2: The experimental results of the dissolution process of lime samples containing 4.3% of MgO in the model slag

№ of test	1300°C		1400 °C		1500 °C		1600°C	
	Time, s	Mass of lime dissolved in the slag phase, g	Time, s	Mass of lime dissolved in the slag phase, g	Time, s	Mass of lime dissolved in the slag phase, g	Time, s	Mass of lime dissolved in the slag phase, g
1	30	0.01	30	0.01	30	0.03	30	0.06
2	60	0.005	60	0.06	60	0.06	60	0.12
3	90	0.01	90	0.07	90	0.08	90	0.22
4	120	0.01	120	0.11	120	0.14	120	0.37
5	180	0.02	180	0.23	180	0.23	180	0.56
6	300	0.05	300	0.26	300	0.4	300	0.75
7	600	0.09	600	0.31	600	0.52	600	0.82
8	900	0.13	900	0.29	900	0.55	900	0.8
9	1200	0.16	1200	0.31	1200	0.53	1200	0.81
10	1500	0.21	1500	0.34	1500	0.53	1500	0.76
11	1800	0.19	1800	0.34	1800	0.52	1800	0.84
12	2400	0.19	2400	0.35	2400	0.53	2400	0.82

Table 10-3: The experimental results of the dissolution process of lime samples containing 5.6% of MgO in the model slag

№ of test	1300°C		1400 °C		1500 °C		1600°C	
	Time, s	Mass of lime dissolved in the slag phase, g	Time, s	Mass of lime dissolved in the slag phase, g	Time, s	Mass of lime dissolved in the slag phase, g	Time, s	Mass of lime dissolved in the slag phase, g
1	20	0.01	20	0.01	20	0.02	20	0.03
2	60	0.01	60	0.03	60	0.05	60	0.07
3	90	0.01	90	0.04	90	0.07	90	0.13
4	180	0.02	180	0.08	180	0.13	180	0.16
5	600	0.06	600	0.16	600	0.27	600	0.40
6	900	0.09	900	0.20	900	0.33	900	0.51
7	1200	0.11	1200	0.21	1200	0.33	1200	0.51

8	1500	0.12	1500	0.22	1500	0.32	1500	0.52
9	1800	0.14	1800	0.21	1800	0.33	1800	0.50
10	2400	0.15	2400	0.22	2400	0.33	2400	0.52

Table 10-4: The experimental results of the dissolution process of lime samples containing 6.2% of MgO in the model slag

№ of test	1300°C		1400 °C		1500 °C		1600°C	
	Time, s	Mass of lime dissolved in the slag phase, g	Time, s	Mass of lime dissolved in the slag phase, g	Time, s	Mass of lime dissolved in the slag phase, g	Time, s	Mass of lime dissolved in the slag phase, g
1	20	0	20	0.01	20	0.01	20	0.01
2	60	0.01	60	0.03	60	0.02	60	0.03
3	90	0.02	90	0.04	90	0.03	90	0.08
4	180	0.03	180	0.06	180	0.11	180	0.19
5	600	0.06	600	0.11	600	0.20	600	0.25
6	900	0.07	900	0.11	900	0.20	900	0.27
7	1200	0.08	1200	0.12	1200	0.21	1200	0.27
8	1500	0.10	1500	0.14	1500	0.22	1500	0.29
9	1800	0.09	1800	0.13	1800	0.22	1800	0.27
10	2400	0.1	2400	0.12	2400	0.21	2400	0.28

Table 10-5: The experimental results of the dissolution process of lime samples containing 7.6% of MgO in the model slag

№ of test	1300°C		1400 °C		1500 °C		1600°C	
	Time, s	Mass of lime dissolved in the slag phase, g	Time, s	Mass of lime dissolved in the slag phase, g	Time, s	Mass of lime dissolved in the slag phase, g	Time, s	Mass of lime dissolved in the slag phase, g
1	20	0.000	20	0.003	20	0.005	20	0.005
2	60	0.010	60	0.010	60	0.020	60	0.020
3	90	0.020	90	0.030	90	0.050	90	0.060
4	180	0.030	180	0.060	180	0.080	180	0.090
5	600	0.040	600	0.080	600	0.130	600	0.170

10 Experimental results of the study of lime dissolution containing various amounts of MgO in model slag

6	900	0.050	900	0.070	900	0.130	900	0.190
7	1200	0.050	1200	0.080	1200	0.140	1200	0.200
8	1500	0.050	1500	0.090	1500	0.150	1500	0.190
9	1800	0.040	1800	0.090	1800	0.150	1800	0.210
10	2400	0.055	2400	0.080	2400	0.140	2400	0.180

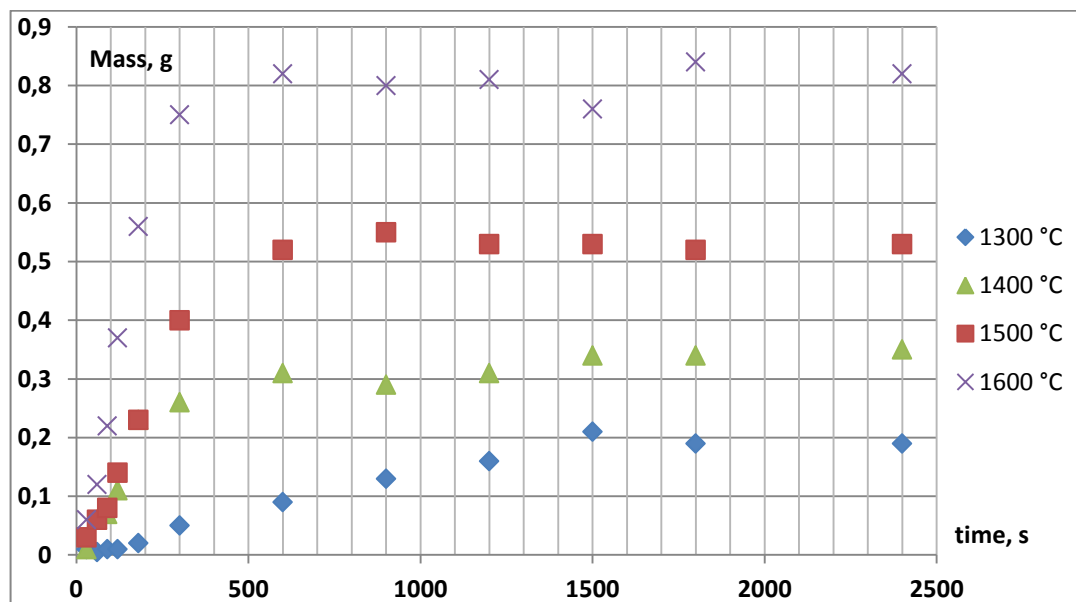


Figure 10-6: The dependence of the amount of dissolved lime containing 4.3% of MgO on contact time with slag

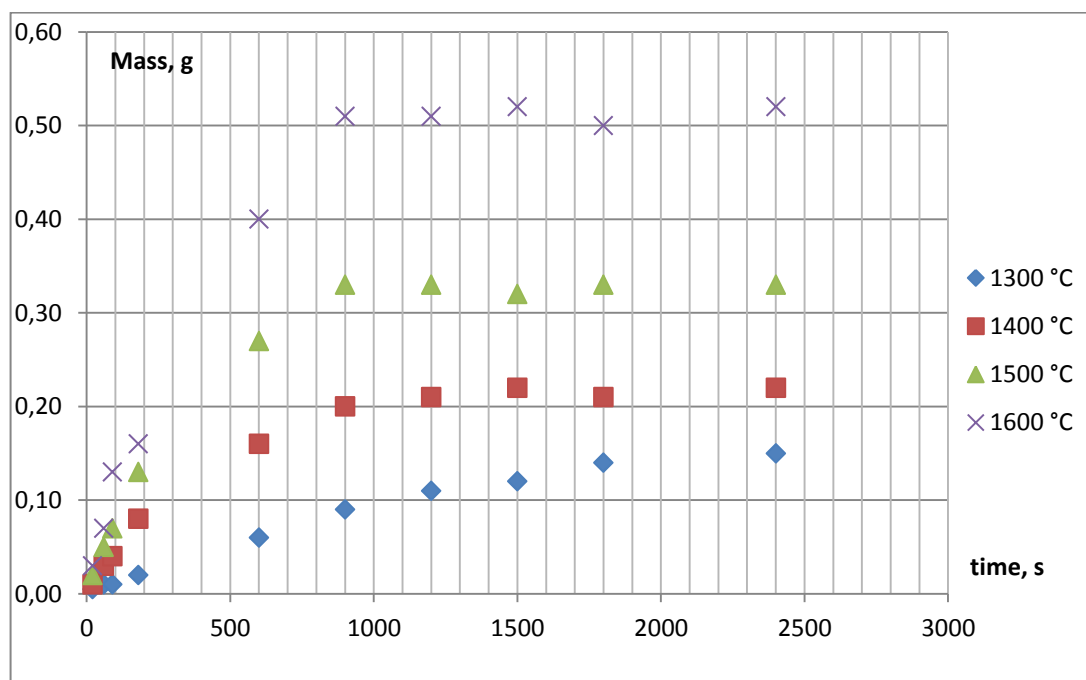


Figure 10-7: The dependence of the amount of dissolved lime containing 5.6% of MgO on contact time with slag

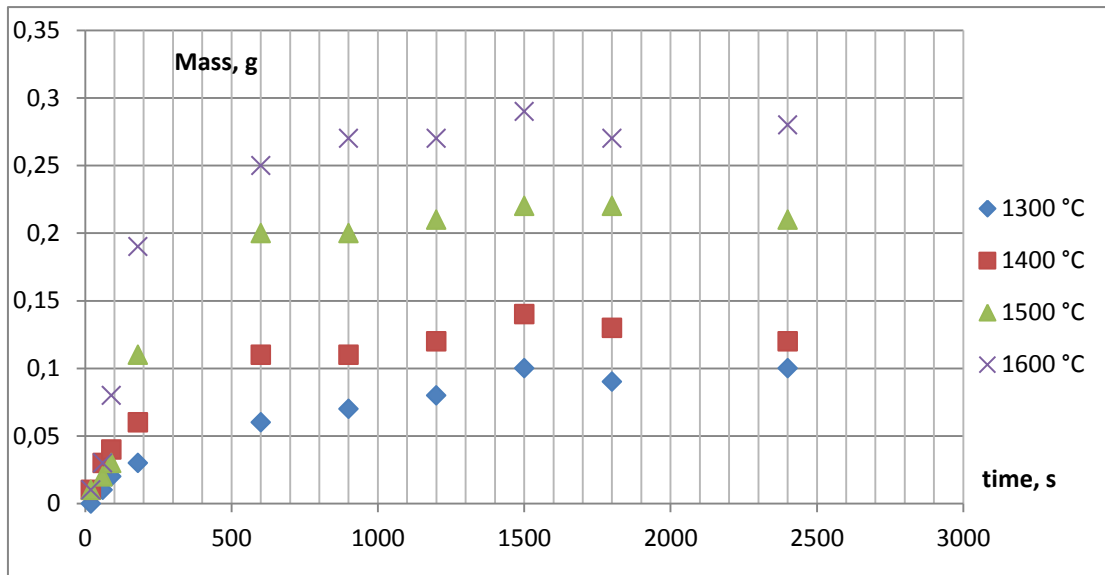


Figure 10-8: The dependence of the amount of dissolved lime containing 6.2% of MgO on contact time with slag

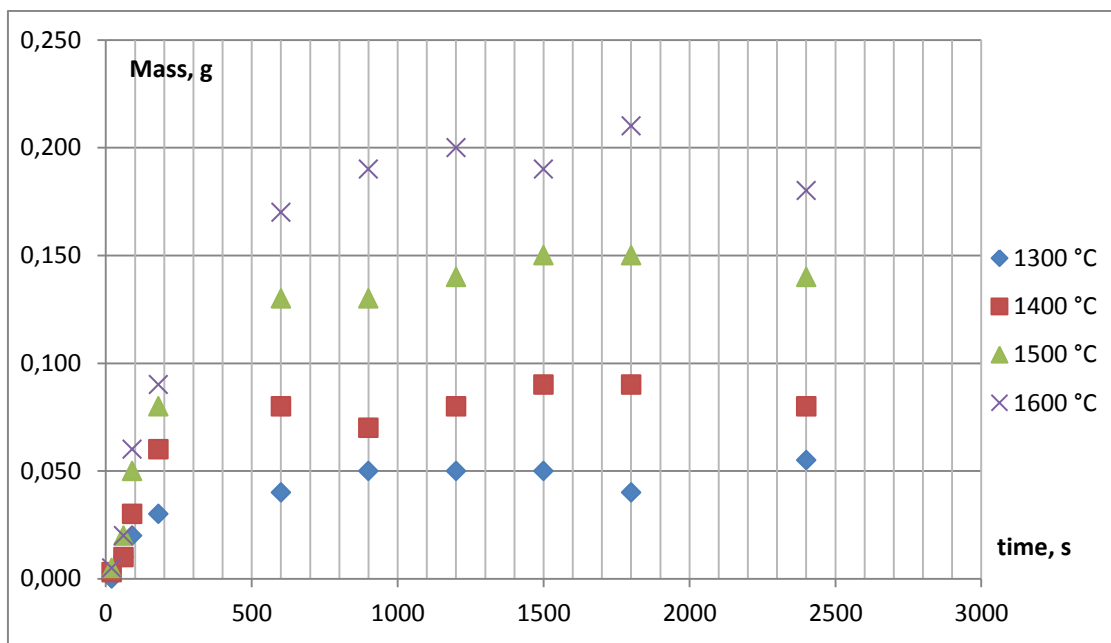


Figure 10-9: The dependence of the amount of dissolved lime containing 7.6% of MgO on contact time with slag

It is evident from the experimental data that as model slag becomes saturated with calcium oxide, the mass of the lime samples ceases to change with the increasing contact time. Slag saturation with calcium oxide occurs at any given temperature, wherein the amount of dissolved lime increases with the temperature and, respectively, the equilibrium concentration of calcium oxide in the slag (saturation concentration) raises as well.

One of the characteristics of slag saturation with calcium oxide is the formation of dicalcium silicate on the surface and in the volume of lime particles, which prevents further diffusion of CaO in the melt phase [60,61]. Ca_2SiO_4 is formed due to the dissolution of lime in the slag with a high concentration of silica, which is contained in the model slag (35% SiO_2) used in the experiment.

Dicalcium silicate is indicated in the X-Ray spectrum of the final slag composition (Figure 10-10). However, FeO content in the slag and MgO content in lime have an important role. FeO is capable to penetrate into the cracks of poorly soluble dicalcium silicate surface layer, and to form with MgO a solid solution of magnesiowustite $(\text{Fe, Mg})\text{O}$ with a melting point greater than 1750°C hindering the process of lime dissolution (Figure 10-9). [1,30,60–62]

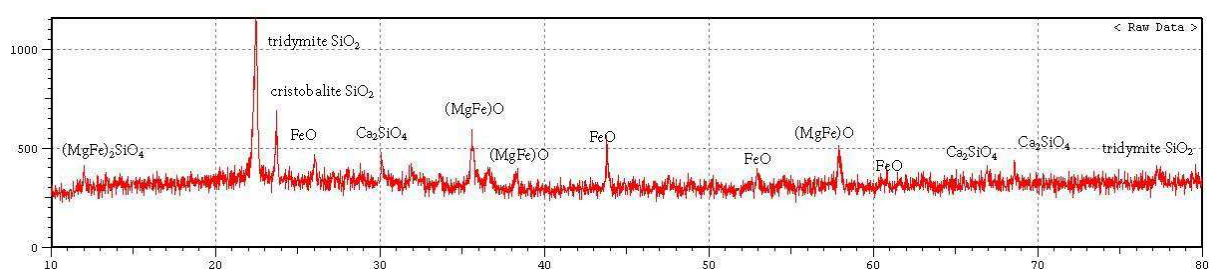


Figure 10-10: The X-Ray spectrum of the final slag after lime dissolution containing 4.3% of MgO

The values of the equilibrium concentration of CaO in relation to the magnesium content in lime at various temperatures are presented in Table 10-6. The observed drop in the equilibrium concentration of CaO in the slag samples with the increasing content of MgO in lime can be explained by an increase of magnesiowustite and dicalcium silicate concentration in the surface layer and in the volume of lime, and as a consequence the greater thickness of formations further complicating the process of lime dissolution.

Table 10-6: Equilibrium concentration (saturation concentration) of CaO in model slag at different temperatures of lime dissolution process.

№	MgO content in lime, %	Equilibrium concentration of CaO in the slag, % at temperatures °C			
		1300	1400	1500	1600
1	2	28.3-28.4	34.0-34.3	38.2-38.6	45.5-45.8
2	4.3	26.2-26.5	30.6-30.8	35.4-35.5	41.0-41.2
3	5.6	24.9-25.0	27.1-27.4	30.1-30.3	34.7-34.8
4	6.2	23.4-23.6	24.7-24.8	27.2-27.3	29.1-29.3
5	7.6	21.9-22.0	23.0-23.1	24.9-25.0	26.4-26.5

There is a correlation between the linear rate of the dissolution of lime with different MgO content and the saturation concentration of calcium oxide in slag at

different temperatures, as seen in Figures 10-11 – 10-14. With the increasing concentration of CaO in the slag, the rate of the samples' dissolution drops.

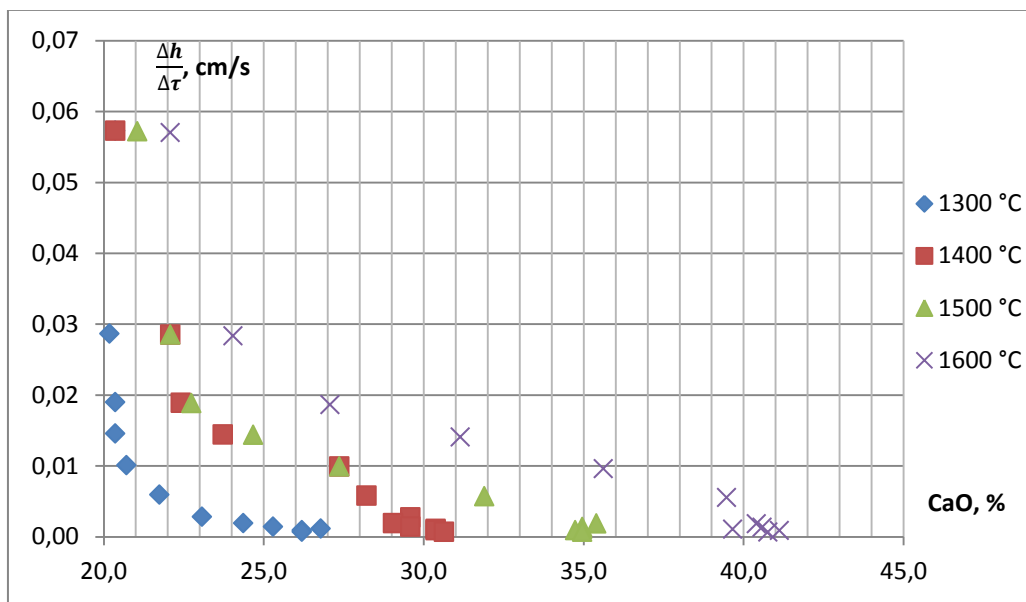


Figure 10-11: The dependence of the linear rate of dissolution of lime samples containing 4.3% of MgO on the CaO content in slag

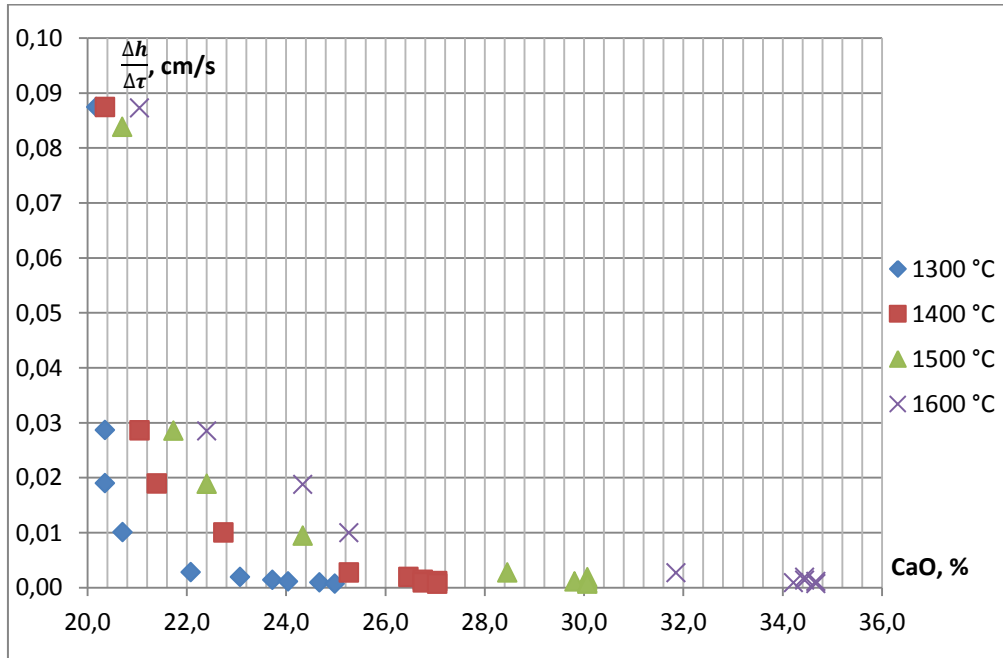


Figure 10-12: The dependence of the linear rate of dissolution of lime samples containing 5.6% of MgO on the CaO content in slag

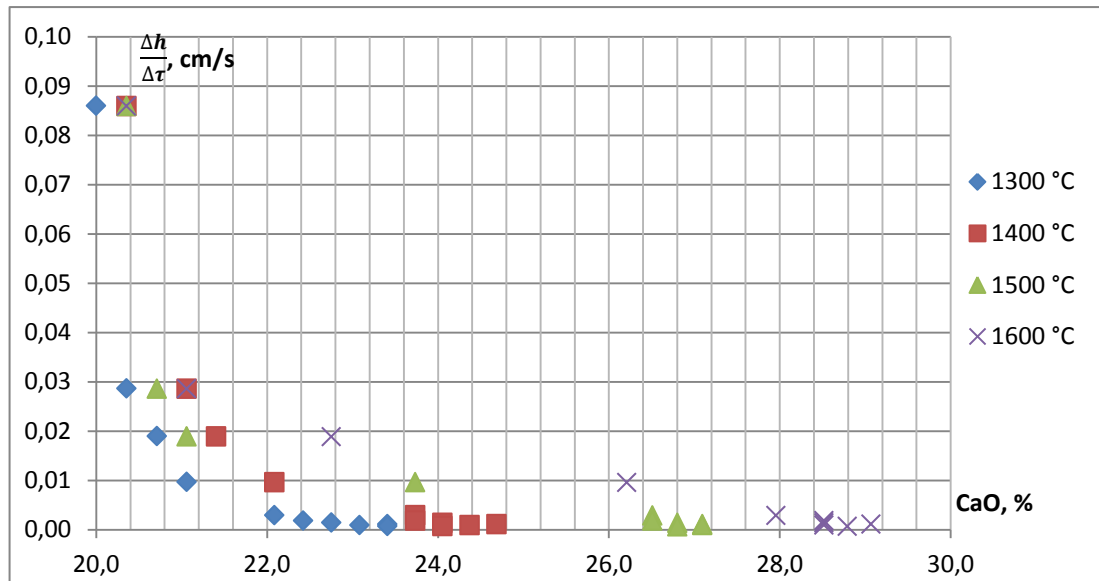


Figure 10-13: The dependence of the linear rate of dissolution of lime samples containing 6.2% of MgO on the CaO content in slag

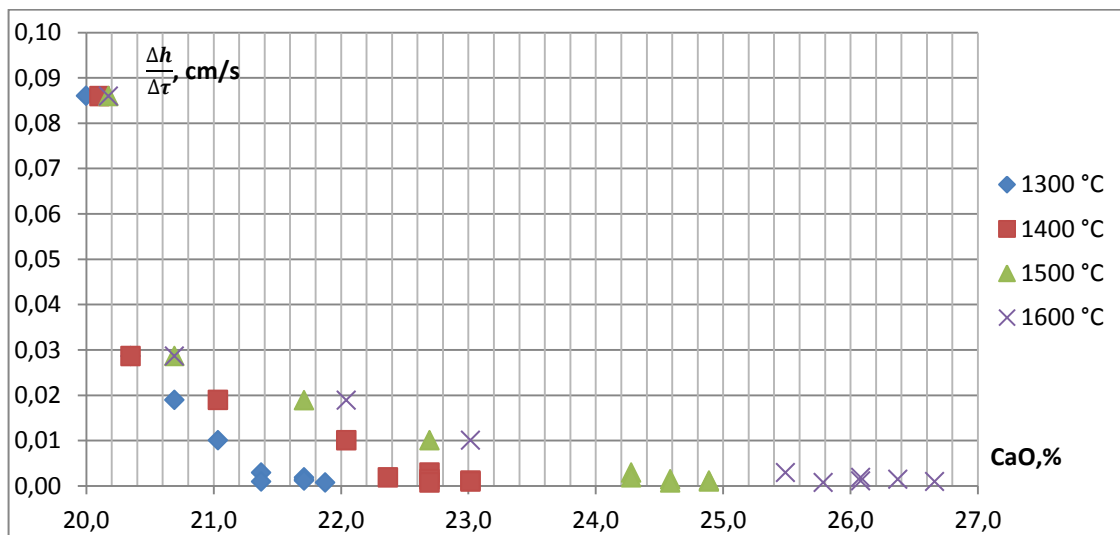


Figure 10-14: The dependence of the linear rate of dissolution of lime samples containing 7.6% of MgO on the CaO content in slag

Based on differential equations of mass balance of the dissolving substance and taking into account its transition into the melt phase, and accumulation in the consistently dissolving layers of solid, values of mass transfer coefficients were calculated. The experiment showed an increase in mass transfer coefficients calculated by the equation (4-34) until the saturation of slag with lime was reached (see Figure 10-15).

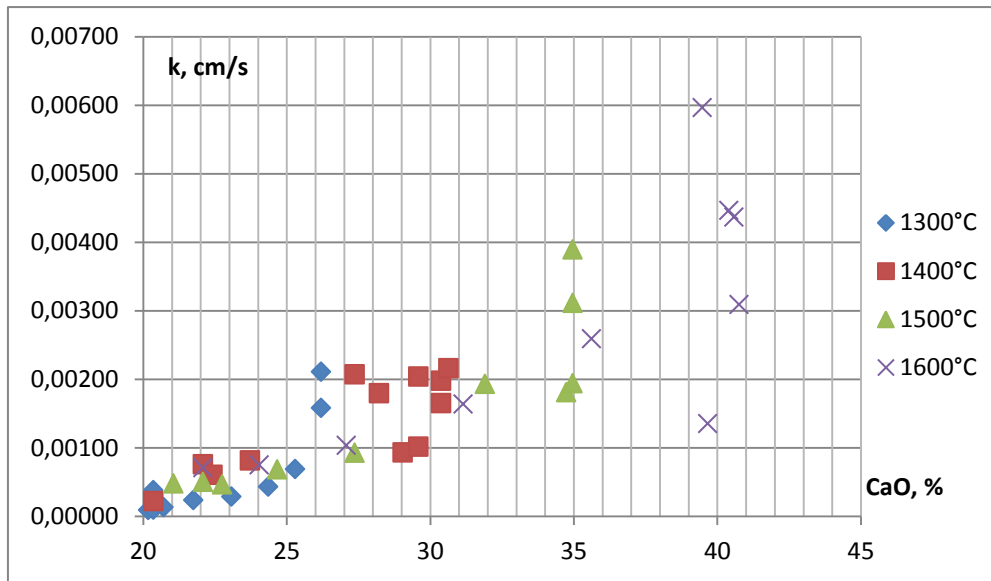


Figure 10-15: The values of calculated mass transfer coefficients of lime dissolution containing 4.3% of MgO.

According to similarity theory, when large particles (greater than 1 cm in diameter) are dissolving, the mass transfer coefficient is dependent on particle size and continuously increases as the dissolution of the lime in the slag progresses at a Reynolds number $Re > 500$; yet still less than a critical value:

$$k = 1,06 \left(\frac{\Delta\rho g}{\rho_{liq}} \right)^{1/4} \frac{D^{2/3}}{h^{1/4} \nu^{1/6}} \quad (10-1)$$

where $\Delta\rho$ - is the density difference between solids and liquid melt; ρ_{liq} - is the density of the melt; g - is the acceleration of free fall; ν - is the kinematic viscosity; D - is the diffusion coefficient; h - is the linear size of the dissolving sample.

According to B. Baptizmansky [23] the mass transfer coefficient is greatly influenced by the slag composition and the value of the mass transfer coefficient can increase with the rising basicity of the slag, in spite of the lower concentration gradient. Therefore, mass transfer coefficients are only of use for an approximate estimation of the dissolution time of large solid lime particles in the melt.

The influence of MgO content in lime on its rate of dissolution should be emphasized. The increase in the concentration of MgO in lime slows down the dissolution rate of the samples. In the work [1,30] authors measured the rate of calcined dolomite samples $\text{CaCO}_3 \cdot \text{MgCO}_3$ dissolution in the slag with the composition $\text{Fe}_x\text{O} \cdot \text{CaO} \cdot \text{SiO}_2$, containing FeO from 20 to 65%. Authors suggested a limitation of the MgO diffusion in the slag containing FeO more than 20% through the surface layer at the interface.

To prove the limitation of the dissolution rate of samples with the increasing MgO concentration, in this thesis, the values of CaO diffusion in the liquid slag are derived from the experimental data.

10.1 The calculation of the diffusion coefficients of lime dissolution in model slag containing various amounts of MgO

The rate of the heterogeneous process, which is limited by the diffusion, is described by the following equation according to Fick's first law:

$$w = \frac{1}{(-1)_s} \left(\frac{dm}{dt} \right)_{x=0} = D \left(\frac{\partial c(x,t)}{\partial x} \right)_{x=0} \quad (10-2)$$

where $x=0$ is the origin of the coordinates, which is placed on a surface of solid body and is inwardly directed into the melt (the propagation of the diffusion). The following equation is used to describe a semi-infinite linear diffusion when the substance diffuses along the length of the cylinder, and the reacting surface is the bottom of the cylinder. In terms of non-stationary spatial semi-infinite spherical diffusion Fick's second law can be represented by the next equation (10-3) [29]:

$$w = D \left(\frac{\partial c(R, t)}{\partial R} \right)_{R=r} \quad (10-3)$$

which is expressed in the linear form:

$$w = \sqrt{\frac{D}{\pi}} \frac{c}{\sqrt{t}} + \frac{Dc}{r} \quad (10-4)$$

where w is the rate of diffusion; r – is the sphere radius; C – CaO concentration in the slag, expressed in mol/m^3 .

Taking into account the correlation between the amounts of reacted substance and time, the diffusion coefficient of lime can be determined, as long as the value of the solid surface is known. The linear dependence of mass change rate of calcium oxide samples $w = \frac{1}{s} \frac{dM}{dt}$ on the value of $\frac{c}{\sqrt{t}}$ is evident in Figures 10-16 and 10-17. The lime diffusion coefficient values in the molten slag were calculated using the tangent of the angle.

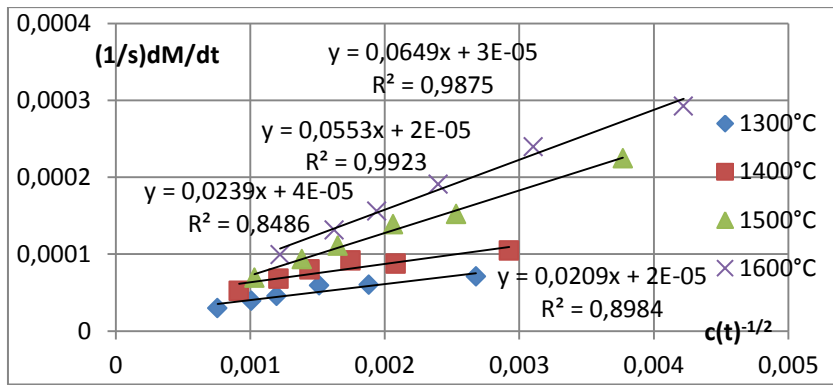
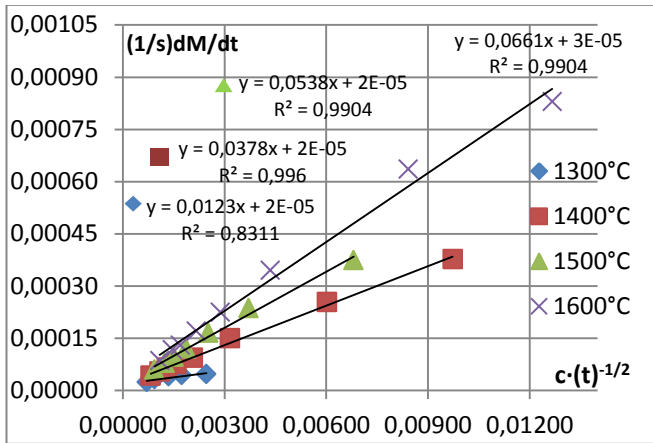
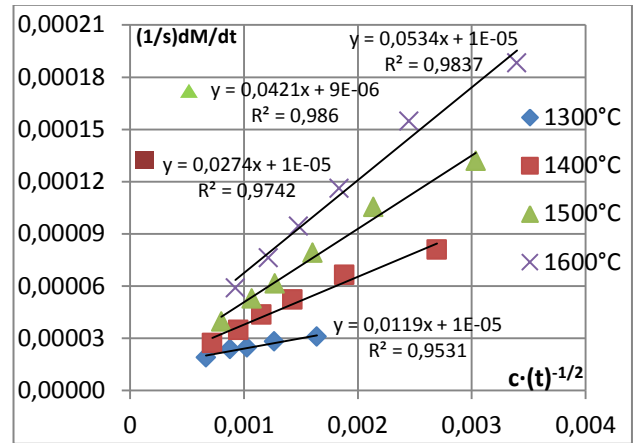


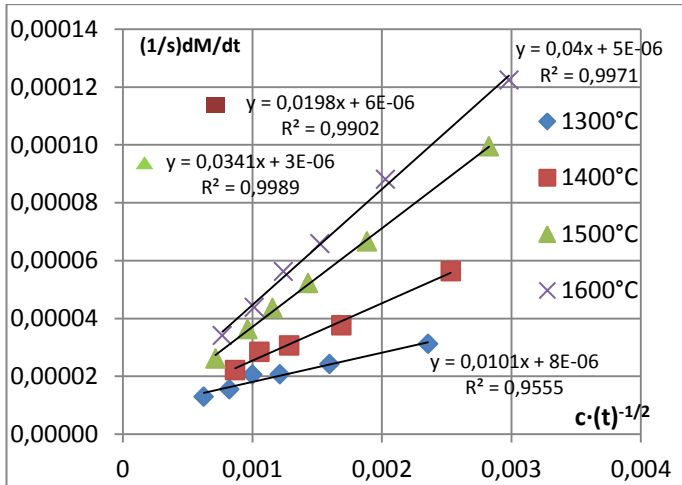
Figure 10-16: The dependence of the dissolution rate of lime samples containing 2% of MgO on the value of $\frac{c}{\sqrt{t}}$.



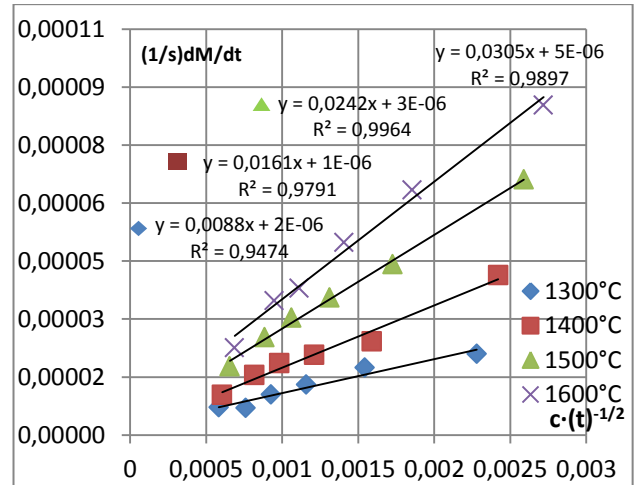
a) – The dependence of the dissolution rate of lime samples containing 4.3% MgO on the value of $\frac{c}{\sqrt{t}}$.



b) – The dependence of the dissolution rate of lime samples containing 5.6% MgO on the value of $\frac{c}{\sqrt{t}}$.



c) – The dependence of the dissolution rate of lime samples containing 6.2% of MgO on the value of $\frac{c}{\sqrt{t}}$.



d) – The dependence of the dissolution rate of lime samples containing 7.6% of MgO on the value of $\frac{c}{\sqrt{t}}$.

Figure 10-17: The dependence of the dissolution rate of lime samples on the value of $\frac{c}{\sqrt{t}}$.

The results obtained are consistent with the conclusions made by Umakoshi. et. al. [30] about limitation of lime dissolution process by magnesium oxide in slag systems with FeO content above 20%.

The values of the calculated diffusion coefficients (spatial semi-infinite diffusion in comparison with the non-stationary linear process) of mass transfer are shown in Table 10-7.

Table 10-7: The values of diffusion coefficients of lime dissolution in slag (SD- spatial diffusion and LD-linear diffusion).

T °C	D, cm ² /s								
	SD	SD	LD	SD	LD	SD	LD	SD	LD
	2% MgO	4.3% MgO		5.6% MgO		6.2% MgO		7.6% MgO	
1	1.37·10 ⁻³	1.66·10 ⁻⁵	0.91·10 ⁻⁵	6.15·10 ⁻⁶	4.52·10 ⁻⁶	5.31·10 ⁻⁶	3.14·10 ⁻⁶	3.80·10 ⁻⁶	1.53·10 ⁻⁶
2	2.64·10 ⁻³	10.56·10 ⁻⁵	2.83·10 ⁻⁵	4.29·10 ⁻⁵	1.26·10 ⁻⁵	1.81·10 ⁻⁵	1.02·10 ⁻⁵	1.26·10 ⁻⁵	0.38·10 ⁻⁵
3	9.6·10 ⁻³	19.60·10 ⁻⁵	5.27·10 ⁻⁵	9.15·10 ⁻⁵	2.83·10 ⁻⁵	5.80·10 ⁻⁵	1.66·10 ⁻⁵	2.80·10 ⁻⁵	0.91·10 ⁻⁵
4	1.32·10 ⁻²	30.16·10 ⁻⁵	7.85·10 ⁻⁵	14.95·10 ⁻⁵	5.02·10 ⁻⁵	7.85·10 ⁻⁵	2.29·10 ⁻⁵	4.53·10 ⁻⁵	1.38·10 ⁻⁵

1 refers to 1300°C, 2-1400°C, 3-1500°C and 4-1600°C

Derived diffusion coefficient values for the linear and spatial process of mass transfer are in satisfactory agreement with each other. Dependence of the dissolution rate of samples on the variable $\frac{c}{\sqrt{t}}$ is approximated by linear correlation with high reliability, which suggests that the chosen spatial model is adequate. It is noteworthy that the calculated from the experimental data D values are comparable with the value of $2.7 \cdot 10^{-5}$ cm²/s, presented by Matsushima et.al. [60] for CaO dissolution in slag with the composition: 20% FeO-40% SiO₂- 40% CaO at 1400°C.

The difference in the values of the diffusion coefficients is explained by the difference in slag and samples composition. In the case when convective fluctuations occur in the high temperature metallurgical system, in the equations of the first and second Fick's laws' effective diffusion coefficient, D_{ef}, is introduced instead of the molecular diffusion coefficient D.

The effective diffusion coefficient values are six to eight times higher than the molecular diffusion coefficient and result in 200-1000 cm²/s, as shown in the study of mass transfer processes in a boiling liquid bath using radioactive indicators [23].

In the turbulent medium substance concentration in the volume of each liquid phase is approximately constant. However, in these conditions, the role of molecular diffusion still remains significant, since at the interface there are thin unstirred boundary layers in which the mass transfer is carried out by molecular diffusion.

According to the results derived, the diffusion coefficient values decrease with the increasing content of MgO in lime at the same temperatures and increase with the

increasing temperature and constant MgO values. By raising the content of MgO from 2 to 7.6% the D value decreased by a factor of 5 to 8.

The experimental data confirms the linear dependence of $\ln D$ on the inverse temperature $1/T$ according to the equation (10-5), as shown in (Figures 10-18 and 10-19):

$$\ln D = \ln D_0 - \frac{E_D}{R} \frac{1}{T} \quad (10-5)$$

The calculated mean value of the diffusion activation energy using a tangent of the angle is 198.7 ± 17.0 kJ/mol for lime containing 2% of MgO and 230.2 ± 14.0 kJ/mol for limes containing 3.4-7.6% of MgO. High values of diffusion energy are typical for slag systems, for example, the diffusion energy of phosphorus oxide in the silicate slags is 170 kJ/mol. and in the aluminate slags - 200 kJ/mol. [62]

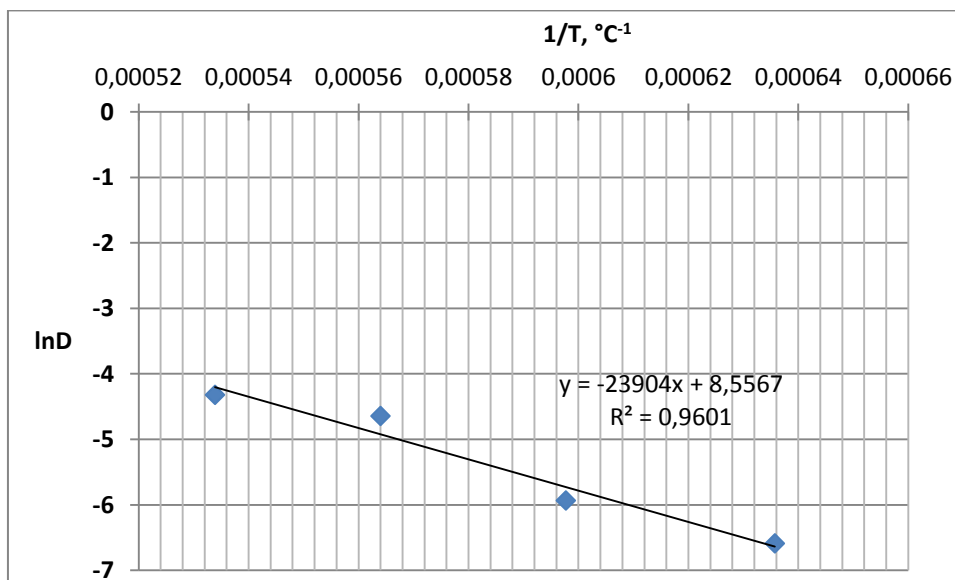


Figure 10-18: The dependence of the logarithm of the diffusion coefficient on the inverse temperature

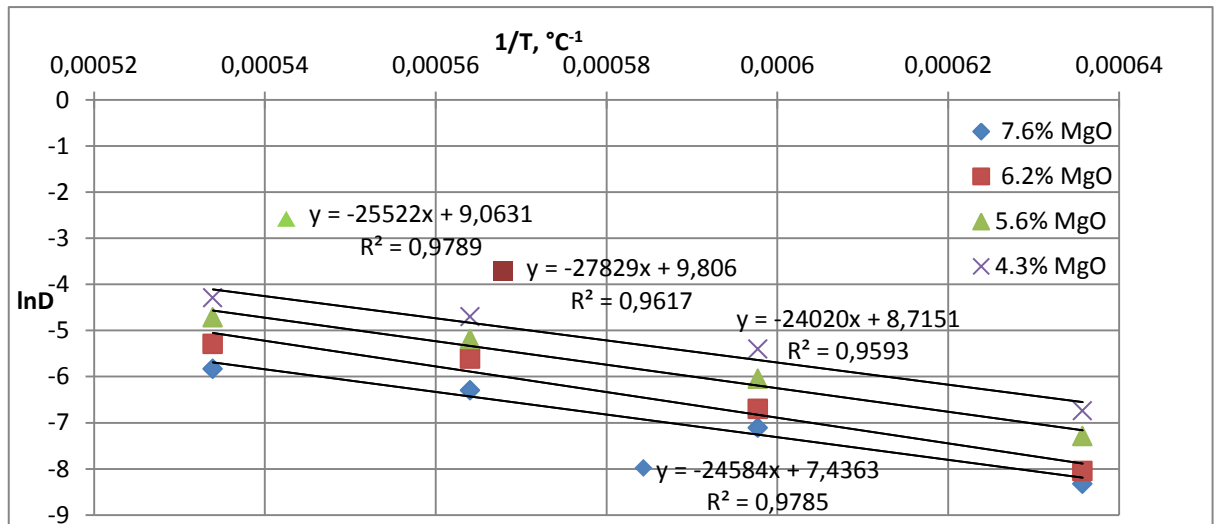


Figure 10-19: The dependence of the logarithm of the diffusion coefficient on the inverse temperature

The elevated levels of diffusion activation energy of calcium oxide in the slag is due to the work that must be applied to bring CaO atoms from the volume of the solid phase onto the interface, where they are in an (e.g. activated) energetically unfavorable state.

Derived kinetic parameters of the lime dissolution process, containing various amounts of MgO, allow for implementing slag formation in the magnesium oxide saturation area. The slag of this composition have less aggressive effect on the refractory lining of the converter. According to the theory of metallurgical thermodynamics no interaction at the interface of the two phases takes place in the case of equality of the concentration of the diffusing component and the saturation concentration.

The following conclusions are summarized below:

1. The kinetics of model slag saturation with lime containing different amounts of MgO in the process of lime dissolution, in a non-stationary diffusion at temperatures of 1300-1600°C has been studied.
2. To describe the kinetics of dissolution of solid body in the molten slag differential equations derived from the total mass balance of the dissolving substance have been applied. The total mass balance considers the transition of the dissolving substance into the melt phase and its accumulation in the consistently soluble layers of solid.
3. It was revealed that with the increasing content of magnesium oxide from 2 to 7.6% in the technical lime saturation concentration of calcium oxide in the slag decreases 1.2-1.6 times depending on the temperature of the process of lime dissolution.

The equilibrium concentration of CaO in the slag melt is influenced by the content of FeO in the slag and MgO content in lime. Magnesium and iron oxides form a solid

magnesiowustite solution ((Fe, Mg)O) and silicates of Ca and Mg in form of dense poorly soluble film on the surface and in the volume of lime. The raise in the MgO content leads to increase in the thickness of formations and as a consequence, limits the dissolution of lime.

4. It was found that, despite a decrease in the concentration gradient, as the saturation of slag with lime progresses, the mass transfer coefficients are increasing, which value is largely dependent on slag composition and particle size of the lime.

5. The influence of MgO content in lime on its rate of dissolution has been revealed. The increase in the concentration of MgO in lime results in slower dissolution rates of samples, which indicates the limitation of the process by MgO diffusion in slag. Formation of chemical compounds based on magnesium oxide inhibits diffusive transport of CaO and MgO in the melt and results in the cessation of diffusion.

6. Diffusion coefficients were calculated on the basis of the experimental data under the conditions of non-stationary linear and spatial semi-infinite diffusion. The linear dependences of the dissolution rate of samples on the variable $\frac{c}{\sqrt{t}}$ derived with high reliability consider the chosen spatial model adequate. It was revealed that the diffusion coefficients decrease in approximately 5–8 times with the double increase in the content of MgO (from 2 to 7.6%) and increase with the raising temperature (1300°C to 1600°C) at constant MgO content by a factor of 15-20.

7. The linear dependence of diffusion coefficients logarithm on the inverse temperature has been derived. The calculated mean value of the diffusion activation energy is 230.2 ± 14.0 kJ/mol. The high value of diffusion energy is due to the great degree of viscosity of the slag melt and elevated “energy consumption” of the calcium oxide. This occurs for output through the interface lime-slag, which is film-coated by solid and liquid solutions, and chemical compounds on the basis of CaO and MgO.

11 The results of experimental study of dolomite dissolution containing 20, 50 and 80% MgO

In this Chapter the kinetics of dolomite dissolution containing 20, 50 and 80% of MgO in model slag (20% CaO, 45%FeO and 35%SiO₂) has been studied. It is worth mentioning that dolomite materials have different preparation procedures compared to lime materials described in Chapter 10 and were provided by Voestalpine Stahl Linz.

The results of the experiment with dolomite containing 20% of MgO are presented in Table 11-1. The amount of the dissolved samples is presented as function of contact time in Figure 11-1.

Table 11-1: The experimental results of the dissolution process of dolomite samples containing 20% of MgO in the model slag

№ of test	1300°C		1400 °C		1500 °C		1600°C	
	Time, s	Mass of lime dissolved in the slag phase, g	Time, s	Mass of lime dissolved in the slag phase, g	Time, s	Mass of lime dissolved in the slag phase, g	Time, s	Mass of lime dissolved in the slag phase, g
1	20	0.0090	20	0.0200	20	0.0250	20	0.0300
2	60	0.0100	60	0.0420	60	0.0540	60	0.0840
3	90	0.0420	90	0.0950	90	0.1140	90	0.1540
4	180	0.0650	180	0.1240	180	0.1580	180	0.2110
5	600	0.1250	600	0.1540	600	0.2140	600	0.3250
6	900	0.1750	900	0.2580	900	0.3110	900	0.4020
7	1200	0.2120	1200	0.2750	1200	0.3950	1200	0.5140
8	1500	0.2130	1500	0.3150	1500	0.4120	1500	0.5800
9	1800	0.2130	1800	0.3200	1800	0.4050	1800	0.5710
10	2400	0.2140	2400	0.3100	2400	0.4150	2400	0.5740

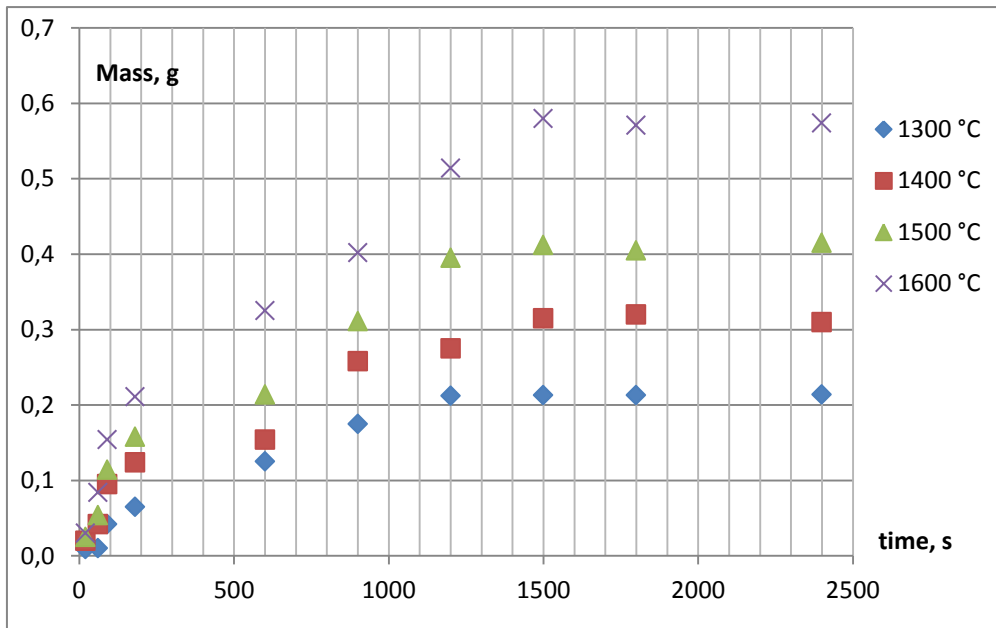


Figure 11-1: The dependence of the amount of dissolved dolomite containing 20% MgO on the contact time with slag

Based on the experimental data it is evident, that the amount of the dissolved dolomite ceases to change after time interval of 1500 seconds where the saturation of the slag with lime takes place. The amount of dissolved lime increases with the temperature and, respectively, the saturation concentration of calcium oxide in the slag raises as well. Equilibrium concentration of calcium oxide in the slag phase at 1300°C is 25.8%, 28.05% at 1400°C, 30.1% at 1500°C and 33.4 at 1600°C.

The relation between the linear rate of samples dissolution $\frac{\Delta h}{\Delta \tau}$ and the saturation concentration of CaO in slag is presented on Figure 11-2. With the increasing concentration of CaO in the slag the dissolution rate of samples drops due to the decrease in the concentration gradient $(CaO\%)_{sat} - (CaO\%)$.

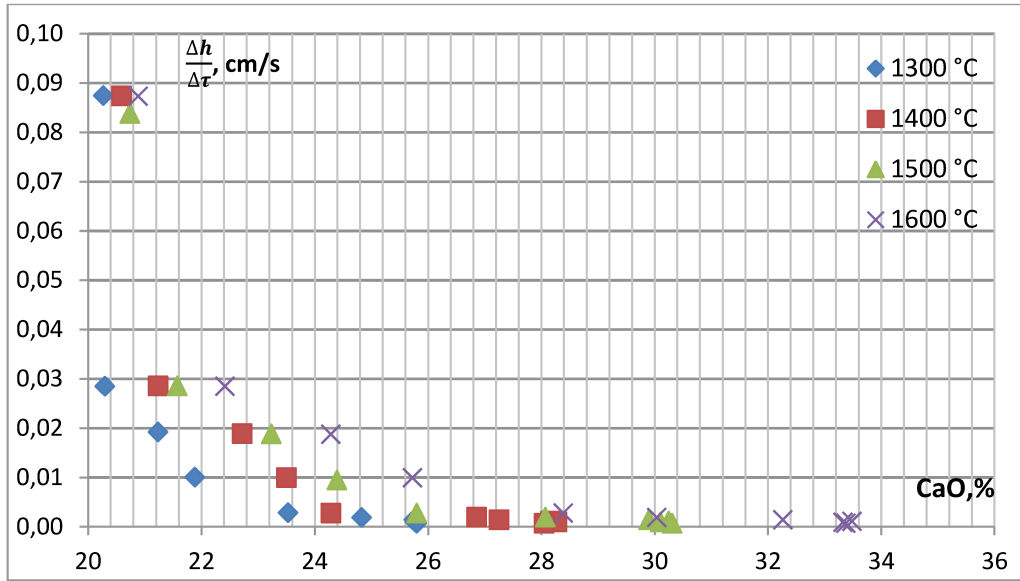


Figure 11-2: The dependence of the linear rate of dissolution of dololime samples on the CaO content in the slag

Calculated Activation energy of the dissolution process of dololime using tangent of the angle (see Figure 11-3) is 64.4 ± 5.3 kJ/mol. The value derived indicates the diffusion limiting step in the process of dololime dissolution in model slag.

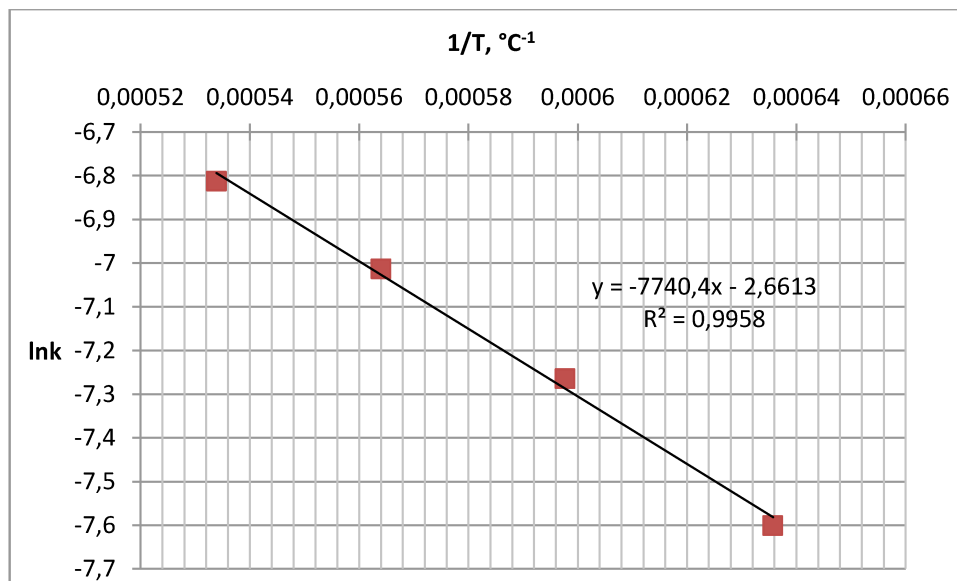


Figure 11-3: The dependence of the logarithm of the mass transfer coefficient on the inverse temperature

The linear dependence of mass change rate of dololime samples $w = \frac{1}{s} \frac{dM}{dt}$ on the value of $\frac{c}{\sqrt{t}}$ is shown in Figure 11-4. The dololime diffusion coefficient values in the molten slag were calculated using the tangent of the angle.

Dependence of the dissolution rate of samples on the variable $\frac{c}{\sqrt{t}}$ is approximated by linear correlation.

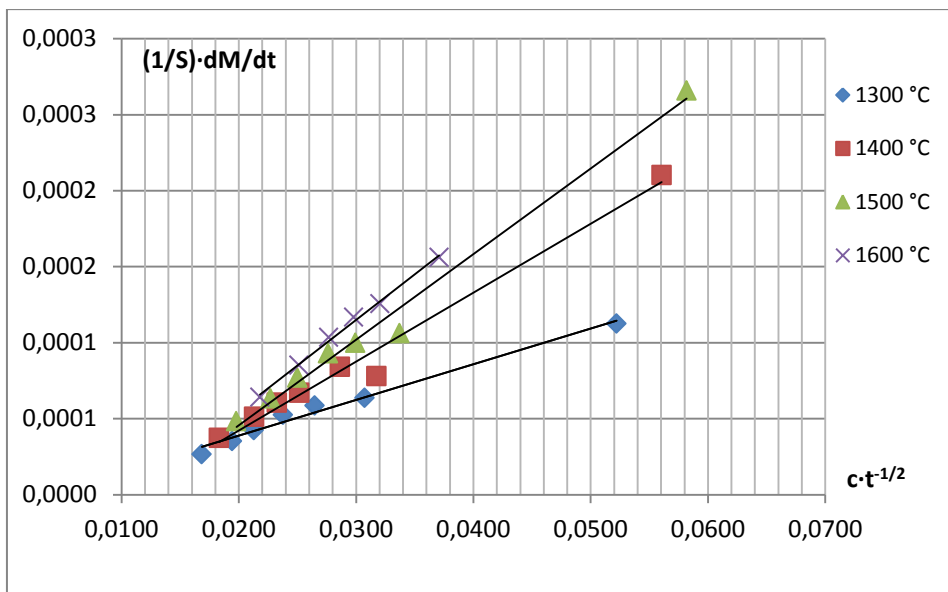


Figure 11-4: The dependence of the dissolution rate of lime samples containing 20% of MgO on the value of $\frac{c}{\sqrt{t}}$.

The linear dependence of $\ln D$ on the inverse temperature $1/T$ according to the equation (10-5) is shown in Figure 11-5.

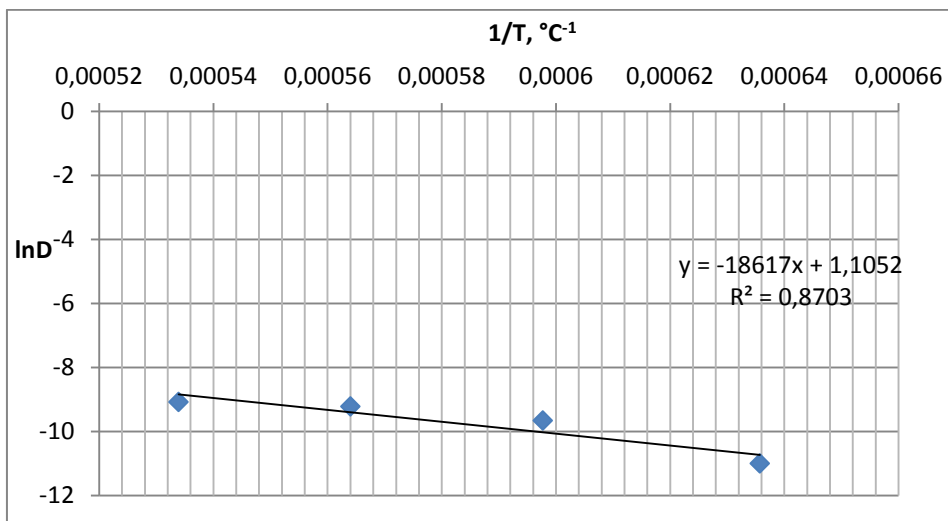


Figure 11-5: The dependence of the logarithm of the diffusion coefficient on the inverse temperature

Using equations (10-4) and (10-5) Diffusion coefficients and Diffusion activation energy with the value of 154.7 ± 9 kJ/mol were calculated. Despite the general tendency for the drop in the Diffusion coefficient values with the increasing MgO content in the material, diffusion coefficients of this dololime are higher than those for lime dissolution, see Table 11-4. Such behavior is due to the higher porosity of

material and different preparation procedures. Porosity investigations of lime and dololime samples using BET/BJH desorption method were carried out to support the conclusion made and are presented in Table 11-2.

Table 11-2: Porosity measurements of lime samples

	MgO %						
	2%	4.3%	5.6%	6.2%	7.6%	20%	50%
Surface Area, m²/g	16.697	14.541	14.300	8.290	8.278	16.599	14.380
Pore Volume, cm³/g	0.0120	0.0123	0.01042	0.0079	0.008	0.021	0.015
Pore r, Å	5.582	6.894	8.120	9.201	10.826	12.440	17.391

The results of Experiment with dololime containing 50% MgO are shown in Table 11-3. The amount of the dissolved samples is presented as function of time in Figure 11-6.

Table 11-3: The experimental results of the dissolution process of dololime samples containing 50% of MgO in the model slag

№ of test	1300°C		1400 °C		1500 °C		1600°C	
	Time, s	Mass of lime dissolved in the slag phase, g	Time, s	Mass of lime dissolved in the slag phase, g	Time, s	Mass of lime dissolved in the slag phase, g	Time, s	Mass of lime dissolved in the slag phase, g
1	20	0.0054	20	0.0045	20	0.0178	20	0.0199
2	60	0.0075	60	0.0175	60	0.0258	60	0.0211
3	90	0.0102	90	0.0254	90	0.0413	90	0.0410
4	180	0.0258	180	0.0459	180	0.0755	180	0.0985
5	600	0.0758	600	0.1124	600	0.1458	600	0.1789
6	900	0.0985	900	0.1458	900	0.2145	900	0.2547
7	1200	0.1198	1200	0.1995	1200	0.2548	1200	0.2998
8	1500	0.1233	1500	0.1991	1500	0.2799	1500	0.3005
9	1800	0.1245	1800	0.1978	1800	0.2758	1800	0.3145
10	2400	0.1250	2400	0.1985	2400	0.2874	2400	0.2999

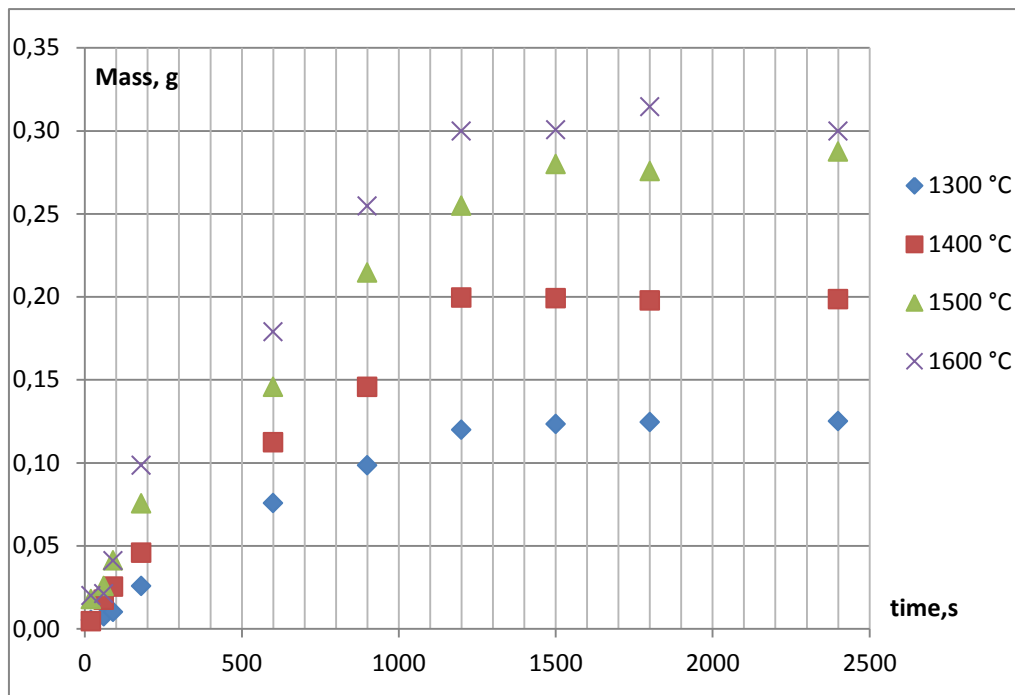


Figure 11-6: The amount of dolomite containing 50% MgO dissolved on contact time with slag

As it is seen on the Figure 11-6, the amount of the dissolved dolomite ceases to change after time interval of 1700 seconds. The amount of dissolved material increases with the temperature. Equilibrium concentration of calcium oxide in the slag phase at 1300°C is 21.7%, 22.7% at 1400°C, 23.8% at 1500°C and 23.9% at 1600°C. This agrees with the literature [3,57] and is significantly lower than the saturation of pure CaO and limes used in the experiment.

The relation between the linear rate of samples dissolution $\frac{\Delta h}{\Delta \tau}$ and the saturation concentration of CaO in slag is presented on Figure 11-7. With the increasing concentration of CaO in the slag the dissolution rate of samples drops due to the decrease in the concentration gradient $(CaO\%)_{sat} - (CaO\%)$.

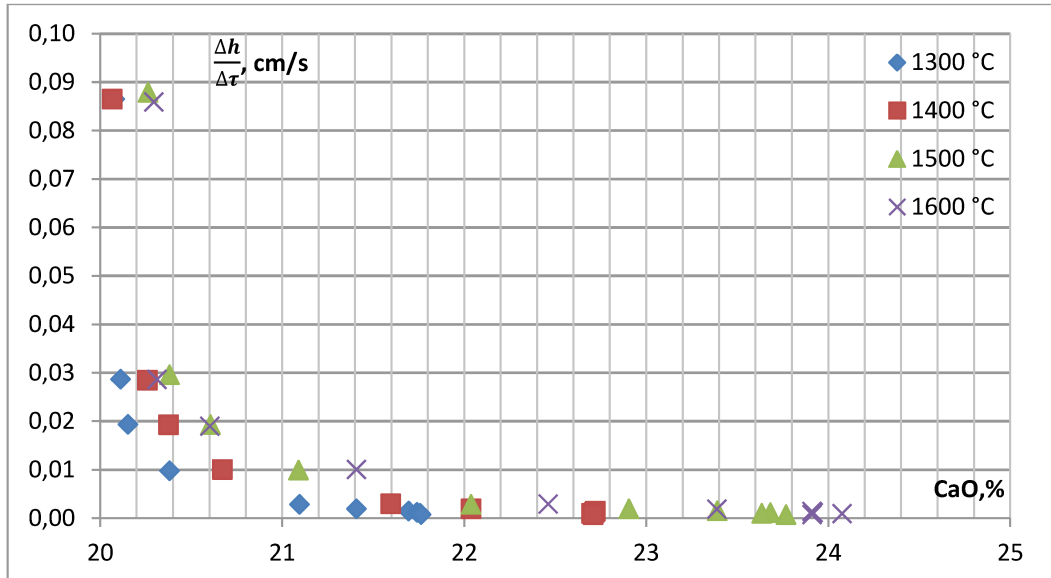


Figure 11-7: The dependence of the linear rate of dissolution of dolomite samples on the CaO content in the slag

Calculated Activation energy of dolomite dissolution in model slag using tangent of the angle on the Figure 11-8 is 74.9 ± 6.7 kJ/mol.

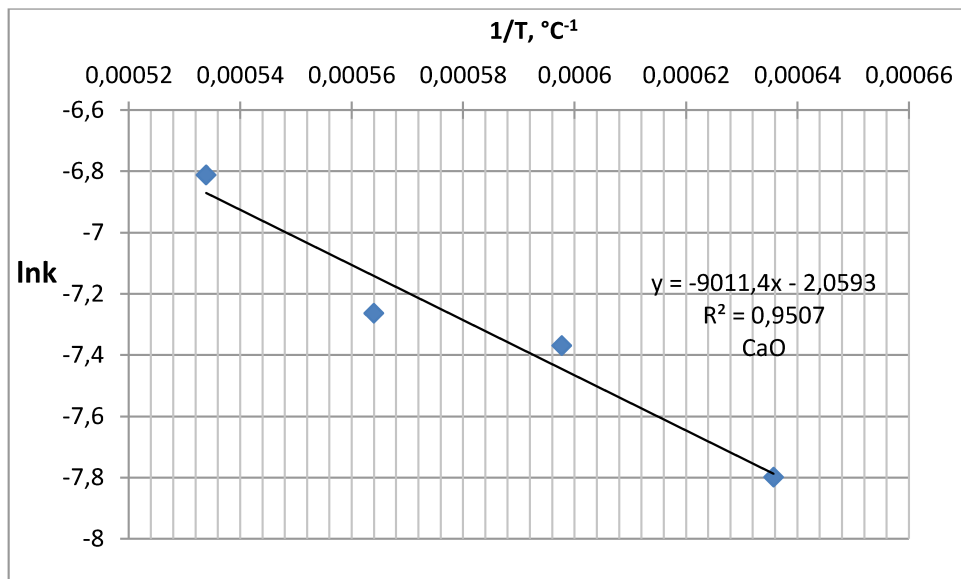


Figure 11-8: The dependence of the logarithm of mass transfer coefficients on the inverse temperature

The dependence of the dissolution rate of samples on the variable $\frac{c}{\sqrt{t}}$ is approximated by linear correlation. The dolomite diffusion coefficient values in the molten slag were calculated using the tangent of the angle.

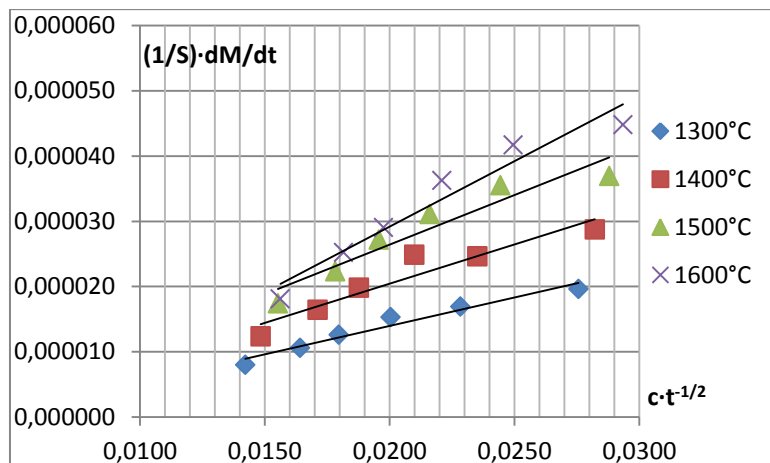


Figure 11-9: The dependence of the dissolution rate of lime samples containing 50% of MgO on the value of $\frac{c}{\sqrt{t}}$.

The linear dependence of $\ln D$ on the inverse temperature $1/T$ according to the equation (10-5) is shown in Figure 11-10.

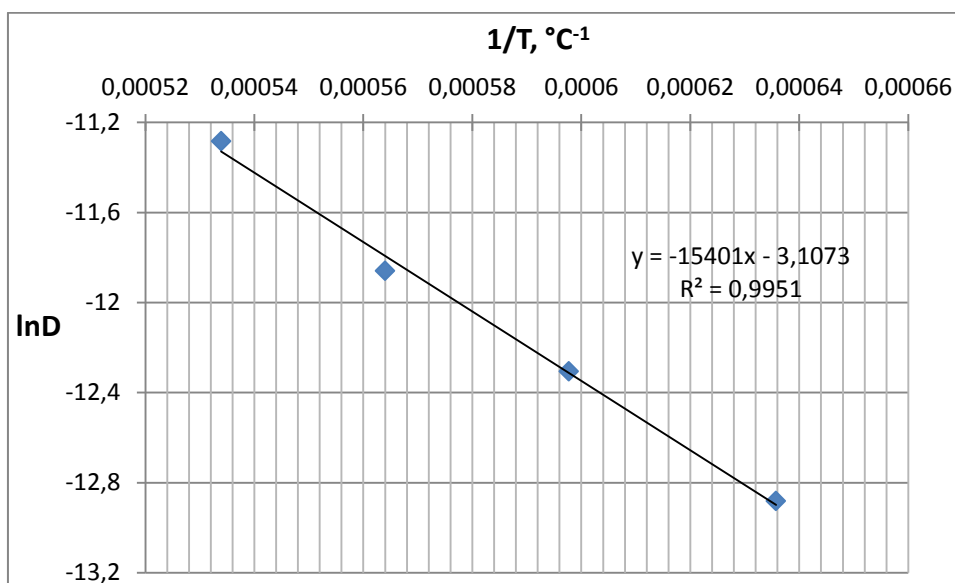


Figure 11-10: The dependence of the logarithm of the diffusion coefficient on the inverse temperature

The diffusion coefficient values of dolomite material containing 50% MgO are essentially lower than those of other materials (CaO and limes containing 2 to 7.6% MgO) used in the experiment. Here the tendency for the drop in the diffusion coefficient with the increasing MgO content in the dissolving material is observed.

11 The results of experimental study of dolomite dissolution containing 20, 50 and 80% MgO

Table 11-4: The derived diffusion coefficients for dolomite dissolution containing 20 and 50% MgO

T, °C	D, cm ² /s	
	20% MgO	50% MgO
1300	$1.66 \cdot 10^{-5}$	$2.54 \cdot 10^{-6}$
1400	$6.36 \cdot 10^{-5}$	$4.52 \cdot 10^{-6}$
1500	$9.85 \cdot 10^{-5}$	$7.07 \cdot 10^{-6}$
1600	$11.30 \cdot 10^{-5}$	$1.26 \cdot 10^{-5}$

Finally, the dissolution experiment with dolomite containing 80% MgO has been carried out. The results are summarized in Table 11-5.

Table 11-5: The experimental results of the dissolution process of dolomite samples containing 80% of MgO in the model slag

№ of test	1300°C		1400 °C		1500 °C		1600°C	
	Time, s	Mass of lime dissolved in the slag phase, g	Time, s	Mass of lime dissolved in the slag phase, g	Time, s	Mass of lime dissolved in the slag phase, g	Time, s	Mass of lime dissolved in the slag phase, g
1	20	0.0012	20	0.0008	20	0.0011	20	0.0009
2	60	0.0047	60	0.0009	60	0.0016	60	0.0011
3	90	0.0045	90	0.0021	90	0.0055	90	0.0014
4	180	0.0075	180	0.0046	180	0.0075	180	0.0045
5	600	0.0111	600	0.0081	600	0.0115	600	0.0120
6	900	0.0101	900	0.0088	900	0.0142	900	0.0113
7	1200	0.0089	1200	0.0095	1200	0.0136	1200	0.0154
8	1500	0.0112	1500	0.0110	1500	0.0162	1500	0.0171
9	1800	0.0102	1800	0.0120	1800	0.0154	1800	0.0178
10	2400	0.0098	2400	0.0121	2400	0.0149	2400	0.0175

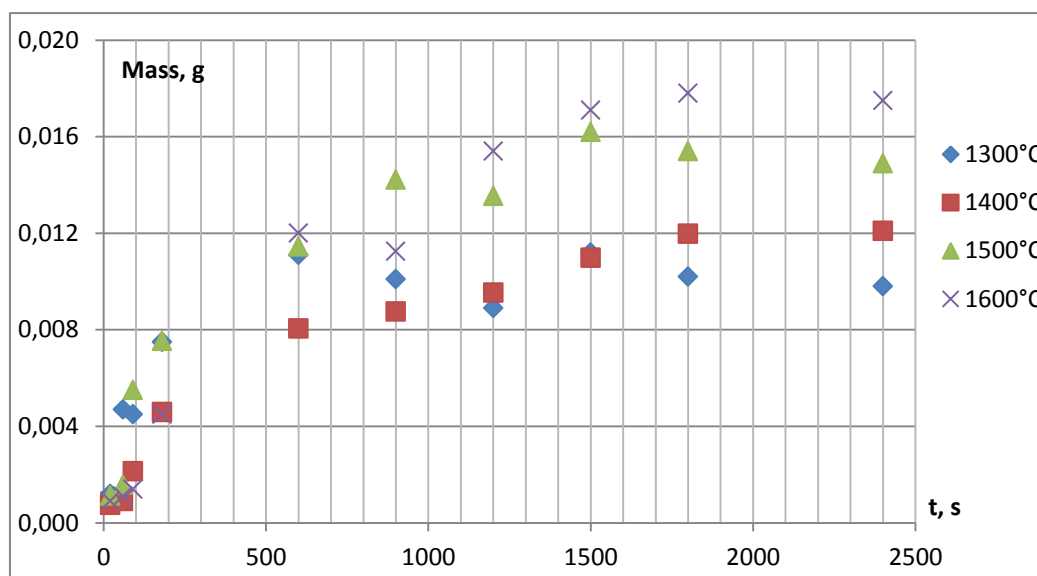


Figure 11-11: The dependence of mass of the dissolving sample on contact time with slag

As it is evident from the experiment the dissolved mass of the dolomite material containing 80%MgO in slag is insufficient. With such a low value of the dissolved sample mass it is not possible to conduct any kinetic calculations. It is worth mentioning, that the repetition of the dissolution test with this material did not show any further progress.

As a result of the experiment, the values of lime and dolomite Diffusion activation energy are summarized in Table 11-6.

Table 11-6: Activation energy of Diffusion for lime and dolomite samples

№	MgO content, %	Diffusion energy values, kJ/mol	Activation energy of the heterogeneous dissolution reaction, kJ/mol
1	2.0 ÷ 7.6	198.7±17 ÷ 230.0±14	-
2	20	154.7±9	64.4±5.3
3	50	128±11	74.9±6.7

The differences in the derived diffusion activation energy values attributed to different structure of the crystal lattice of lime samples used in the experimental study. An elementary act of diffusion is to move atom from one node of the lattice to the other one, if there is a concentration gradient in the system. Therefore, diffusion occurs throughout the volume of the crystalline lime sample by replacing one atom in the crystal lattice on the other, which leads to the formation of chemical compounds. To implement such atomic jumps it is necessary to overcome the potential barrier due to the presence of the force field of the crystal lattice. Therefore, the diffusion process requires very high activation energies comparable with the lattice energy.

However, if there is diffusion along grain boundaries, where there are many disorders in the crystal structure like vacancies, dislocations or pores, the activation energy can be relatively low as observed with dololime samples containing 20 and 50% MgO.

Thus, the diffusion activation energy characterizes the energy of atoms in the crystal lattice. The higher its value, the greater the amount of energy required for the transition of an atom from one equilibrium position in a lattice to another. Excess energy required for this transfer acquired by atom from neighbour atoms due to the constant exchange in the kinetic energy.

Since the activation energy is an exponential function of diffusion coefficient, it has a great effect on it and the diffusion coefficient in solids rises very rapidly with the increasing temperature. Such relation is described by the Arrhenius equation.

12 CFD calculations

ANSYS Fluent software has been used here to simulate the dissolution flow for the process of lime or CaO dissolution in the converter slag in order to demonstrate the impact of the flow on the overall process.

An important role is served by lime and slag densities. The general image of the dissolution is possible to observe by using ANSYS Fluent [63] program. Depending on the difference between densities of the dissolving material and slag, the flow rate and the direction of the flow will vary. When the density of lime is lower than the density of slag, lime particles will float up onto the melt and 'sink' in the bulk melt if the density of lime is higher than slag density.

An important part of the simulation was the direction of the dissolution. By the visual observation of the cylinder lime samples after the dissolution the reduction in size was observed mainly in the bottom of the cylinders.

Two different cases have been simulated considering the density difference between the dissolving material and slag. Taking into consideration the input data derived from the experiment, the flow has been simulated demonstrating its movement in two different directions due to the density difference. In the first case the density of lime of 3.9 g/cm^3 was higher than CaO-FeO-SiO₂ model slag density of 3.0 g/cm^3 , where dissolving lime particles went in the direction of 'down-flow' in the melt. In the second case lime density was lower and particles went in the direction of 'up-flow'. During the dissolution of solid component the flow influences the boundary layer and increases the distance between high and low concentration zones of the component in the melt, thus, the flow can enhance the dissolution process and also can be indicated by high values of the diffusion coefficient. As the dissolution of sample progresses, diffusion increases significantly with the influence of the flow.

Another parameter influencing the flow is viscosity. Viscosity of the melt is decreasing with the dissolution of basic oxides, such as CaO and MgO. Melts with high concentration of SiO₂ have high viscosity. CaO ions break SiO₂ continuous chain and, therefore, the viscosity decreases, as well as with the raise in temperature.

As it is evident from the simulation results on Figures 12-1 and 12-2 the density difference between dissolved material and melt describes the behavior of the material whether its particles will move up or 'sink' in the melt. If material density is lower (see Figure 12-1) the saturation will be reached faster, as the dissolving particles will float up, however, in the bulk phase of the melt saturation may be not reached. If the dissolving material density is higher (see Figure 12-2), particles will move deeper in the bulk phase of the melt which allows reaching the saturation in the deep layers of the slag, consistently moving upwards. In addition, the shape of the sample is also affected by the flow depending on its direction.

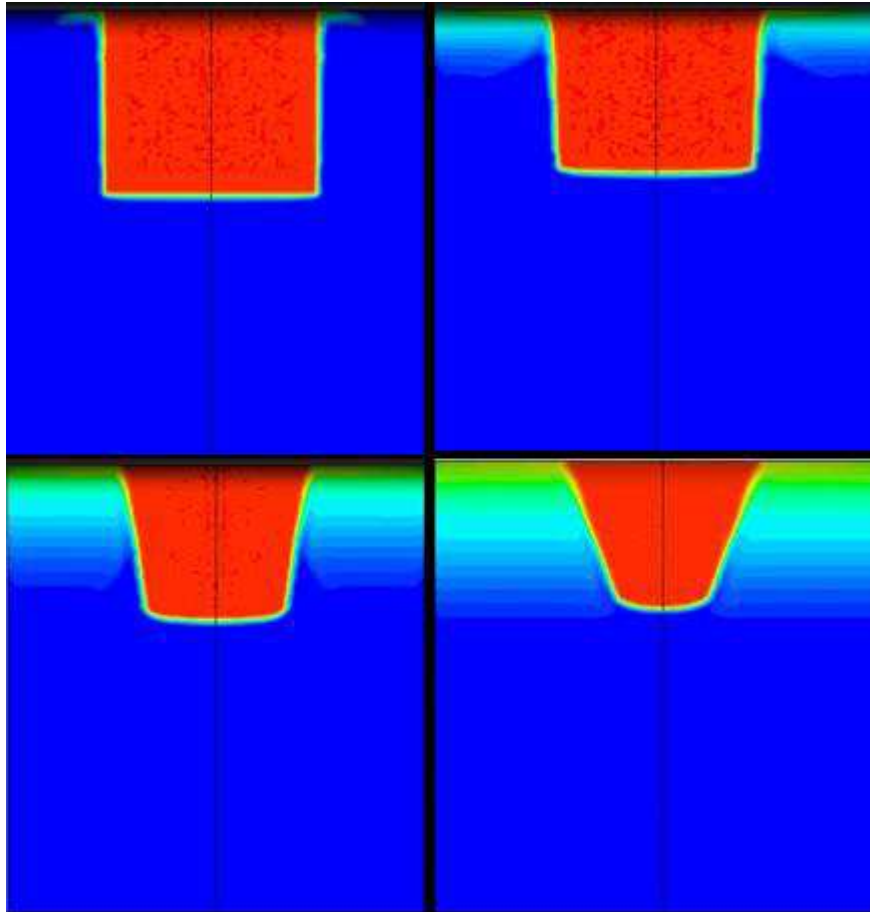


Figure 12-1: Simulation of up-flow of the dissolving sample

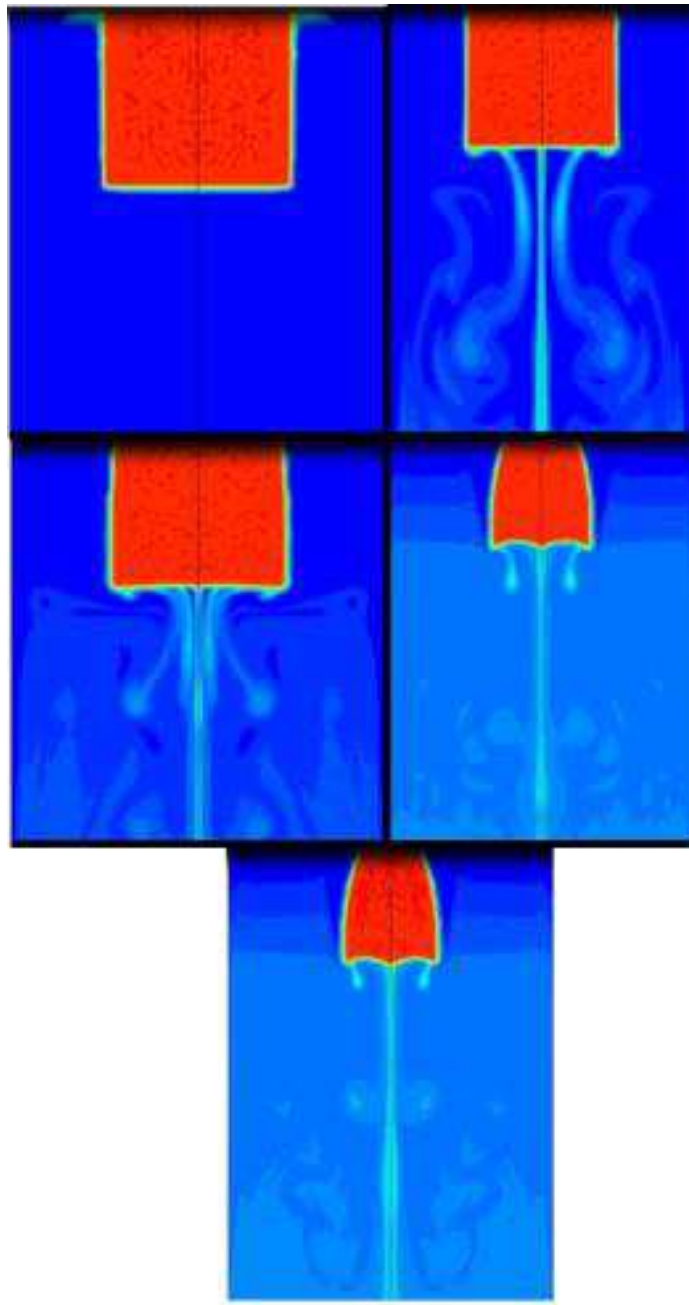


Figure 12-2: Simulation of down-flow of the dissolving sample

After experiment visual observation of the cylindrical samples indicated that the dissolution mainly took place in the bottom of the cylinder. In order to investigate the influence of the flow the rotating cylinder experiment has been carried out.

13 Rotating cylinder experiment

In the stagnant experimental series the influence of the flow was not defined, thus, the experiment with rotating sample has been conducted. A schematic illustration of the experimental setup is shown in Figure 13-1. It equipped with a motor enabling 180rpm, Platinum-Rhodium thermocouple, Molybdenum rotation rod, sampling rod centring system to stabilize the rotation of the rod and Argon gas inlet.

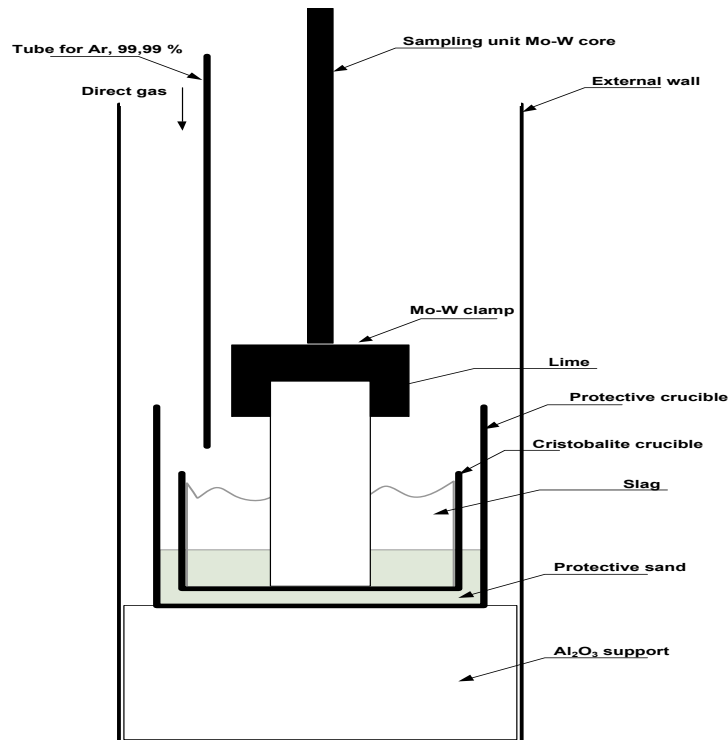


Figure 13-1: Schematic setup of vertical high temperature furnace

100 grams of model slag with the following composition 20% CaO, 35% SiO₂, 45% FeO was placed in magnesia crucible. The inertness of crucible material was investigated in Chapter 7.1. The cylindrical samples of 4 different limes containing 4.3-7.6% of MgO were prepared 2.5 cm long with diameter of 2.4 cm and density of 3.2 g/cm³. The samples were introduced into the molten slag and rotated for a predetermined time. Samples were then withdrawn from the melt, cooled down to the room temperature and weighted on the analytical balance. The experiment carried out under temperatures of 1400 and 1500°C. Calculation of Diffusion coefficient was carried out using equation (13-1) [29]:

$$\frac{1}{s} \frac{dm}{dt} = 0.2D^{2/3}v^{-1/6}n^{1/2}C \quad (13-1)$$

where: $\frac{dm}{dt}$ is the mass change of the rotating cylinder in time (g/s), S is cylinder surface (cm^2), D is Diffusion coefficient (cm^2/s), ν is kinematic viscosity (cm^2/s), equal to the ratio of the dynamic viscosity η (Pa·s) to density ρ (g/cm^3), n is number of evolutions per s, (s^{-1}), C is CaO concentration (g/cm^3).

The results of the experiments are summarized in the Tables 13-1 – 13-4.

Table 13-1: Experimental results of lime dissolution containing 4.3% MgO

Slag and lime properties	Temperature	
	1400°C	1500°C
Initial mass of lime cylinder, g	28.94	29.05
Initial CaO content in slag, %	20	20
Final mass of lime cylinder, g	12.85	5.09
Mass of dissolved lime, g	16.09	23.95
CaO content in lime, %	91.4	91.4
MgO content in lime, %	4.3	4.3
dm CaO, g	14.71	21.9
Rotation time t, s	600	600
CaO concentration in slag, g/cm ³	0.9568	1.0816
Revolutions per sec, n (180 rpm)	3	3
D, cm ² /s for rotation	1.343E-04	2.03E-04
Spatial diffusion	1.06E-04	1.96E-04
Linear diffusion	2.83E-05	5.25E-05

Table 13-2: Experimental results of lime dissolution containing 5.6% MgO

Slag and lime properties	Temperature	
	1400°C	1500°C
Initial mass of lime cylinder, g	29.02	29.50
Initial CaO content in slag, %	20	20
Final mass of lime cylinder, g	18.95	15,01
Mass of dissolved lime, g	10.07	14.49
CaO content in lime, %	91.1	91.1
MgO content in lime, %	5.6	5.6

dm CaO, g	9.17	13.20
Rotation time t, s	600	600
CaO concentration in slag, g/cm³	0.84807	0.99558
Revolutions per sec, n (180 rpm)	3	3
D, cm²/s	6.227E-05	1.49E-04
Spatial diffusion	4.29E-05	9.15E-05
Linear diffusion	1.26E-05	2.83E-05

Table 13-3: Experimental results of lime dissolution containing 6.2% MgO

Slag and lime properties	Temperature	
	1400°C	1500°C
Initial mass of lime cylinder, g	28.50	28.75
Initial CaO content in slag, %	20	20
Final mass of lime cylinder, g	23.36	21.24
Mass of dissolved lime, g	5.14	7.51
CaO content in lime, %	91.6	91.6
MgO content in lime, %	6.2	6.2
dm CaO, g	4.71	6.88
Rotation time t, s	600	600
CaO concentration in slag, g/cm³	0.75205	0.80007
Revolutions per sec, n (180 rpm)	3	3
D, cm²/s	3.491E-05	6.761E-05
Spatial diffusion	1.81E-05	5.80E-05
Linear diffusion	1.02E-05	1.66E-05

Table 13-4: Experimental results of lime dissolution containing 7.6% MgO

Slag and lime properties	Temperature	
	1400°C	1500°C
Initial mass of lime cylinder, g	28.90	28.45
Initial CaO content in slag, %	20	20
Final mass of lime cylinder, g	25.81	22.72
Mass of dissolved lime, g	3.09	5.73
CaO content in lime, %	90.1	90.1
MgO content in lime, %	7.6	7.6
dm CaO, g	2.78	5.16
Rotation time t, s	600	600
CaO concentration in slag, g/cm ³	0.70714	0.76151
Revolutions per sec, n (180 rpm)	3	3
D, cm ² /s	1.737E-05	3.929E-05
Spatial diffusion	1.26E-05	2.80E-05
Linear diffusion	0.38E-05	0.91E-5

To calculate mass transfer coefficient of the immersed general solid body into the melt under the convection flow equation (13-1) involving J-factor can be applied. [30]

$$J = St \cdot Sc^\beta = \alpha \cdot Re^\gamma \quad (13-2)$$

Another useful correlation proposed by Eisenberg et.al [64] for mass transfer specifically from a solid cylinder in a liquid under the convection flow:

$$\frac{k}{U} = 0.079 \cdot Re^{-0.3} Sc^{-0.644} \quad (13-3)$$

where α, β and γ are empirical coefficients, St is a Stanton number, defined as (k/U) , Sc is the Schmidt number $(\eta/\rho D)$, Re is the Reynolds number $(\rho d U/\eta)$; k is the mass transfer coefficient (m/s), η is the viscosity of the fluid (Pa·s), U is the peripheral speed of rotation of the cylinder (m/s), d is the diameter of the cylinder (m), ρ is the density of liquid (kg/m^3), D is the diffusion coefficient (m^2/s).

Derived mass transfer coefficients using equation (13-2) are presented in Table 13-5.

Table 13-5: Mass transfer coefficients of lime dissolution under forced convection

k, cm/s	4.3%	5.6%	6.2%	7.6%
1400	2.30E-03	1.40E-03	9.65E-04	6.15E-04
1500	3.00E-03	2.46E-03	1.48E-03	1.04E-03

The mass transfer coefficients derived here are similar to those reported by Umakoshi et.al: $4.7 \cdot 10^{-4}$ to $1.7 \cdot 10^{-3}$ cm/s [30] and Fruehan et.al: $4.5 \cdot 10^{-4}$ to $2.5 \cdot 10^{-5}$ cm/s. [59]

Figure 13-2 shows microscopic raster images (SEM Tesla XRAY Oxford) of lime containing 4.3, 7.6 and 80% MgO, after 5 minutes of immersion in the melt at 1500 C, and the phase composition of samples carried out with a powder diffractometer "Bruker D2 Phaser". Sample containing 80% of magnesium oxide was prepared by Voestalpine Stahl Linz consisting of periclase (MgO) and portlandite ($\text{Ca}(\text{OH})_2$) phases. The sample was prepared in the shape of cylinder according to the methodology described earlier. During kinetic experiment after the contact time up to 2400 seconds dissolution of sample was not observed. Microscopic investigation of lime containing 80% MgO was carried out for detection of formed solid compounds blocking the dissolution. Due to the capillary effects after 5 minutes of contact with a melt samples become impregnated with slag. Slag fills the inner and outer pores of lime and is distributed in samples in the form of compounds, consisting of high-temperature silicates of calcium, magnesium and iron, and also magnesiowustite, based on the results of X-ray diffraction analysis. According to the intensities of the characteristic spectral lines, for example of magnesiowustite, it is

evident that with the increasing concentration of MgO in lime its concentration increases as well.

Chemical compounds formed during the dissolution of the lime in the slag inhibit the diffusion of MgO and CaO in the bulk slag and limit their dissolution in the melt. Growth of the phase formations limits the diffusion transport of CaO and MgO in the melt until the complete cessation of diffusion, which leads to the drop of MgO concentration in the slag with the raise of magnesium oxide concentration in lime.

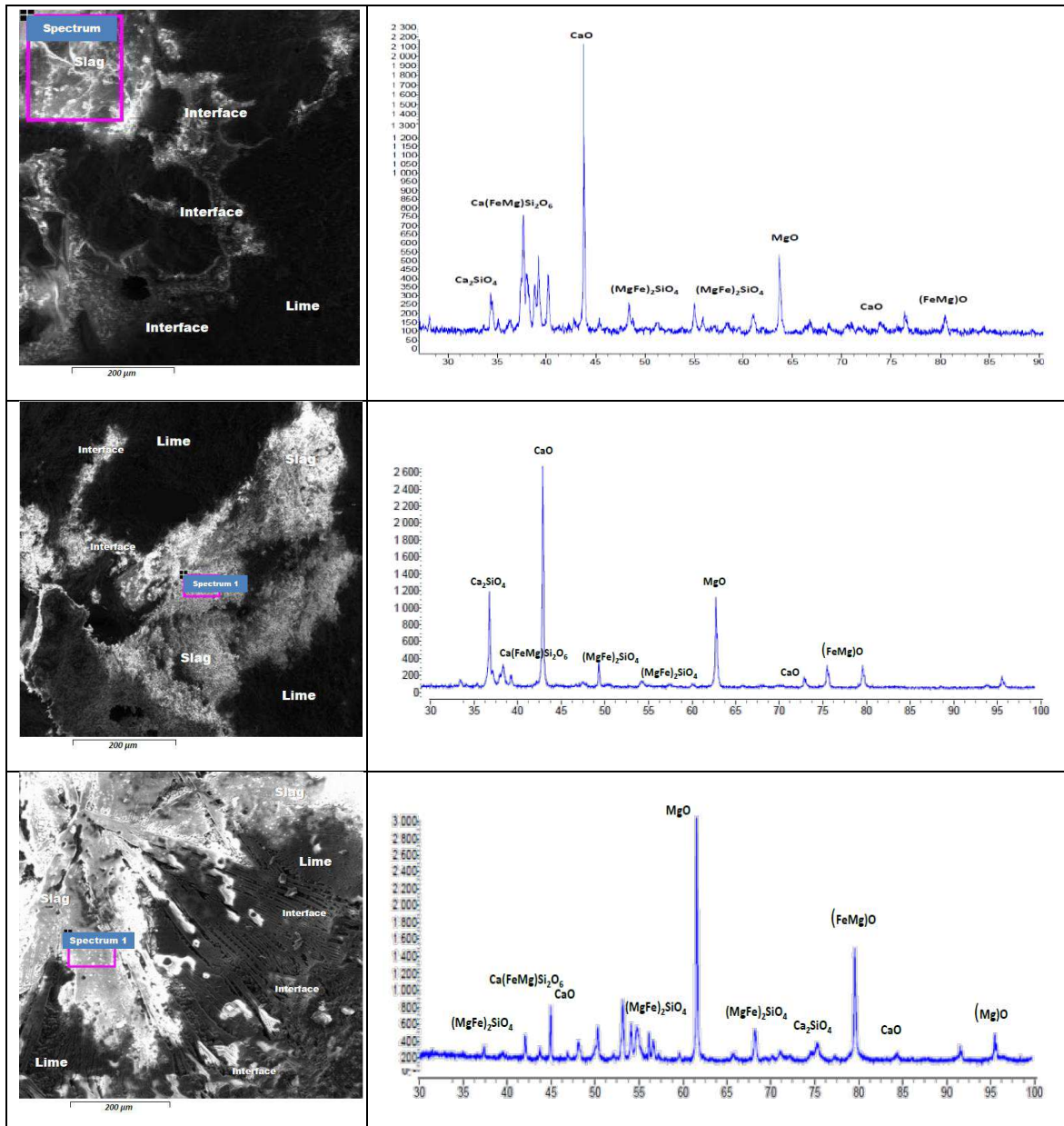


Figure 13-2: Microscopic raster images of lime containing 4.3 (upper) 7.6 (middle) and 80% MgO (bottom).

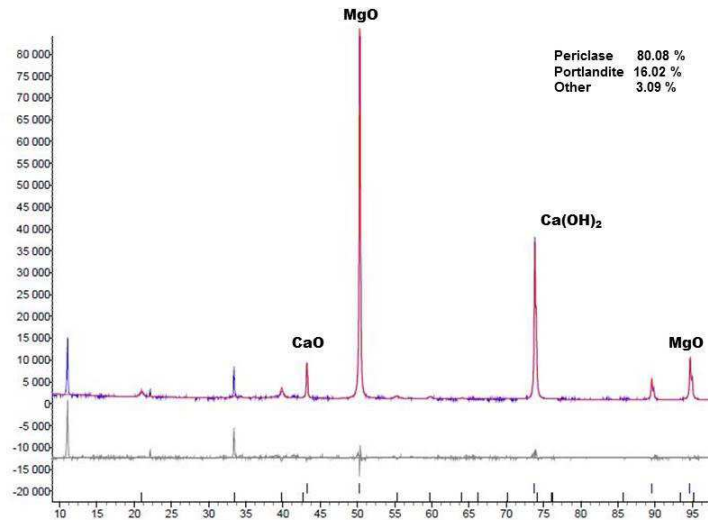


Figure 13-3: The X-Ray spectrum of dololime containing 80%MgO

To intensify the processes of dissolution of calcium and magnesium oxides in slags the rate-limiting step should be defined.

The sign of the outer diffusion is the dependence of the dissolution rate of lime on rate of the melt moving with respect to the dissolving material. The increase in the relative velocity of the fluid reduces the effective thickness of the diffusion boundary layer and, thus, raises the dissolution rate.

Satisfactory agreement of diffusion coefficient values obtained in the case of a rotating cylinder and calculated in the case of non-stationary diffusion in the absence of stirring, defines that the outer diffusion is not the rate-limiting step. The dissolution rate controlled by internal diffusion depends on the thickness, structure and density of the solid film formed on the surface of the dissolved material which further prevents the dissolution. The rate of dissolution is independent from the stirring rate, when process takes place in the area of inner diffusion, and that is observed during the experiment with rotating sample. Intradiffusion resistance is due to diffusion through the solid-state layer, like magnesiowustite, formed on the surface of soluble lime samples. Such solid poorly soluble phases were observed on the surface and in the volume of lime samples (Figure 13-2).

It is worth mentioning that the diffusion in the presence of phase transitions is the most complicated case of chemical diffusion. One of the ways to reduce or lower the diffusion resistance is crumbling of lime. Therefore, subtle or fine grinding of lime will substantially weaken the diffusion resistance. In case of formation of an insoluble reaction film, its thickness, comparable with the sizes of the particles will be small and will not cause substantial diffusion resistance.

14 Summary

The kinetics of pure calcium oxide and lime dissolution in a non-steady-state diffusion at temperatures of 1300-1500°C has been studied. It was found that with the increasing concentration of CaO in the slag the dissolution rate of samples dropped, due to the decrease in the diffusion concentration gradient $(CaO\%)_{sat} - (CaO\%)$. It was also found that the mass transfer coefficient increases due to the reduced size of the dissolving CaO or lime sample, and is explained by the decrease in the thickness of the boundary layer. Calculated value of the apparent activation energy of the heterogeneous dissolution reaction was less than 200kJ/mol indicating the limitation of the dissolution process by diffusion of CaO. After reaching the saturation the values of CaO mass transfer coefficient reduce due to the formation of solid phases (dicalcium $2CaO \cdot SiO_2$ and tricalcium silicate $3CaO \cdot SiO_2$), enveloping lime particles. SEM and XRD methods were applied in order to investigate the phases.

Mass transfer coefficients of MgO dissolution in slag have been calculated. Low values of the effective MgO mass transfer coefficients in comparison with CaO characterize the limitation of the dissolution process of lime in slag by the diffusion of MgO. This is applied for slag systems containing more than 20% of FeO.

The dissolution of lime containing different amounts of MgO in the model slag in a non-stationary diffusion at temperatures of 1300-1600°C has been studied. The experimental results derived showed that with the increasing content of magnesium oxide from 2 to 7.6% in the technical lime saturation concentration of calcium oxide in the slag decreases 1.2-1.6 times depending on the temperature of the process of lime dissolution.

Magnesiowustite solution ((Fe, Mg)O) in form of dense poorly soluble bulk formation in conjunction with (Ca, Mg and Fe) silicates on the surface and in the volume of lime were observed. The raise in the MgO content leads to increase in the amount of phases formed and as a consequence, limit the dissolution of lime until the complete cessation of diffusion.

The influence of MgO content in lime on its rate of dissolution has been investigated. The increase in the concentration of MgO in lime results in slower dissolution rates of samples, which indicates the limitation of the diffusion process through the low-permeable MgO surface film of silicates and solid phases at the interface.

It was revealed that the diffusion coefficients decrease by factor of 5–8 with the double increase in the content of MgO (from 2 to 7.6%) and increase with the raising temperature (1300°C to 1600°C) at constant MgO content by a factor of 15-20.

The calculated mean value of the diffusion activation energy is 198 ± 17.0 and 230.2 ± 14.0 kJ/mol. The high value of diffusion energy is due to the great degree of viscosity of the slag melt and elevated “energy consumption” of the calcium oxide. This occurs for output through the interface lime-slag, which is film-coated by solid and liquid solutions, and chemical compounds on the basis of CaO and MgO.

Experiment carried out under forced convection showed no significant increase in the diffusion coefficients. It was summarized that the process is controlled by the inner diffusion and the major impact has the formation of solid phases hindering the dissolution of solids. Phases of (Ca, Mg and Fe) silicates in conjunction with magnesiowustite were observed on the surface and in the volume of lime samples.

15 Bibliography

- [1] Dogan, N., G.A. Brooks and M.A. Rhamdhani, Kinetics of Flux Dissolution in Oxygen Steelmaking, *ISIJ Int.* 49 (2009), 10, pp. 1474–1482.
- [2] Deng, T., Study on the dissolution of lime and dolomite in converter slag, *Industrial Engineering and Management*, KTH Royal Institute of Technology, Stockholm, 2012.
- [3] Maruoka, N., A. Ishikawa, H. Shibata and S.-y. Kitamura, Dissolution Rate of Various Limes into Steelmaking Slag, *High Temperature Materials and Processes* 32 (2013), 1.
- [4] Huang, F., N. Maruoka, A. Ishikawa, J. Liu and S.-y. Kitamura, Dissolution Rates of Solid Oxides into Molten Slags, in: D.G. Goski, J.D. Smith (Eds.), *Proceedings of the Unified International Technical Conference on Refractories (UNITECR 2013)*, John Wiley & Sons, Inc, Hoboken, NJ, USA, 2014, pp. 869–874.
- [5] Maruoka, N., Ishikawa, A., Shibata, H. and Kitamura, S.: Competitive dissolution of MgO from Flux and Refractory, *Tohoku University* (2012), CD-Rom.
- [6] Nikitin, Y.P. and Esin, O.A., *Proceedings of Universities, Ferrous metallurgy*.
- [7] World Steel Association, *Steel statistical Yearbook*.
- [8] Turkdogan, E.T., *Fundamentals of steelmaking*, Institute of Materials, London, 1996.
- [9] Ghosh, A. and A. Chatterjee, *Ironmaking and steelmaking: Theory and practice*, Prentice-Hall of India, New Delhi, 2008.
- [10] Moore, C. and R.I. Marshall, *Steelmaking*, Institute of Metals, London, Brookfield, VT, 1991.
- [11] Fruehan, R.J., *The making, shaping and treating of steel*, 11. ed., AISE Steel Foundation, Pittsburgh, Pa., 1998.
- [12] Barker, K.J., *Oxygen Steelmaking Furnace, Mechanical Description and Maintenance Considerations*.
- [13] By John Stubbles, Steel Industry Consultant, *The basic oxygen steelmaking (bos) process*.
- [14] Oeters, F., *Metallurgy of steelmaking*, Verlag Stahleisen, Düsseldorf, 1994.
- [15] Voskoboynikov, V., *General Metallurgy, Production of steel*, 2005.
- [16] Williams, P., Sunderland, M. and Briggs, G., *Ironmaking Steelmaking* 9 (1982), pp. 150.

-
- [17] Pehlke, R.D., *Steelmaking—the jet age*, MTB 11 (1980), 4, pp. 539–562.
- [18] Jackson, A., *Oxygen Steelmaking For Steelmakers*, 1969.
- [19] Tupkary, R.H., *An Introduction to Modern Steel Making*, 2000.
- [20] Chakrabarti, A.K., *Steel making*, Prentice Hall, New Delhi, 2007.
- [21] Pehlke, R.D., *BOF Steelmaking, Theory*, 1975.
- [22] Medzibowskiy, M., *Thermodynamics and Kinetics of Steelmaking Processes*, 1996.
- [23] Baptizmansky, V.I., Okhotskiy V.B., *Physico-chemical basis of the BOF process*, Vishcha Head Publishing House, Donetsk, 1982.
- [24] Filippov, C., *The kinetics of decarbonation process in the molten metal* (1973), pp. 9–15.
- [25] Belyaev, S.V., *Fundamentals of metallurgical and foundry production: students manual* (2016), pp. 211.
- [26] Aksel'rod, L., Laptev, A., and Ustinov, Y, *Increasing resistance of converter lining: refractory materials, technological methods 1-2* (2009), pp. 9.
- [27] [27] Kumar, D., Prasad, G., Vishwanath, S., Ghorui, P., Mazumdar, D., Ranjan, M., and Lal, P., *Iron and Steelmaker* 6 (2007), pp. 521.
- [28] Deng, T. and Du Sichen, *Study of Lime Dissolution Under Forced Convection*, Metall and Materi Trans B 43 (2012), 3, pp. 578–586.
- [29] Stromberg, A. G., Semchenko, D. P., *Physical chemistry, book for chemical special schools*, Vysshaya shkola, Moscow, 2003.
- [30] Umakoshi, M., Mori, K. and Kawai, K., *Trans. Iron Steel Inst. Jpn.* 24 (1984), pp. 532.
- [31] Baker, R., Normanton, A. S., Spenceley, G. D., & Atkinson, R., *Bath Agitation in Oxygen Steelmaking*. *Iron and Steelmaking*.
- [32] Turkdogan, E. T. and J. Pearson, *Activities of constituents of iron and steelmaking slags* 173 (1953), pp. 217–223.
- [33] Choudhary, S.K., Lenka S.N. and Gosh, A., *Tata Search* (2005), pp. 117.
- [34] Boronenkov, V. and O. Esin, *Kinetic equations of multicomponent reactions in the diffusive regime: Ferrous metallurgy* (1970), pp. 17–21.

- [35] Svyazhin, A.G., Mathematical description of the kinetics of metallurgical processes: Ferrous metallurgy, *Izvestiya Vysshikh uchebnykh zavedeniy*. 5 (2008), pp. 7–9.
- [36] Engh, T.A., Principles of Metal Refining, Oxford University Press, UK (1992), pp. 192.
- [37] Ward, R.G., An Introduction to the Physical Chemistry of Iron and Steelmaking, Edward Arnold, London, 1963.
- [38] Sigworth, G.K. and Elliott, G.F., *Metal Science* 8 (1974), pp. 298.
- [39] Barfield, R. N., and J. A. Kitchener., The viscosity of liquid iron and iron-carbon alloys: *Journal of the Iron and Steel Institute* (1955), 180, pp. 324–329.
- [40] Atkins, P.W. and J. de Paula, *Atkins' Physical chemistry*, 8th ed., Oxford University Press, Oxford, New York, 2006.
- [41] Landau, L.D., J.B. Sykes, W.H. Reid and E.M. Lifshitz, *Fluid mechanics*, Second edition (Online-ausg.), Pergamon Press, Oxford, England, 1987.
- [42] Elliot, J.F, Gleiser M. and Ramakrishna, V., *Thermochemistry of Steelmaking*, Addison-Wesley, Reading Mass., USA, 1963.
- [43] Szekely, Von.J. and Themelis, N.J., *Rate Phenomena in Process Metallurgy*, Wiley Interscience, a Division of John Wiley & Sons Inc., New York-London-Sydney-Toronto 44 (1971), 9, pp. 640.
- [44] Davies, J.T., *Turbulence Phenomena. An Introduction to the Elderly Transfer of Momentum, Mass, and Heat, Particularly at Interfaces*, Academic Press, New York-London 45 (1972), 5, pp. 339.
- [45] Turkdogan, E.T., *Fundamentals of Steelmaking*, 2012.
- [46] Newman, A.B., The drying of porous solids diffusion and surface emission equations 27 (1931), pp. 310.
- [47] Bird, R. B., Stewart, W. E. and Lightfoot, E. N., *Transport Phenomena*, Wiley, New York, 1960.
- [48] Pehkle, R.D., Goodell, P.D. and Dunlap, R.W., Iron and Steel Division - Kinetics of Steel Dissolution in Molten Pig Iron, *Trans., AIME* (1965), pp. 1420.
- [49] Perrot, P., *A to Z of thermodynamics*, Oxford University Press, Oxford, New York, 1998.
- [50] Richardson, F.D., *Physical chemistry of melts in metallurgy*, Academic Press, London, New York, 1974.

-
- [51] Bird, R.B., W.E. Stewart and E.N. Lightfoot, Transport phenomena, Rev. 2nd ed., J. Wiley, New York, 2007.
- [52] Welty, J.R., Rorrer, G.L. and Foster, D.G, Fundamentals of momentum, heat and mass transfer, 6th edition, Wiley, Hoboken, NJ, 2015.
- [53] Sherwood, T.K. Pigford, R.L. and Wilke, C.R., Mass Transfer, McGraw-Hill, New York, 1975.
- [54] Medzhibozhskiy, M.Y., Fundamentals of thermodynamics and kinetics of steelmaking processes, Metallurgiya cher. metallov, Kiev, 1979.
- [55] Starikov, V. S., Starikov, V. V. and Temljancev, M. V., Refractories and lining in the ladle metallurgy: Uchebnoe posobie dlja vuzov, Misis, Moscow, 2003.
- [56] Kashcheev, D. I., Strelow, D.D. and Mamykin, P.S., Chemical refractory technology: Metallurgical heat engineering, Internet Engineering, 2007.
- [57] Slag Atlas, 2nd. ed, Verlag Stahleisen, Düsseldorf, Germany, 1981.
- [58] Berezhnoy, A.S., Multicomponent oxide systems, Naukova dumka, Kiev, 1988.
- [59] Fruehan, R. J, Li, Y. and Brabie, L., Dissolution of Magnesite and dolomite in simulated EAF slags.
- [60] Matsushima, M., Yadoomaru, S., Mori, K. and Kawai, Y., Fundamental Study on the Dissolution Rate of Solid Lime Into Liquid Slag, Trans. Iron Steel Inst. Jpn. 17.8 (1977), pp. 442-449.
- [61] Babenko, A., Danilin Y.A., Mukhranov N.V., Levchuk V.V., Krivyh L., Increasing converter lining resistance: Proceedings of the Universities, Ferrous metallurgy 4 (2010), pp. 20.
- [62] Posin, M.E., Research in inorganic Technology. Salts, oxides, acids., Moscow Science (1972), pp. 361.
- [63] ANSYS-Fluent, <http://www.ansys.com/Products/Fluids/ANSYS-Fluent>.
- [64] Eisenberg, M., Tobias, C. W. and Wilke, C.R., Mass Transfer at Rotating Cylinders (1955).

16 List of Figures

Figure 2-1:	BOF and Q-BOP steelmaking with and without combined blowing [12]	6
Figure 2-2:	Schematic section of the BOF [12].....	8
Figure 2-3:	Schematic of operational steps in oxygen steelmaking process (BOF) [13]	10
Figure 4-1:	Laminar (left), turbulent (right) flow [50]	30
Figure 5-1:	Rietveld investigation of phases of LD slag №1	40
Figure 5-2:	Rietveld investigation of phases of LD slag №2.....	40
Figure 5-3:	Microscopic investigation of LD slag phases.....	42
Figure 5-4:	Microscopic investigation of LD slag phases.....	42
Figure 5-5:	Microscopic investigation of LD slag phases.....	43
Figure 5-6:	Microscopic investigation of LD slag phases.....	43
Figure 6-1:	The principle setup of the Gero furnace	47
Figure 6-2:	The principle of the device structure	47
Figure 7-1:	General view of crucibles subjected for the study of the interaction of crucible material with slag.....	53
Figure 7-2:	Pictures of broken BN crucible after test with LD slag at 1500°C.....	54
Figure 7-3:	Pictures of broken BN crucible after test with LD slag at 1600°C.....	54
Figure 7-4:	Characteristic X-ray spectrum of industrial slag after heat treatment in the BN crucible without new formed structure	55
Figure 7-5:	Characteristic X-ray spectrum of new structure formed after heat treatment of industrial slag in the BN crucible	55
Figure 7-6:	Characteristic X-ray spectrum of industrial slag after heat treatment in magnesia crucible	56
Figure 7-7:	Parts of MgO crucible with industrial slag at 1500°C and 1600°C.....	56
Figure 7-8:	Visual control of interaction between slag and crucible at different temperatures and defect of crucible after melting.....	57
Figure 7-9:	Crucible from electrofused magnesite, 2 –Crucible from silica modified to cristobalite	57
Figure 7-10:	The results of qualitative XRD on the presence of cristobalite in the samples of industrial slag.....	58

Figure 7-11:	Characteristic X-ray spectrum of industrial slag without heat treatment	58
Figure 7-12:	Characteristic X-ray spectrum of industrial slag after melting at 1500°C in a quartz crucible.....	59
Figure 7-13:	The distribution of elements according to the intensity	60
Figure 8-1:	Ternary diagram of the system CaO - FeO - SiO ₂ [57].....	63
Figure 8-2:	The X-ray spectrum of model slag №1 melted at 1400°C for 30 min.....	64
Figure 8-3:	The X-ray spectrum of model slag №1 melted at 1500°C for 30 min.....	64
Figure 8-4:	The X-ray spectrum of model slag №1 melted at 1600°C for 30 min.....	65
Figure 8-5:	The X-ray spectrum of model slag №2 melted at 1400°C for 30 min.....	66
Figure 8-6:	The X-ray spectrum of model slag №2 melted at 1500°C for 30 min.....	67
Figure 8-7:	The X-ray spectrum of model slag №2 melted at 1600°C for 30 min.....	67
Figure 8-8:	The X-ray spectrum of model slag №3 melted at 1500°C for 30 min.....	69
Figure 8-9:	The X-ray spectrum of model slag №3 melted at 1600°C for 30 min.....	69
Figure 9-1:	Dependence of the amount of dissolved CaO on the contact time of sample with the slag	73
Figure 9-2:	The dependence of Calcium oxide sample's height on time.....	73
Figure 9-3:	The dependence of the linear rate of CaO samples dissolution on the saturation of slag with calcium oxide	74
Figure 9-4:	The dependence of the mass transfer coefficient values of CaO dissolution in model slag on the dissolution time	75
Figure 9-5:	The dependence of the amount of dissolved CaO sample on contact time of sample with the slag	76
Figure 9-6:	The dependence of calcium oxide sample linear dimensions (height of the cylinder) change on time.....	77

Figure 9-7:	The dependence of the dissolution rate of CaO samples on the calcium oxide concentration in slag.....	78
Figure 9-8:	The dependence of mass transfer coefficient values of CaO dissolution in the industrial slag on the dissolution time	78
Figure 9-9:	The dependence of the amount of the lime dissolved in the industrial slag on time	80
Figure 9-10:	The dependence of the linear rate of lime dissolution on the CaO concentration in the industrial slag	80
Figure 9-11:	The values of calculated mass transfer coefficients of lime in the industrial slag	81
Figure 10-1:	The X-Ray spectrum of the industrial lime containing 4.3% MgO	83
Figure 10-2:	The dependence of the amount of dissolved lime containing 2% of MgO on time.....	84
Figure 10-3:	The dependence of the linear dimensions of lime samples containing 2% of MgO on the dissolution time	85
Figure 10-4:	The dependence of the linear rate of dissolution of lime samples containing 2% of MgO on the CaO content in slag.....	86
Figure 10-5:	Calculated mass transfer coefficients of lime containing 2% MgO	86
Figure 10-6:	The dependence of the amount of dissolved lime containing 4.3% of MgO on contact time with slag	89
Figure 10-7:	The dependence of the amount of dissolved lime containing 5.6% of MgO on contact time with slag	89
Figure 10-8:	The dependence of the amount of dissolved lime containing 6.2% of MgO on contact time with slag	90
Figure 10-9:	The dependence of the amount of dissolved lime containing 7.6% of MgO on contact time with slag	90
Figure 10-10:	The X-Ray spectrum of the final slag after lime dissolution containing 4.3% of MgO.....	91
Figure 10-11:	The dependence of the linear rate of dissolution of lime samples containing 4.3% of MgO on the CaO content in slag.....	92
Figure 10-12:	The dependence of the linear rate of dissolution of lime samples containing 5.6% of MgO on the CaO content in slag.....	92
Figure 10-13:	The dependence of the linear rate of dissolution of lime samples containing 6.2% of MgO on the CaO content in slag.....	93

Figure 10-14: The dependence of the linear rate of dissolution of lime samples containing 7.6% of MgO on the CaO content in slag	93
Figure 10-15: The values of calculated mass transfer coefficients of lime dissolution containing 4.3% of MgO.....	94
Figure 10-16: The dependence of the dissolution rate of lime samples containing 2%of MgO on the value of <i>ct</i>	96
Figure 10-17: The dependence of the dissolution rate of lime samples on the value of <i>ct</i>	96
Figure 10-18: The dependence of the logarithm of the diffusion coefficient on the inverse temperature.....	98
Figure 10-19: The dependence of the logarithm of the diffusion coefficient on the inverse temperature.....	99
Figure 11-1: The dependence of the amount of dissolved dololime containing 20% MgO on the contact time with slag.....	102
Figure 11-2: The dependence of the linear rate of dissolution of dololime samples on the CaO content in the slag	103
Figure 11-3: The dependence of the logarithm of the mass transfer coefficient on the inverse temperature.....	103
Figure 11-4: The dependence of the dissolution rate of lime samples containing 20% of MgO on the value of <i>ct</i>	104
Figure 11-5: The dependence of the logarithm of the diffusion coefficient on the inverse temperature.....	104
Figure 11-6: The amount of dololime containing 50% MgO dissolved on contact time with slag	106
Figure 11-7: The dependence of the linear rate of dissolution of dololime samples on the CaO content in the slag	107
Figure 11-8: The dependence of the logarithm of mass transfer coefficients on the inverse temperature.....	107
Figure 11-9: The dependence of the dissolution rate of lime samples containing 50% of MgO on the value of <i>ct</i>	108
Figure 11-10: The dependence of the logarithm of the diffusion coefficient on the inverse temperature.....	108

Figure 11-11: The dependence of mass of the dissolving sample on contact time with slag	110
Figure 12-1: Simulation of up-flow of the dissolving sample.....	113
Figure 12-2: Simulation of down-flow of the dissolving sample	114
Figure 13-1: Schematic setup of vertical high temperature furnace	115
Figure 13-2: Microscopic raster images of lime containing 4.3 (upper) 7.6(middle) and 80% MgO (bottom).	120
Figure 13-3: The X-Ray spectrum of dololime containing 80%MgO	121

17 List of Tables

Table 2-1:	The duration of Basic Oxygen Steelmaking process stages [16]	13
Table 5-1:	The elemental composition of the industrial slags carried out by X-ray fluorescence method	38
Table 5-2:	The elemental composition of the industrial slag №1 by SEM.....	38
Table 5-3:	Industrial slags phase composition (XRD analysis of slag carried out by MCL-Leoben)	39
Table 5-4:	The results of quantitative X-ray analysis of the industrial slag №1.....	39
Table 5-5:	The results of quantitative X-ray analysis of the industrial slag № 2.....	39
Table 5-6:	Comparison of XRD and Rietveld results for investigation of Industrial slag phase composition.....	41
Table 6-1:	The composition of model slag	45
Table 6-2:	The quantitative composition of model slag.....	46
Table 6-3:	The composition of the industrial limes provided by Voestalpine Linz.....	48
Table 6-4:	The composition of other elements for lime samples.....	48
Table 7-1:	Properties of the refractory materials [55].....	50
Table 7-2:	Intensities of slag melted in various crucibles at 1500°C	59
Table 7-3:	Detected phases of industrial slag after melting at 1500°C in different crucibles: quartz, magnesia and boron nitride	60
Table 8-1:	Identified phases of model slag №1.....	65
Table 8-2:	Identified phases of model slag №1 compared with phase diagram and literature.....	66
Table 8-3:	Identified phases of model slag №2.....	68
Table 8-4:	Composition of model slag №2 compared with phase diagram and literature.....	68
Table 8-5:	Composition of model slag №3 melted at 1400°C, 1500°C, 1600°C compared with phase diagram and literature	70
Table 9-1:	The experimental results of the dissolution process of CaO samples in the model slag	72
Table 9-2:	The results of experimental studies of CaO dissolution in the industrial slag.....	76

Table 9-3:	Experimental results of the dissolution of cylindrical lime samples in the industrial slag	79
Table 10-1:	The experimental results of the dissolution process of lime samples containing 2% of MgO in the model slag.....	84
Table 10-2:	The experimental results of the dissolution process of lime samples containing 4.3% of MgO in the model slag.....	87
Table 10-3:	The experimental results of the dissolution process of lime samples containing 5.6% of MgO in the model slag.....	87
Table 10-4:	The experimental results of the dissolution process of lime samples containing 6.2% of MgO in the model slag.....	88
Table 10-5:	The experimental results of the dissolution process of lime samples containing 7.6% of MgO in the model slag.....	88
Table 10-6:	Equilibrium concentration (saturation concentration) of CaO in model slag at different temperatures of lime dissolution process.	91
Table 10-7:	The values of diffusion coefficients of lime dissolution in slag (SD- spatial diffusion and LD-linear diffusion).	97
Table 11-1:	The experimental results of the dissolution process of dololime samples containing 20% of MgO in the model slag.....	101
Table 11-2:	Porosity measurements of lime samples	105
Table 11-3:	The experimental results of the dissolution process of dololime samples containing 50% of MgO in the model slag.....	105
Table 11-4:	The derived diffusion coefficients for dololime dissolution containing 20 and 50% MgO	109
Table 11-5:	The experimental results of the dissolution process of dololime samples containing 80% of MgO in the model slag.....	109
Table 11-6:	Activation energy of Diffusion for lime and dololime samples.....	110
Table 13-1:	Experimental results of lime dissolution containing 4.3% MgO	116
Table 13-2:	Experimental results of lime dissolution containing 5.6% MgO	116
Table 13-3:	Experimental results of lime dissolution containing 6.2% MgO	117
Table 13-4:	Experimental results of lime dissolution containing 7.6% MgO	118
Table 13-5:	Mass transfer coefficients of lime dissolution under forced convection	119
Table 18-1:	The chemical composition of the initial and final slag.....	135

18 Appendix

The mass balance of slag composition before and after the dissolution was conducted to confirm the inertness of SiO₂ crucibles. Due to the complexity of the analysis a certain deviation within the error is appropriate.

The chemical composition presented as oxides, of the initial and final slag after the dissolution of lime containing 4.3-7.6% MgO at the highest temperature of experiment (1600°C) is shown in Table 18-1.

Table 18-1: The chemical composition of the initial and final slag

Slag	MgO content in lime, %	Composition, %				
		CaO	SiO ₂	FeO	MgO	other
Initial	-	20.00	35.00	45.00	-	-
Final (XRF), 1600°C	4.3	40.36	25.93	31.83	1.38	0.50
Final (calculation), 1600°C		41.84	24.82	31.91	1.30	0.13
XRF, 1600°C	5.6	35.85	26.20	36.52	1.32	0.11
calculation, 1600°C		35.16	27.78	35.71	1.28	0.07
XRF, 1600°C	6.2	31.02	33.90	34.10	0.88	0.10
calculation, 1600°C		29.10	30.58	39.41	0.82	0.09
XRF, 1600°C	7.6	26.40	31.28	41.53	0.71	0.08
Calculation, 1600°C		25.79	32.11	41.28	0.75	0.07

Initial mass of slag =2g, after the dissolution of 4.3% lime mass of slag was 2.82g

Lime 4.3% 1600°C	Initial slag Content, %	Initial Mass, g	Slag content after lime dissolution, % (XRF)	Mass after the dissolution, g	M end-M initial, g
	CaO 20%	0.4	CaO 40.36	1.13	0.74
	SiO ₂ 35%	0.7	SiO ₂ 25.93	0.73	0.03
	FeO 45%	0.9	FeO 31.83	0.89	0
			MgO 1.38	0.04	0.04
			Other 0.50	0.01	0.01

Initial mass of slag =2g, after the dissolution of 5.6% lime mass of slag was 2.52g

Lime 5.6% 1600°C	Initial slag Content, %	Initial Mass, g	Slag content after lime dissolution, % (XRF)	Mass after the dissolution, g	M end-M initial, g
	CaO 20% SiO ₂ 35% FeO 45%	0.4 0.7 0.9	CaO 35.85 SiO ₂ 26.20 FeO 36.52 MgO 1.32 Other 0.11	0.90 0.66 0.92 0.035 0	0.5 -0.04 0.02 0.035 0

Initial mass of slag =2g, after the dissolution of 6.2% lime mass of slag was 2.28g

Lime 6.2% 1600°C	Initial slag Content, %	Initial Mass, g	Slag content after lime dissolution, % (XRF)	Mass after the dissolution, g	M end-M initial, g
	CaO 20% SiO ₂ 35% FeO 45%	0.4 0.7 0.9	CaO 31.02 SiO ₂ 33.90 FeO 34.10 MgO 0.88 Other 0.10	0.70 0.71 0.70 0.025 0	0.30 0.01 0 0.025 0

Initial mass of slag =2g, after the dissolution of 7.6% lime mass of slag was 2.18g

Lime 7.6% 1600°C	Initial slag Content, %	Initial Mass, g	Slag content after lime dissolution, % (XRF)	Mass after the dissolution, g	M end-M initial, g
	CaO 20% SiO ₂ 35% FeO 45%	0.4 0.7 0.9	CaO 26.40 SiO ₂ 31.28 FeO 41.53 MgO 0.71 Other 0.08	0.58 0.68 0.91 0.02 0	0.18 0.02 0.01 0.02 0

Curriculum Vitae



Cheremisina Elizaveta Alexandrovna

Leoben Waasenstrasse, 24/5 Austria

+43680 2200080

Elizaveta.Cheremisina@unieoben.ac.at

elisa-alex@mail.ru

Date of birth: 27.12.1990

Employment History

BASF SE (The Chemical company) Ludwigshafen, Germany Jul/Sept 2012

- Internship working in the department of non-destructive testing, corrosion testing, corrosion inspection and failure inspection studying methods for cracks and defects inspection
- Completing work in the sales department completing negotiations
- Offering support to the management team

Montanuniversität 6 Month Scholarship/Grant 2012 **Exchange Semester 2011 - 2012**

- Based in the raw materials department studying diamond drilling technology for my thesis

Kola peninsula GMK-subsiary of Norilsk Nickel 2011 **Monchegorsk, Kola Peninsula, Russian Federation**

- Assisting with optimising Platinum/Palladium production processes and other noble metals
- Preparing reports to management

Volkhov Aluminium Smelter Internship 2009

- Studying aluminium/copper electro processes, hydrometallurgical processes, leaching and extraction

Education and further training

Montanuniversitaet Leoben, Austria

2013 – 2016

PhD in Ferrous Metallurgy

Project: Collaboration with Voestalpine Linz, Voestalpine Donawitz & Siemens VAI (Primetals technologies)

Thesis: Kinetics of CaO and MgO dissolution in the converter steelmaking process

Saint-Petersburg State Mining University (Mineral Resources University) 2008 – 2013

MSc Metallurgical Engineering in Non-Ferrous Metallurgy

Classification: 4.9 (5 is HM)

Thesis: Gallium absorption on anionites from circulating alkaline solutions from aluminium production

Oriental Institute Certificate in the Japanese language 2008 – 2013

Certificate in Japanese language proficiency; N4, JLPT 日本語能力試験 2012

Lomonosovskaya Gymnasium №73

1997 – 2008

Continuous professional development

Publications

Cheremisina, E., Schenk, J., Nocke, L., Paul, A., Wimmer, G. (2016)

ISIJ International, Vol 57 №2

Influence of magnesium oxide content on kinetics of lime dissolution in steelmaking slags

Cheremisina, E.; Schenk, J.; Tappeiner, T.; Panhofer, H. (2015)

Proceedings of the 26th International Symposium on Transport Phenomena

Kinetic characteristics of calcium oxide dissolution in steelmaking slags

Cheremisina, E.; Schenk, J.; Tappeiner, T.; Sormann, A.; Wimmer, G. (2015)

Proceedings of Asia Steel International conference

Kinetics of lime dissolution in steelmaking slags

Cheremisina O.V, Cheremisina E.A, El-Salim S.Z

Mining Institute journal. 2013 T. 202, pp 228-230

Indicators and air monitoring

Chirkst D.E., Cheremisina E.A., Cheremisina, O.V., Ponomareva M.A.

Russian Journal of Non-Ferrous Metals, 2013, Vol. 54, No. 3, pp. 201–208. Peer-reviewed

Sorption of Gallium from the Alkali solutions Based on Anionites

Al-Salim S.Z., Cheremisina O.V., Cheremisina, E.A, Migalovskaya E.D., Kleshchenko R.V.

Russian Journal of Physical Chemistry B, Volume 6, Issue 5, September 2012, Pages 637-642, peer-reviewed

Improving the analytical characteristics of adsorption semiconductor sensors based on adsorption SnO₂ using photon simulation

Patents: Method of determining concentration of element in substance of complex chemical composition RU 2524454C1

Research: Kinetics of lime dissolution in the converter steelmaking process

Languages: Russian (native), fluent in English, good Japanese and German. Chinese and Slovenian basic.

IT skills: MS Office, AutoCAD, Factsage, Gambit ANSYS fluent

Scientific Interests:

- Thermodynamics and kinetics of metallurgical processes
- Sorption and Ion exchange
- Phase transformations
- Lime dissolution in the converter slags
- Primary Metallurgy and Metallurgical Process
- Refractories , Corrosion
- Thermodynamics and kinetics of heterogeneous systems
- Oxygen steelmaking
- Slag metallurgy
- High temperature metallurgical processes